Structural Seismic Analysis of the Great Portico of Medina Azahara

Delft University of Technology

TU Delft

Structural Seismic Analysis of the Great Portico of Medina Azahara

by

Wouter Kroon

to obtain the Master of Science degree
in Civil Engineering
Track: Structural Engineering

at the Delft University of Technology
Faculty of Civil Engineering and Geosciences

Author:	Wouter Kroon (4916603)	
Thesis supervisors:	Dr. R. Esposito	Applied Mechanics, CEG, TU Delft
	Dr. B. Zapico-Blanco	Department of Building Structures and Geotechnical Engineering, Universidad de Sevilla
	Dr. S. Sharma	Applied Mechanics, CEG, TU Delft
	Prof. Dr. Ir. M.A.N. Hendriks	Concrete Structures, CEG, TU Delft
Date:	November, 2025	

Cover picture: Calero Clavero, 2023

TU Delft

Acknowledgements

This thesis finalizes my studies at Delft University of Technology for both the bachelor of civil engineering and master of structural engineering. I have studied for several years at the TU Delft and I am truly grateful for all the opportunities it has given me to broaden my knowledge and improve myself. I am grateful to all the Professors and lecturers, who showed me the beautiful world of civil engineering and engaged me in their own expertise. I am also grateful to my fellow students, who helped me along the way and especially to those who became close friends and shared struggles and successes.

I would like to thank my thesis committee: Dr. Rita Esposito, Dr. Beatriz Zapico-Blanco, Prof. Dr. Ir. Max Hendriks and Dr. Satya Sharma, for supervising and guiding the, sometimes very difficult, process. Thanks to Dr. Rita Esposito, first of all for setting up the thesis-proposal and sparking my enthusiasm for the topic. For your guidance, you always had helpful advice to help me move forward in my research and always tried to keep me on track. For your patience in what became quite a long process, you always stayed positive even at the smallest steps of progress. Thanks to Dr. Beatriz Zapico-Blanco, for including me into your project and giving me a first look into the world of actual research. For refining the scope of my research to fit my abilities and your research. For your feedback and help with specific aspects of my research, it has helped me greatly. Thanks to Prof. Dr. Ir. Max Hendriks, for your insights during our meetings, it has helped me to widen my perspective on the research and cleared up many things I had overlooked. Special thanks to Dr. Satya Sharma, without your support I would not have been able to finish this thesis project. You always had answers to my many questions. Even when you were busy with your own work, you had time to help me. I am truly grateful for all our meetings and conversations.

I am grateful to all my friends I made at DSZ WAVE. You have been an important part of my time in Delft. The time I spend with you all were always a great way to get my mind of studies. In you all, I found support and love, which helped me through the good and the bad times. You feel like a second family. Especially all the guys from Gents 2, who have been my second brothers for the past few years (AHOE).

To my long-time friends, who always spark joy and make me smile. To Cynrîk, for your unwavering support and all the conversations we had about life. To my family, who loved and supported me in all my choices. To my parents, for paving the way and giving me all the opportunities to choose my own life. To my dad, who has been my greatest example. To my mom, for your unconditional love. And lastly to my brother, you will always be my first and best friend.

Kroon, Wouter

Summary

The Great Portico of Medina Azahara is a prominent remnant of the 10th-century Caliphate of Córdoba. Once the monumental entrance to the Caliph's palace complex, it is now a partially preserved four-arched masonry structure. The site is a UNESCO World Heritage monument of major cultural significance. Ensuring its structural integrity is vital for conservation and heritage management. This study investigates the seismic response of the existing remains of the Great Portico using finite element modelling and nonlinear pushover analysis. It aims to identify its dominant vibration modes, primary failure mechanisms, and the points of concern for damage due to seismic loading.

The study adopted a continuum homogeneous modelling strategy. Multiple three-dimensional finite element models were constructed in an iterative approach, to enable a sensitivity analysis on specific aspects of the structure. The initial model included only a single building material. Later models included three materials, interface elements at important structural interfaces and a more accurate model geometry. Due to lack of in-situ measurements, the model geometry was approximated based on detailed drawings of the structure. All models used solid elements and later models also incorporated structural interface elements at important interfaces. Boundary conditions fixed the column bases, and loading consisted of the self-weight followed by a modal pushover analysis. The dominant eigenmodes were determined using an eigenmode analysis. Three materials were defined: limestone masonry, brick masonry and limestone. The mechanical properties incorporated in the study, were based on literature concerning the Mosque-Cathedral of Córdoba and available structural codes for concrete and masonry structures. Limestone and brick masonry were modelled with a total strain-based crack model, while limestone blocks were modelled linear elastic isotropic. Two types of structural interface elements were modelled and assessed comparatively: discrete cracking elements and combined cracking-shearing-crushing elements.

From the results of the eigenmode analyses, it was revealed that both in-plane and out-of-plane modes significantly influence the seismic response. Therefore both the in-plane and out-of-plane responses of the structure were analysed. The in-plane response is characterized by tensile cracking in the arches' brick masonry and at the interfaces between brick masonry and limestone blocks. The out-of-plane response had the most critical failure mechanism. Cracking in the limestone masonry initiated at the bases and mid-height of the columns, leading to tensile failure and toppling of the second arch. However, the overall capacity of the Great Portico, estimated at approximately 1.0 g, is relatively high compared to results from shake-table tests on masonry structures. Sensitivity analyses demonstrated that halving the tensile strength had minimal influence on global capacity, while reducing stiffness decreased peak base shear but did not alter failure modes. Crushing was observed only at high displacements, well after tensile cracking dominated the response, confirming that tensile failure controls the seismic vulnerability. Model comparisons showed that, introducing multiple materials and interface elements had only limited impact on the overall seismic response of the structure. For the out-of-plane behaviour, the simplest model was adequate, whereas for the in-plane behaviour, the most detailed model best represented its response.

In conclusion, this study indicates that the remaining part of the Great Portico is most vulnerable under out-of-plane loading, leading to tensile cracking in the limestone masonry of the columns. The in-plane response, while stronger, is controlled by cracking within the brick masonry in the arches and at the interfaces between the brick masonry and limestone blocks. Crushing failure is not governing for both mechanisms.

The findings for the Great Portico from this research can serve as a reference for similar analyses at Medina Azahara and the Mosque-Cathedral of Córdoba, contributing to their sustainable preservation against seismic risk.

Contents

1

Introduction

1.1. Background

Once the capital city of the first Umayyad Emirate of Córdoba and later the Caliphate of Córdoba, the current city of Córdoba, in Andalusia, Spain, hosts a large historical heritage. The best preserved remnants of the Caliphate are the Mosque-Cathedral of Córdoba and the historical city of Medina Azahara, both declared a World Heritage Site by the UNESCO World Heritage Centre (2025). Both sites hold great importance for the region. The Mosque-Cathedral is one of the biggest tourist attractions of Andalusia and a great example of Spain's Islamic history. Medina Azahara is the largest archaeological site of Spain. Preservation of both sites is therefore of major importance for the city and the region.

Quite some research has been performed on both structures, for example about the architectural significance of the Mosque-Cathedral (Hildebrand, 2012 & Hidalgo Fernández and Ortiz-Cordero, 2020) and on certain restoration research performed on the structure (Palomar et al., 2023). Other research about the city of Medina Azahara are for example about its historical/archaeological significance, conservation in the context of tourism (García Hernández and de la Calle Vaquero, 2010) and study about the materials, such as the research performed by Blanco-Varela et al. (1997) on the mortar used at the site of Medina Azahara, but little research is performed on structural analysis of structures at both sites, which would be necessary to ensure the structural integrity of these structures and thus their preservation. An earthquake would likely be the greatest natural cause of damage to the city of Medina Azahara and the Mosque-Cathedral. Research performed by Rodríguez-Pascua et al. (2023) showed evidence of seismic damage at Medina Azahara, such as dropped key stones and tilted walls, from earthquakes in the 11th and 12th century, which could have been a reason for the abandonment and partial destruction of the city (Rodríguez-Pascua et al., 2023). The structural response to seismic loading could therefore be a key research-point for the future conservation of both heritage sites. For this report a specific structure, the Great Portico of Medina Azahara, was chosen to further investigate this key research-point.

Once a structure consisting of fourteen arches, the Great Portico was the entrance to heart of the Alcázar, the palace of the Caliph. From this gallery the Caliph reviewed his troops training on the open square in front of the Great Portico, known as the Plaza de Armas or al-Muzara (Calero Clavero, 2023). Nowadays the structure consists of four segmented arches, one being a horseshoe-shaped arch, which was the central arch of the gallery and is slightly wider and taller than the other arches (Calero Clavero, 2023). The Great Portico in its current state is shown in Figure 1.1. The structure was built using three identifiable building-materials. The main building-material is limestone-and-lime-mortar masonry. The arches consist of components of clay-brick-and-lime-mortar masonry and limestone sequentially. The use of lime mortar is assumed based on a study on the Mosque-Cathedral (Requena García de la Cruz et al., 2023) and the assumption of similar building techniques for the two structures.

Figure 1.1: The Great Portico of Medina Azahara (Calero Clavero, 2023)

1.2. Research Questions and Objectives

The research aims to investigate the structural behaviour of the Great Portico subjected to seismic loading, including a sensitivity analysis on two mechanical properties of the limestone masonry. The main scope of the research could be described by the following research-question: **What is the structural response of the remaining structure of the Great Portico of Medina Azahara subjected to seismic loading?**

To support the main scope, the following sub-research points will be addressed in the report:

- Which eigenmode dominates the seismic response of the structure? Is it a single mode or multiple?
- What are the main failure modes of the structure? And what are the points of concern for seismic damage?
- What effect has a deviation of the value of a certain mechanical property (tensile strength or stiffness) of the limestone masonry on the structural behaviour?

The results found in this research could be useful for other structures on the site of Medina Azahara, as well as the Mosque-Cathedral, due to the use of similar natural stone at both sites and, in case of the Mosque-Cathedral, a similar structure (i.e. a structure consisting of double-layered arches, see Figure 1.2). This research could therefore be used as reference and further research on the site of Medina Azahara and the Mosque-Cathedral.

1.3. Research Methodology

This study implements a continuum homogeneous modelling approach. Several finite element models were built and used to investigate the seismic response of the four-arched structure. The models were made in the DIANA FEA 10.7 software environment (DIANA FEA B.V., 2023), using the constitutive laws and loading types defined in the software. The mechanical properties are mainly taken from literature and partially verified by experimental testing. The seismic loading is modelled by a global modal pushover load. All conclusions drawn in this report are based on the results from the pushover analyses.

Figure 1.2: Hypostyle hall, Mosque-Cathedral of Córdoba: double-layered arches (Mirmobiny, 2015)

1.4. Outline of Report

The report consists of six chapters. Chapter 1 introduces the study and presents the main scope of the research. Chapter 2 elaborates on the current state of research on the structural dynamic behaviour of stone (masonry) arches and on the modelling of masonry structures. Chapter 3 gives a detailed description of the research approach and the development of the finite element models. Chapter 4 outlines the results of the eigenmode and pushover analyses. Lastly, Chapter 5 discusses the research methodology and the results and Chapter 6 draws the final conclusions and lists recommendations for further research.

2

State of the Art

The research utilizes numerical finite element models to analyse the remaining structure of the Great Portico, a historical (predominantly) masonry arch structure. This chapter reviews established research on the dynamic behaviour of masonry arches and examines the various modelling strategies employed for masonry structures.

2.1. Structural dynamic behaviour of masonry arches

For the analysis of the structural behaviour of masonry arches is usually referred to the principles stated by Jacques Heyman. Heyman (1966) formalized the *"safe" theorem* and the *uniqueness theorem*. The theories state that a masonry arch-structure is safe if there exists a line of thrust in equilibrium with the external loads contained entirely within the thickness of the masonry and, if the external loading is proportional increased by a load factor to form the required amount of hinges in the line of thrust to transform the structure in a mechanism, that load factor at collapse is unique (Heyman, 1966). Heyman used the following three assumptions about stone masonry for his formulations: Stone masonry has no tensile strength: tensile forces are not transmissible within masonry, stone has an infinite compressive strength: there is no danger of crushing and sliding failure cannot occur: friction is high enough to prevent the stone blocks from sliding on one another. These assumptions allow plastic theory to be applied to masonry arches (Heyman, 1969).

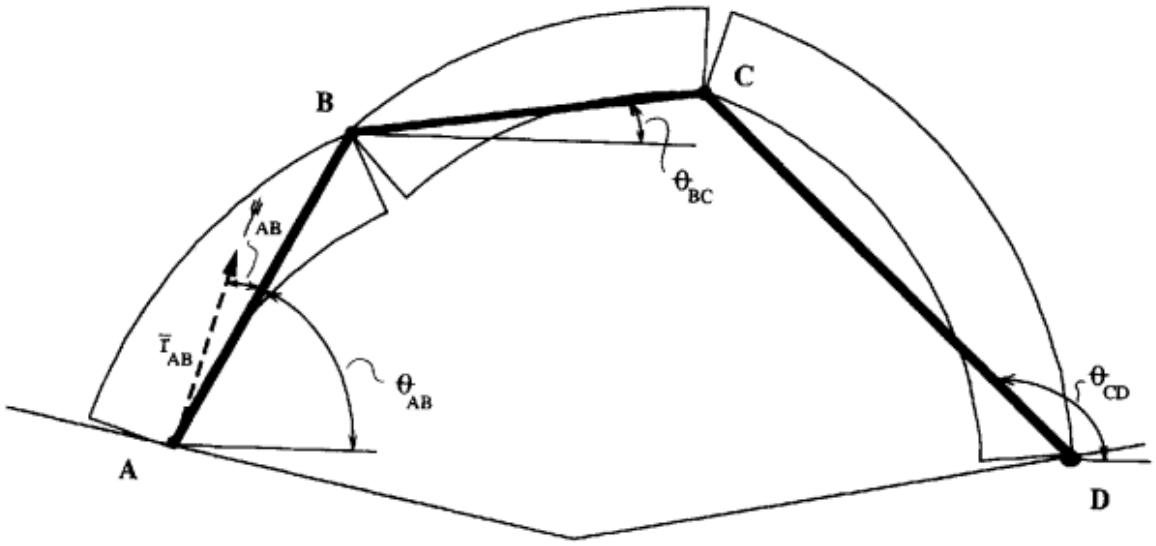

Figure 2.1: Four-link rigid body mechanism motion of an arch (Oppenheim, 1992)

Building on Heyman's theoretical framework, Oppenheim (1992) examined the dynamic response of an unreinforced masonry arch by idealizing the structure as a four-link rigid body mechanism subjected to a base motion. In his paper, *Introduction to dynamics of stone arches*, Clemente (1998) used the four-link rigid body mechanism and the uniqueness theorem to describe an arch turning into a mechanism at an unique peak ground acceleration level (mechanism at $PGA \geq \lambda g$, g is the gravitational acceleration). Oppenheim studied this one possible failure mode: direct overturning as a four-link mechanism. He found that an arch geometry establishes good resistance to earthquake excitation. The ground acceleration must exceed a rather high threshold before any mechanism motion would develop. However, once that threshold has been passed the arch has relatively modest resistance before failure (Oppenheim, 1992). Oppenheim discusses two more failure conditions: pounding and sliding. Pounding could cause fracturing, resulting in the decrease of the effective thickness of the arch significantly weakening the structure. Sliding will occur when the tangential-normal ratio exceeds the friction coefficient. Failure occurs if a block slides beyond the geometric limits (Oppenheim, 1992).

2.2. Modelling of masonry structures

Modelling masonry structures is an intricate task given the complexity of the mechanics of masonry. Masonry has a composite character, combining stone or brick with mortar joints, giving it highly variable and brittle mechanical properties. In the case of historical structures, complex geometry adds to the modelling complexity. They often include straight or curved members, such as arches (e.g. the Great Portico), vaults, domes and buttresses (Roca et al., 2010). Other difficulties can be presented by limited material data, historical modifications and damage, and long-term effects (Roca et al., 2010). Roca et al. (2010) lists the following desirable features for modelling historical masonry structures: an adequate description of the geometry, morphology and damage, non-linear constitutive equations, the interaction with soil/foundation and adjacent structures, the stages experienced by the structure (in particular, the construction process), and long-term effects, such as creep. The paper by Roca et al. (2010) analyses approaches to modelling historical masonry structures. From classical analytical approaches, like the work by Coulomb and Couplet, who describes the failure mechanism of an arch when enough plastic hinges have developed in the structure (Heyman, 1976), to current finite and discrete element analyses.

D'Altri et al. (2020) provide a detailed overview of the different modelling strategies for the computational analysis of unreinforced masonry structures. In the paper four strategies are classified: block-based models, continuum models, macroelement models and geometry-based models (D'Altri et al., 2020).

Block-based models are built block-by-block with mortar (or dry) joints. These models give a representation of the actual masonry and give the ability to model structural details. Block-based models give a clear representation of the failure modes and detailed insights in the weakest part of the structure. However, due to their high computational demand and complex assembly of the model, these models are mainly suited for smaller scale structures (D'Altri et al., 2020).

In continuum models, masonry is modelled as a continuum deformable body. Prime advantage is that the mesh discretization does not have to follow the heterogeneous configuration of the masonry. Making it more suitable for larger scale structures than the block-based models. Two approaches are given to model the mechanical complexities of masonry: the direct approach, which uses continuum constitutive laws that can approximate the mechanical response of masonry and the homogenization procedure and multi-scale approach, which tries to represent masonry from homogenization processes, typically based on Representative Volume Elements (RVEs) (D'Altri et al., 2020).

Macroelement models (or equivalent frame models) model the masonry structure in equivalent panel-scale structural components. This approach is mainly used in the global seismic response analysis of masonry buildings. Macroelement models are widely used in the seismic analysis of masonry structures, due to their simplified modelling approach and, therefore, limited computational effort. However assumed in these models is that local failure modes, mainly associated with the out-of-plane response, are prevented (D'Altri et al., 2020).

In geometry-based models, typically the structural equilibrium and/or collapse of the masonry structure, modelled as a rigid body, is investigated through limit analysis-based solutions, based on either static or kinematic theorems. The use of this approach is limited, but it could give useful insights in the equilibrium states and, therefore, the safety of masonry structures, as well as predict the collapse mechanism in complex masonry structures (D'Altri et al., 2020).

The four different approaches have their uses, because of their specific strengths. However, all masonry

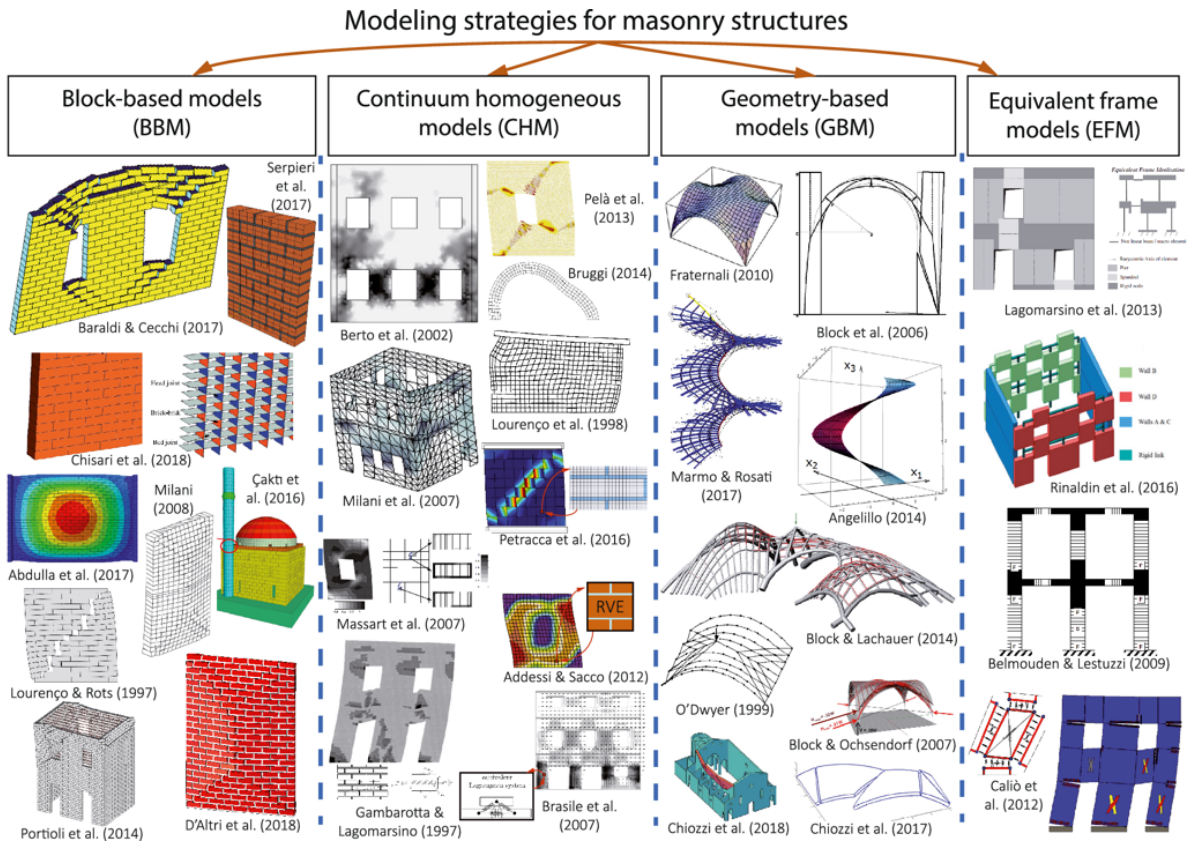

Figure 2.2: Modelling strategies for masonry structures (D'Altri et al., 2020)

structures encounter the same complexities. Roca et al. (2010) concludes that, despite advancements in modelling, analysing historical masonry structures is a challenging task. Encountered difficulties are complex geometry, materials, morphology and present condition. The modelling of the mechanical behaviour of masonry is in particular demanding, due to its brittle nature and composite character (Roca et al., 2010).

3

Research Approach and Model Development

This chapter elaborates on the approach taken in the research of the structural seismic response of the Great Portico. It will go over the specifications of the finite element models used to perform the pushover analyses of the structure. Secondly, the procedure for defining the material properties is outlined.

3.1. Model Specifications

The seismic vulnerability assessment of the Great Portico at Medina Azahara was performed using 3D finite element models. This section outlines the general specifications and considerations applied in the modelling process.

3.1.1. Overview of the Modelling Approach

An iterative approach was taken in the study of the seismic response of the Great Portico. This approach enabled a sensitivity analysis of specific structural aspects of the Great Portico. Initially defining a single-material model and expanding it to a model including three different building materials and interface elements. Notably, during the initial iterations of the modelling process, the top part of the right-most arch was included in the model, despite its absence in the current state of the structure. As seen in Figure 3.2a, the top section is no longer present in reality; however, it was incorporated in early models to evaluate its influence on the seismic response and for sensitivity analyses conducted in this research, which will be discussed in Chapter 4. A total of 4 models were created. The materials mentioned in the description of the models below are the materials mentioned in Section 1.1 and described in Section 3.2. In the models with all three materials, the materials were modelled according to the configuration specified in Section 3.2. The models are listed below:

1. Single-material-model: A single-material model, consisting of stone masonry, including the top of right most arch.
2. Tri-material-model: A model including the three defined materials, consisting of limestone masonry, brick masonry and limestone blocks, including the top of the right most arch.
3. Interface-model: A model including the three defined materials, consisting of limestone masonry, brick masonry and limestone blocks, including interface elements, including the top of the right most arch.
4. Final-model: A model including the three defined materials, consisting of limestone masonry, brick masonry and limestone blocks, including the interface elements, excluding the top of the right most arch.

For the interface-model two types of interface elements were adapted, explained in Subsection 3.2.5. Figure 3.1 shows a visual representation of the described iterative approach. The different colours present in the second, third and fourth model indicate the different materials in these models. The bright blue and red colouring between the arch-segments in the interface- and the final-model represent the interface elements

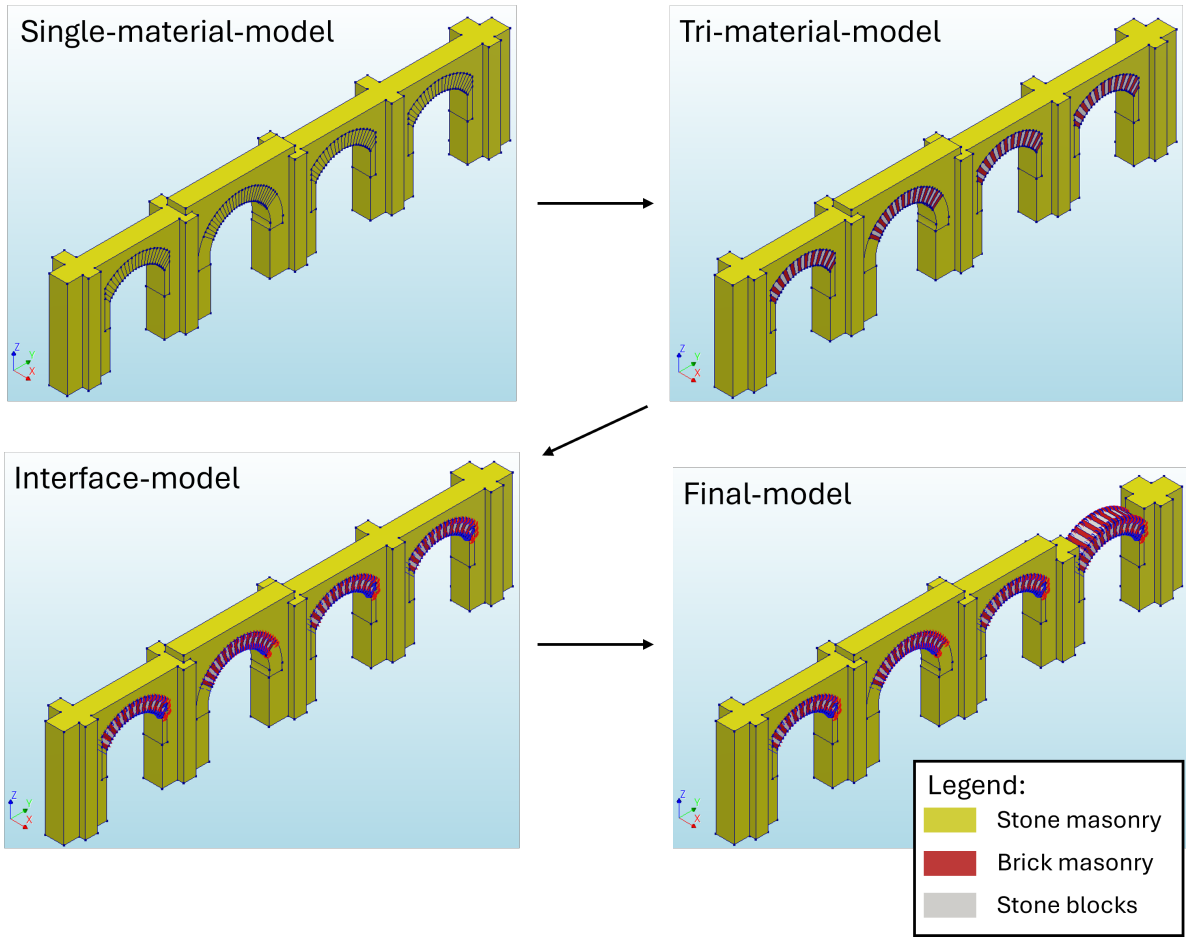

Figure 3.1: Visual overview of the iterative modelling approach

present. The exclusion of the top of the right most arch in the fourth model only removed a part of the structure consisting of stone masonry. Taking a look at Figure 1.1, this corresponds with the current state of the Great Portico.

3.1.2. Model Geometry

The geometric configuration of the standing arch-structure is estimated based on the drawings from Planimetría de Madīnat al-Zahrā' (Almagro Gorbea, 2011) shown in Figure 3.2. There are no current in-situ measurements on the geometry of the structure at the time of constructing the models. These drawings provide a moderately detailed depiction of the structure. While the exact measurements are approximated due to the level of detail in the source material, they are sufficiently accurate to reflect the overall geometry and proportions of the structure. The model dimensions can be found in Figure 3.3.

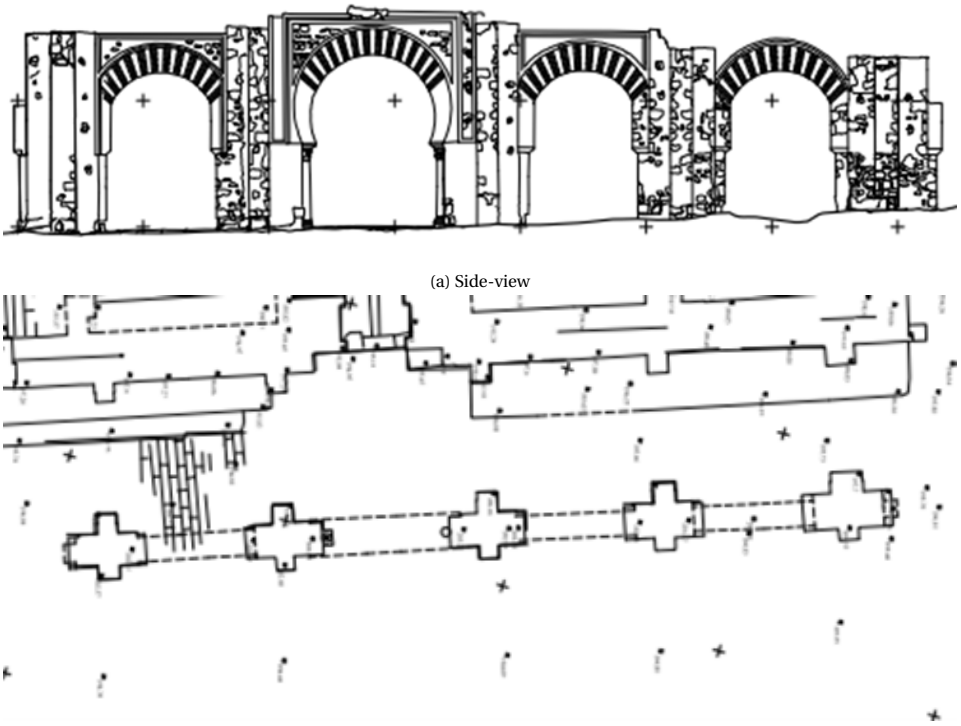

(a) Side-view

(b) Top-view

Figure 3.2: Drawings of the arch-structure in Medina Azahara, Córdoba (Almagro Gorbea, 2011)

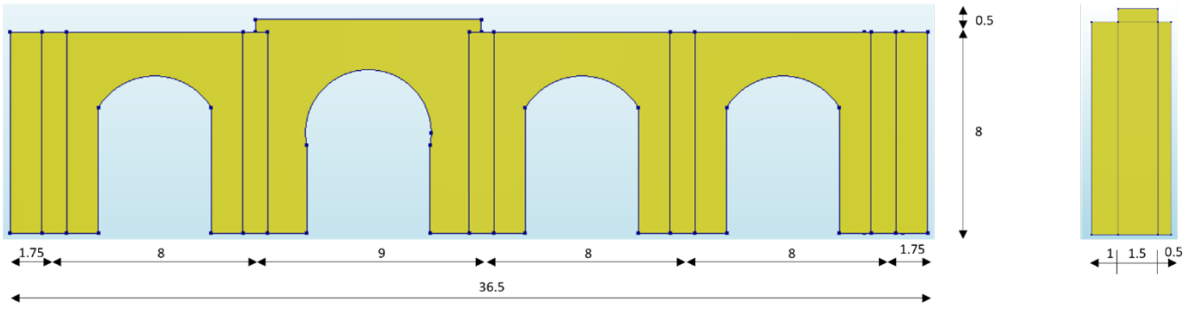

Figure 3.3: Estimated dimensions of the arch-structure in Medina Azahara (in meters)

3.1.3. Finite Element Mesh

The models are constructed in a 3-dimensional space to capture the spatial relationships and physical dimensions of the structure. Figure 3.4 shows the 3D model for the first three models and Figure 3.5 for the final-model. Although both two-dimensional and three-dimensional modelling approaches were considered (see Appendix A), the latter was chosen as it would have a more accurate representation of the seismic response of the structure, particularly with regard to out-of-plane behaviour and possible complex failure modes.

An average mesh size of 0.3 meters is applied for all the models. This choice ensures adequate resolution for capturing the significant features of the structure and the stress concentrations at critical locations, while also maintaining computational efficiency. All models were constructed in segments, as shown in Figure 3.4, to facilitate the implementation of different materials in subsequent models while maintaining a consistent mesh across all models. Although a uniform mesh size was used, smaller elements were generated due to curvature at certain points in the structure to better accommodate the local geometry, ensuring that the structural response was accurately represented throughout.

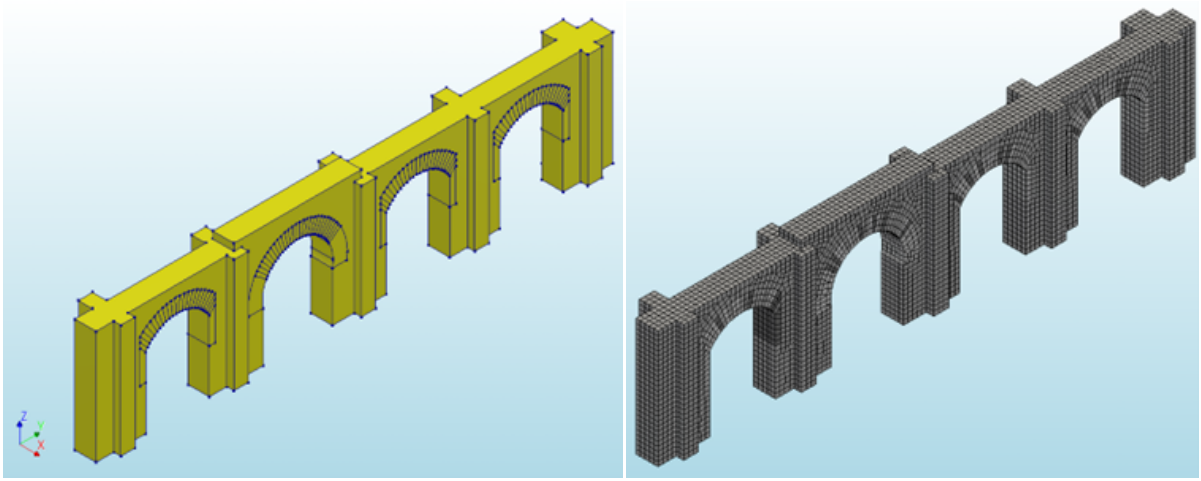

(a) 3D model geometry (b) 3D model mesh

Figure 3.4: 3D finite element model including the top of the right-most arch

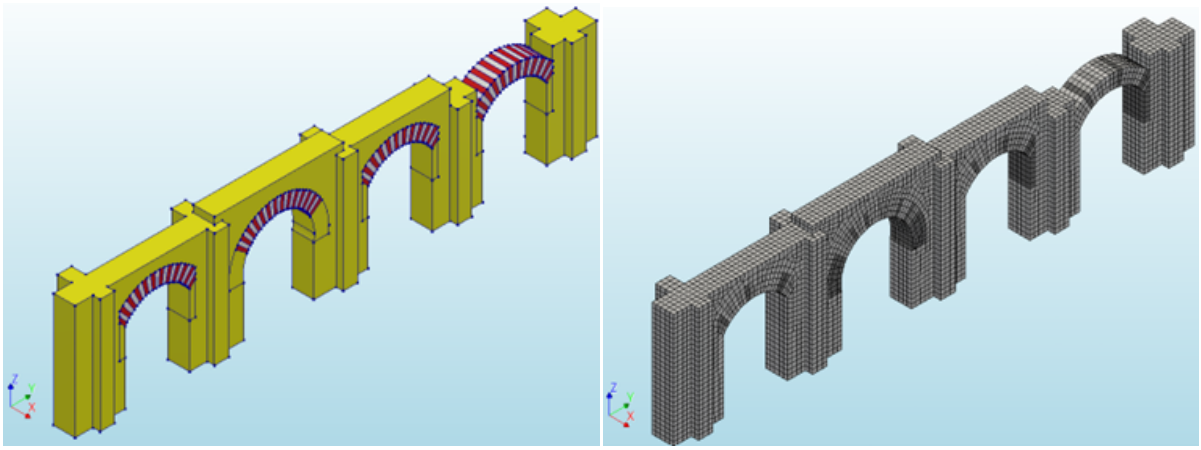

(a) Final-model: 3D geometry (b) Final-model: 3D mesh

Figure 3.5: 3D finite element model of the Great Portico

The structural analysis utilizes solid elements, which are appropriate for capturing the behaviour of the structure and the stress and strain distribution of the materials. The mesh consists primarily of eight-node isoparametric solid brick elements, defined as HX24L in the DIANA FEA Manual (DIANA FEA B.V., 2025). To accommodate the curved edges in the structural model, the mesh consists besides the HX24L-elements of three more solid elements: TE12L (a four-node, three-side isoparametric solid tetrahedron element), PY15L (a five-node isoparametric solid pyramid element) and TP18L (a six-node isoparametric solid wedge element). All elements use linear interpolation (DIANA FEA B.V., 2025), providing a balance between computational efficiency and the capacity to represent force and displacement variations within the structure accurately. The elements are shown in figure Figure 3.6.

Additionally, in later models structural interface elements were incorporated at specific locations, such as mortar joints, to capture potential weaknesses in the structure, and simulate joints with deteriorated mortar. The specific element is a four+four-node linear quadrilateral interface element, named Q24IF (see Figure 3.7). These interface elements are compatible with the structural solid elements.

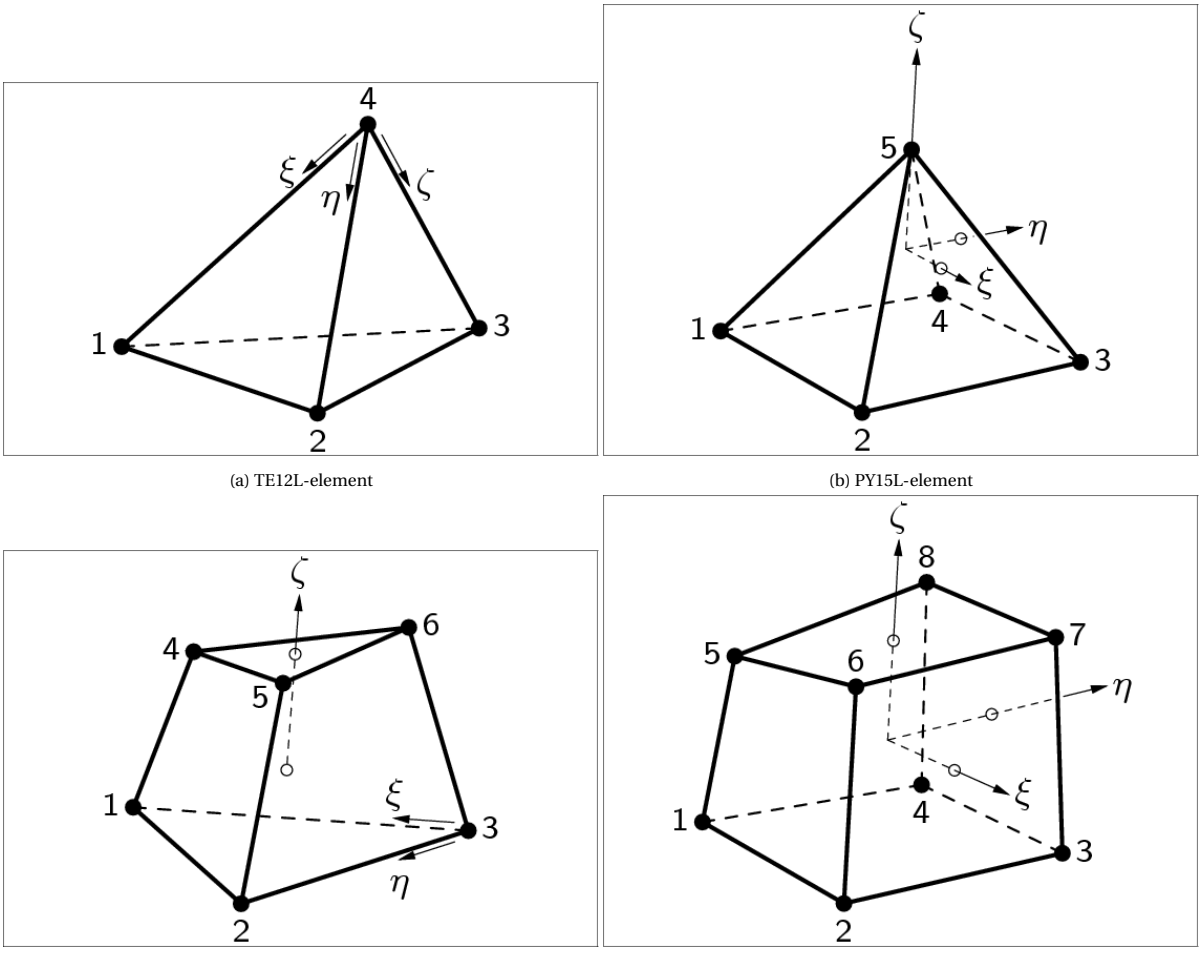

(a) TE12L-element

(b) PY15L-element

(c) TP18L-element

(d) HX24L-element

Figure 3.6: Stuctural solid elements (DIANA FEA B.V., 2025)

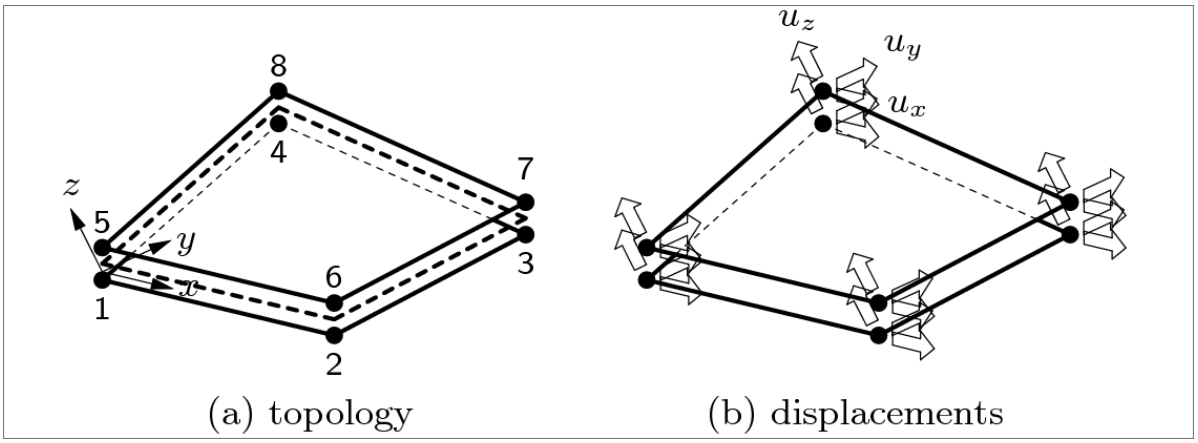

Figure 3.7: Structural interface element: Q24IF (DIANA FEA B.V., 2025)

3.1.4. Boundary and Loading conditions

The structure is free standing, i.e. has no interaction with another structure. The only boundary conditions are defined at the base of each column. The bases are assumed to be fixed to its foundation. In Figure 3.2a a slight inclination in the ground profile can be seen. This inclination is neglected in the model, resulting in a flat base. It was assumed that the neglect of the slight variation in ground level would have minimal impact on the global seismic response of the structure, thereby justifying its exclusion to reduce modelling complexity without significantly compromising result accuracy.

The structure is subjected to first its self weight and then a global modal pushover load in an iterative-incremental method. A structural non-linear analysis was applied. The self weight of the structure was applied in a single step. The modal pushover load was applied in 150 steps of 0.005. The modal pushover loads the structure in a monotonically increasing static force profile proportional to a chosen single mode shape (DIANA FEA B.V., 2025). The relevant eigenmode(s) for the pushover analyses resulted from an eigenmode analysis, explained in Section 4.1. The eigenmode analysis also established the relevance of both an in-plane and out-of-plane pushover analysis.

3.2. Material Properties

The Great Portico's structural model incorporates three distinct materials: limestone masonry, brick masonry, and limestone blocks. The mechanical properties are considered uniform throughout the structure. Due to uncertainties in the exact mechanical values, a conservative approach in deriving these values was chosen. The mechanical values of the materials are given in Table 3.1. The material properties are based on technical codes and relevant research, outlined below.

3.2.1. Constitutive Material Models

The constitutive material model, defined in DIANA (DIANA FEA B.V., 2025), used for the limestone and brick masonry is: total strain based crack model and for the limestone blocks is: linear elastic isotropic. The stress-strain relation in isotropic elasticity can be described by the following equation:

$$\boldsymbol{\sigma}_{xyz} = \frac{E}{(1+\nu)(1-2\nu)} \begin{bmatrix} 1-\nu & \nu & \nu \\ \nu & 1-\nu & \nu \\ \nu & \nu & 1-\nu \end{bmatrix} \boldsymbol{\epsilon}_{xyz} \tag{3.1}$$

The total strain based crack model follows a smeared approach for the fracture energy (DIANA FEA B.V., 2025). The theory used for the three-dimensional application of this approach is proposed by Selby and Vecchio (1993). In this constitutive model the stress is described as a function of the strain. This study uses the rotating-crack-model approach to describe the stress-strain relations, where the relations are evaluated in the principal directions of the strain vector (DIANA FEA B.V., 2025). The stress-strain relation is given in Equation 3.2. In which nst stands for the defined crack coordinate system.

$$\overset{t+\Delta t}{i+1}\boldsymbol{\sigma}_{nst} = \boldsymbol{\sigma}\left(\overset{t+\Delta t}{i+1}\boldsymbol{\epsilon}_{nst}\right) \tag{3.2}$$

An exponential curve is applied for the tensile softening. The curve is given in Figure 3.8a. Important parameters are the tensile strength, f_t, the fracture energy, G_c, and the equivalent length, h_{eq}. The equivalent length, or crack bandwidth, is determined using Rots' element based method (Rots, 1988). In this method the equivalent length is related to the volume of the element. There is specified to be no residual tensile strength and a no reduction model is applied for the Poisson's ratio-reduction.

The compressive behaviour is described by a parabolic softening curve (see Figure 3.8b), formulated by Feenstra (1993). Key parameters are the compressive strength, f_c, the compressive fracture energy, G_c, and the characteristic element lenth, h. Again no residual strength is specified. There is no increase in the compressive strength due to lateral stress confinement and reduction in the strength due to lateral cracking.

3.2.2. Limestone Masonry

The majority of the structure consists of stone masonry, with limestone as the primary material. Figure 3.9 illustrates the configuration of the materials in the numerical models. The real-world configuration of the materials has been replicated as closely as possible without overcomplicating the construction of the numerical models. The mechanical properties of the stone masonry, aside from the fracture energies, are adopted from the study on the Mosque-Cathedral of Córdoba by Requena García de la Cruz et al. (2023).

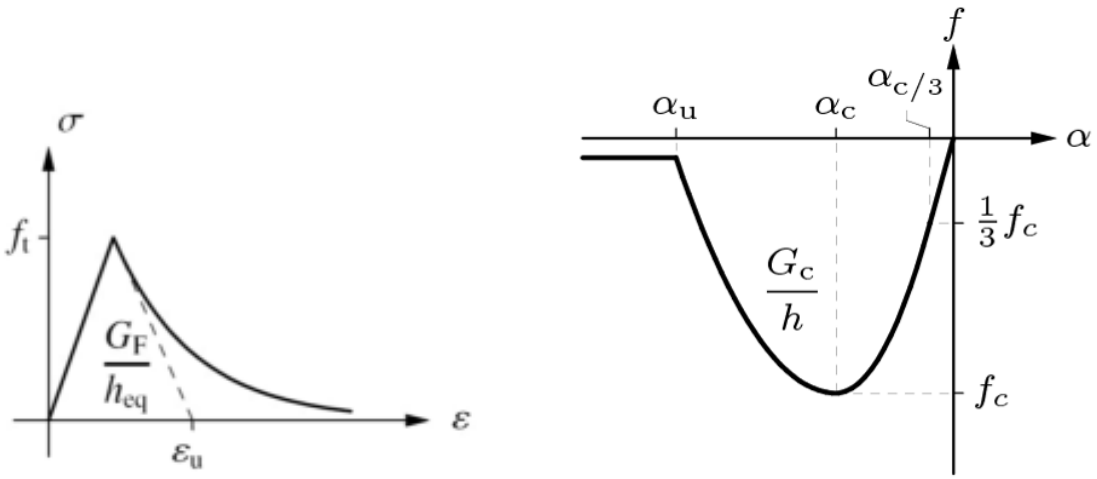

(a) Exponential tensile softening curve (Hendriks and Roosen, 2022)

(b) Parabolic compressive softening curve (DIANA FEA B.V., 2025)

Figure 3.8: Softening curves

Since the original structure of the Mosque-Cathedral was built in the same historical time-period as the city of Medina Azahara, it is assumed that similar materials and construction techniques were employed.

The compressive fracture energy for the stone masonry was derived according to the guidelines set out in the Model Code 90 (CEB and FIB, 1993). While these formulas were originally developed for concrete, it is assumed that Equation 3.3 provides a reliable estimation of the brittle failure in compression, making it appropriate for deriving the compressive fracture energy of the limestone masonry in this structure.

$$G_C = 15 + 0.43 f_c - 0.0036 f_c^2 \tag{3.3}$$

For the tensile fracture energy, the values were derived using Equation 3.4 taken from Structural Masonry Analysis: Recent Developments and Prospects by Lourenço (2008), in which they used the equation for calculating the fracture energy of concrete from Model Code 90 (CEB and FIB, 1993) and the assumption that the relation between the tensile and compressive strength of limestone masonry is 5% (Lourenço et al., 2004).

$$G_F = 0.025(2 f_t)^{0.7} \tag{3.4}$$

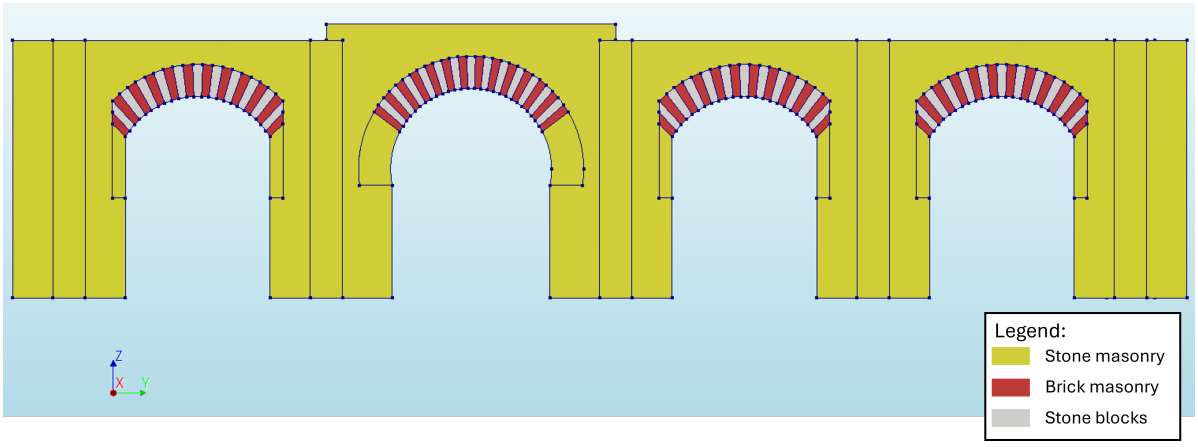

Figure 3.9: Material configuration in the finite element models

Mechanical property	Symbol	Unit	Stone masonry	Brick masonry	Limestone
Compressive strength	f_c	N/mm^2	2.78	3.57	-
Modulus of elasticity	E	N/mm^2	1800	2000	3772.23
Density	ρ	kg/m^3	1800	1800	1644.22
Poisson's ratio	ν	-	0.3	0.2	0.3
Tensile strength	f_t	N/mm^2	0.1	0.21	-
Fracture energy compression	G_C	N/mm	16.17	12.00	-
Fracture energy tension	G_F	N/mm	0.0081	0.0060	-

Table 3.1: Mechanical properties of the materials defined in the structural seismic analysis

3.2.3. Brick Masonry

In addition to stone masonry, the arches feature a combination of brick masonry and limestone blocks. The mechanical properties of the brick masonry, excluding the fracture energies, are also sourced from the study by Requena García de la Cruz et al. (2023).

For the fracture energies in both tension and compression, the model uses values from NPR-9998 specifically from Table F.2 (NEN, 2020). The code provides mean values of material properties for Dutch clay brickwork masonry. In light of the poor quality of the brick masonry in the structure, a 40% reduction was applied to the standard values for fracture energies to reflect this degradation.

3.2.4. Limestone

The limestone blocks used in the arches are modelled as having linear elastic properties, as these blocks are assumed to be stronger and more rigid than the surrounding brick masonry. The linear elastic assumption is a simplification made under the stated premise that cracks and failure will occur in the surrounding brick masonry before these will occur in the limestone blocks.

The material property values for the limestone blocks were taken from an experimental study conducted by a research team from the University of Sevilla, which involved uniaxial compression tests on prismatic samples from three different ashlars (Zapico-Blanco et al., 2025). For conservative modelling, the lowest set of values from this study was applied to the numerical analysis.

3.2.5. Structural interfaces

In last two models interface elements were implemented. These interface elements were modelled between the brick-masonry and stone block segments, therefore simulate the joints between different structural materials. Two types of elements were considered: discrete cracking elements and combined cracking-shearing-crushing (CCSC) elements. The CCSC-elements were considered as its constitutive model describes the mechanisms in masonry joints more accurately.

The constitutive law for discrete cracking is based on a total deformation theory, which expresses the tractions as a function of the total relative displacements, the crack width and the crack slip (DIANA FEA B.V., 2025). The constitutive model for the CCSC-elements is formulated by Lourenço and Rots (1997) and enhanced by Van Zijl (2000). They formulated a two dimensional plane stress interface model based on multi-surface plasticity, comprising a Coulomb friction model combined with a tension cutoff and an elliptical compression cap (DIANA FEA B.V., 2025).

The two sets of properties are given in Table 3.2. Both types consider a low tensile strength and a dummy stiffness, to simulate hard contact between these segments. This is a reasonable assumption, based on close-up pictures of the segments. For the discrete cracking interface elements, brittle tension softening and zero shear traction are assumed to represent limited tensile strength and no shear stiffness after cracking. The combined cracking-shearing-crushing elements consider low cohesion and a compressive strength equal to the compressive strength of the brick masonry. The values of the other mechanical properties are general values taken from literature.

Mechanical Property	Unit	Discrete cracking	CCSC
Normal stiffness modulus-z	N/mm^3	1000	1000
Shear stiffness modulus-x	N/mm^3	500	500
Shear stiffness modulus-y	N/mm^3	500	500
Cracking			
Tensile strength	N/mm^2	0.05	0.05
Fracture energy	N/mm	-	0.0015
Mode-I tension softening criterion	-	Brittle	-
Mode-II shear criterion for crack development	-	Zero shear traction	-
Shearing			
Cohesion	N/mm^2	-	0.1
Friction angle	rad	-	0.4
Dilatancy angle	rad	-	0
Mode-II fracture energy			
Parameter a	mm	-	0
Parameter b	N/mm	-	0.01
Crushing			
Compressive strength	N/mm^2	-	3.57
Factor Cs	-	-	0.01
Compressive inelastic law			
Compressive fracture energy	N/mm	-	12
Equivalent plastic relative displacement	mm	-	0.007

Table 3.2: Mechanical properties of the two types of interface elements

Figure 3.10: Close-up picture of the Great Portico (picture by Luis Manuel Giraldez)

4

Results

This chapter will show the results of the structural analysis of the Great Portico. Firstly the results of the eigenmode analysis of the all four models will be shown. Secondly the results from the pushover analyses will be presented and illustrated. This section includes the results per model, a comparison between the models and a brief sensitivity analysis on the tensile strength of the stone-masonry material and its stiffness.

4.1. Eigenmode Analysis

These eigenmode analyses were performed to determine the critical modes of the Great Portico structure to use in the pushover analysis. The critical modes have a much higher mass participation factor compared to the other modes. The eigenmode analysis of the first model determined if both IP-pushover and OOP-pushover analyses were carried out and which modes were relevant for both directions. The subsequent eigenmode analysis were performed to verify the assumptions made based on the first model also applied for each successive refined model.

The table below lists the 5 modes with the highest participation factor from the eigenmode analysis of the first model. The general participation factors are given in absolute values. P. F. Tx and P. F. Ty are the participation factors for translation in the x-direction, out-of-plane direction, and the y-direction, in-plane direction, respectively. The coordinate system with respect to the structure is shown in Figure 9, as well as all subsequent figures showing the model of the structure.

Table 4.2 lists the 5 modes with the highest participation factor from the eigenmode analysis of the second and third model. The incorporation of the interfaces only slightly changes the stiffness and does not change the weight of the structure, key factors for determining the eigenmodes, therefore the second and third model yield the same results. The results are very similar to those of the single-material-model. One could conclude from the slightly higher eigenfrequencies that the general stiffness of the structure is slightly higher in the second and third model. Looking at the chosen material properties this is expected, considering the stiffness for both the brick-masonry and stone blocks is higher.

The results for the fourth model are given in Table 4.3. The slightly higher frequencies could be explained by a similar stiffness, but lower weight of the structure. One important thing should be noted: the relevant mode for the in-plane dynamic behaviour for the fourth model is the 5th mode instead of the 6th mode.

Mode	**Freq**(Hz)	**Participation Factor**	**P. F. Tx**	**P. F. Ty**
1	4.17	18.45	18.58	-0.01
2	4.86	4.27	4.07	0.25
3	5.59	6.95	6.99	-0.01
5	8.79	2.60	1.41	1.18
6	8.87	21.60	-0.11	21.69

Table 4.1: Eigenmode analysis of the single-material-model

Mode	Freq(Hz)	Participation Factor	P. F. Tx	P. F. Ty
1	4.21	18.58	18.71	-0.01
2	4.92	4.14	3.92	0.26
3	5.71	6.49	6.53	-0.01
5	9.14	3.11	1.29	1.82
6	9.23	21.58	-0.14	21.71

Table 4.2: Eigenmode analysis of the tri-material-model and the interface-model

Mode	Freq(Hz)	Participation Factor	P. F. Tx	P. F. Ty
1	4.24	17.00	17.13	-0.02
3	6.54	8.39	8.46	-0.02
4	7.70	4.22	3.87	0.37
5	9.35	20.52	-0.22	20.70
6	9.49	3.96	1.27	2.67

Table 4.3: Eigenmode analysis of the final-model

The following observations could be made from the results of the eigenmode analyses: of the five eigenmodes with the highest participation factor only one has an in-plane mode shape and the participation factor of the leading in-plane mode is only slightly higher than the participation factor of the leading out-of-plane mode. Based on these observations both the in-plane and out-of-plane responses were considered in the seismic analyses. For the in-plane dynamic behaviour only the one mode was considered. For the out-of-plane behaviour, analysis was restricted to eigenmode 1, as its participation factor is at least twice that of the subsequent mode, thereby providing a sufficiently accurate representation of the response without the inclusion of additional modes and complicating the analysis. Figures 9 and 10 show the mode shape of the considered eigenmode for in-plane and out-of-plane dynamic behaviour of all four models of the Great Portico, respectively.

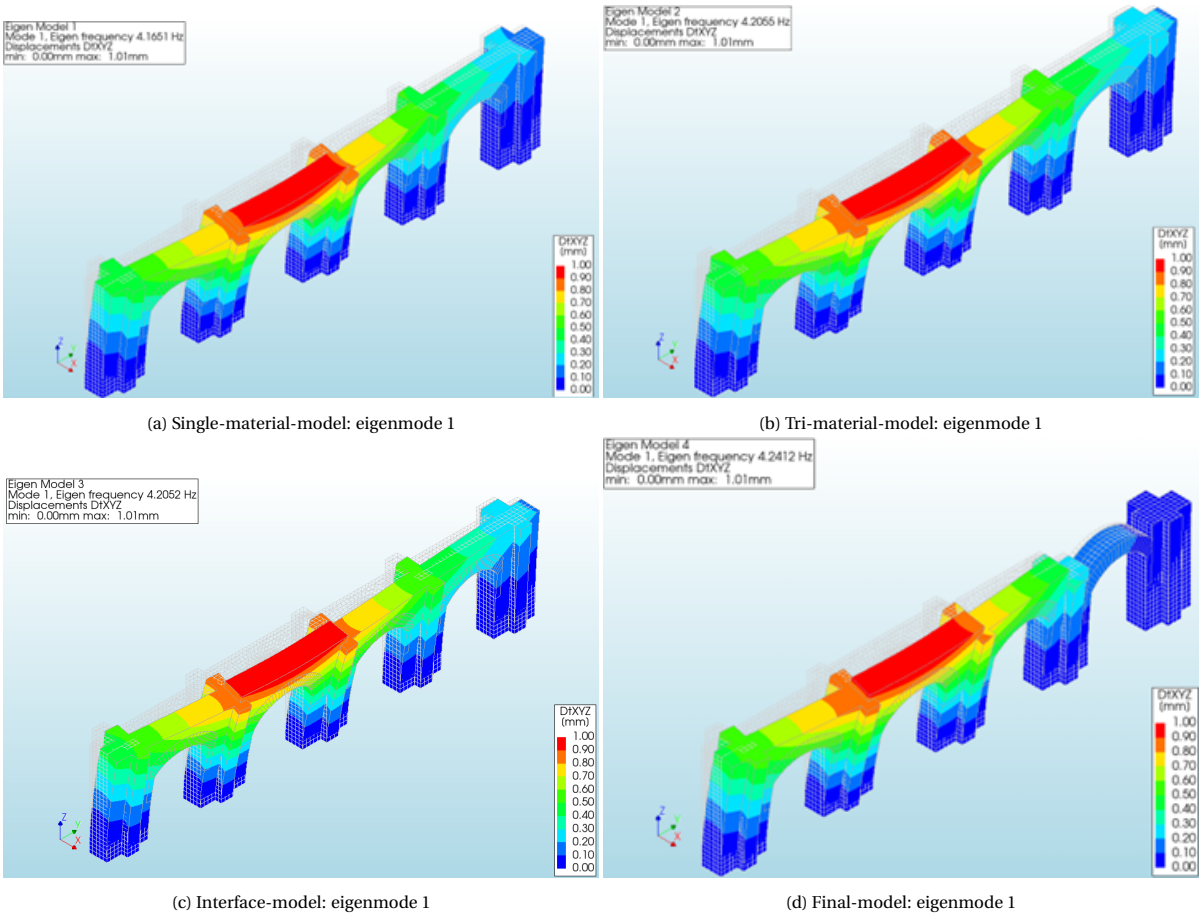

(a) Single-material-model: eigenmode 1

(b) Tri-material-model: eigenmode 1

(c) Interface-model: eigenmode 1

(d) Final-model: eigenmode 1

Figure 4.1: Eigenmode analysis: out-of-plane mode (Deformation scaling factor: 2000)

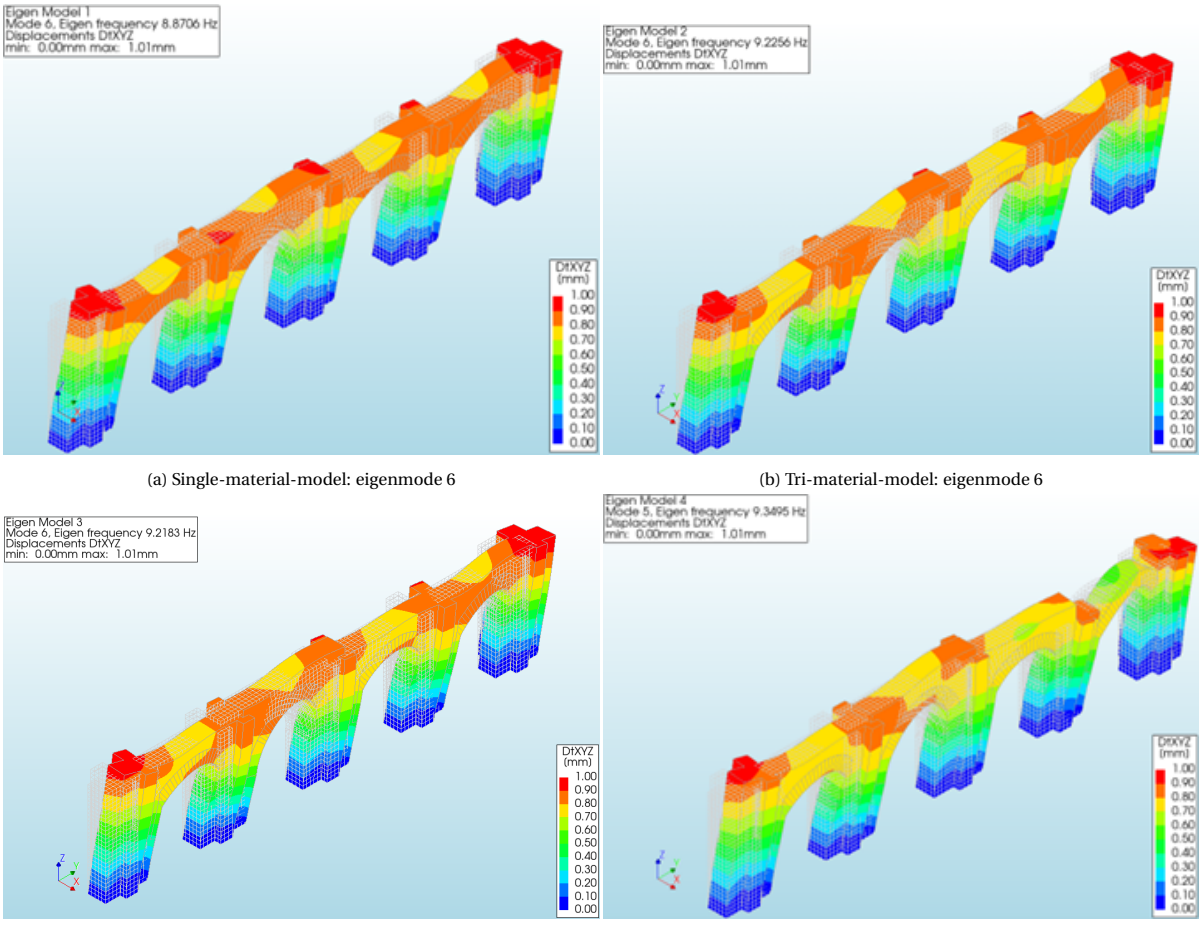

(a) Single-material-model: eigenmode 6

(b) Tri-material-model: eigenmode 6

(c) Interface-model: eigenmode 6

(d) Final-model: eigenmode 5

Figure 4.2: Eigenmode analysis: in-plane mode (Deformation scaling factor: 2000)

4.2. Nonlinear Pushover Analysis

4.2.1. Single-material-model

The graph below gives the comparison between the in-plane (IP) and out-of-plane (OOP) pushover analysis for the normalized base shear over the maximum displacement in the structure. For the IP-pushover analysis the maximum displacement can be found at the top of the far right column and for the OOP-pushover analysis this place is at the top at the middle of the second arch from the left. The graph is shown up to a displacement of 15 mm. After this point the analysis gets less reliable as the analysis does not converge every step before the set limit of 100 iterations, due to the high displacements and cracking in the structure. Much smaller increases in the pushover force would be required to analyse the behaviour further. This would increase the running time of the analysis significantly. Therefore analysing the response for higher displacements was deemed less important considering the scope of the research.

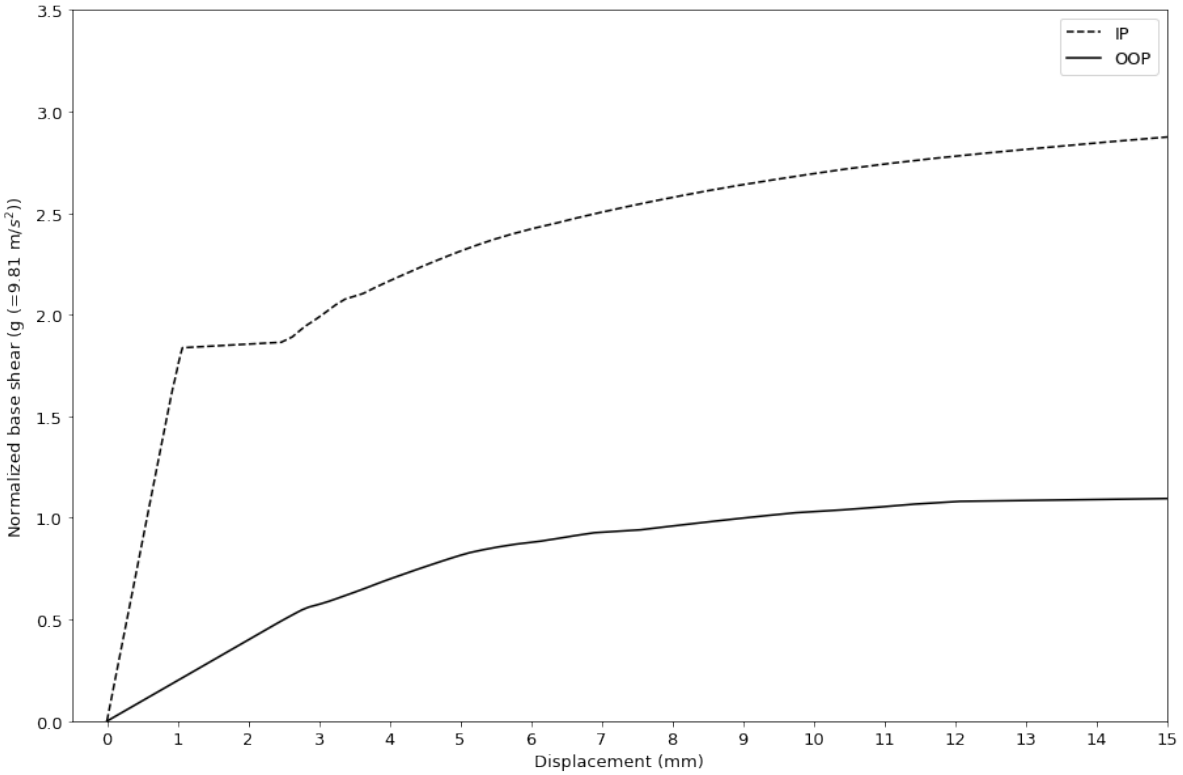

Figure 4.3: Single-material-model: pushover analysis

Based on the graph, the following observations can be made about the response:

- In both analyses an initial elastic response is visible, but the IP-response exhibits a much higher initial stiffness.
- The OOP-response gradually flattens after the initial response suggesting a stable response with no sudden brittle failure up to end of the analysis.
- The IP-response has a sudden rapid decrease in stiffness. In the figures of the crack development (Figure 4.7) can be seen that this is caused by the formation of a large crack in the stone-masonry in the top of the right-most arch next to the far column.
- The IP-response shows a higher load bearing capacity due to a higher in-plane stiffness of the overall structure, but has potential of sudden brittle failure at the peak elastic response.

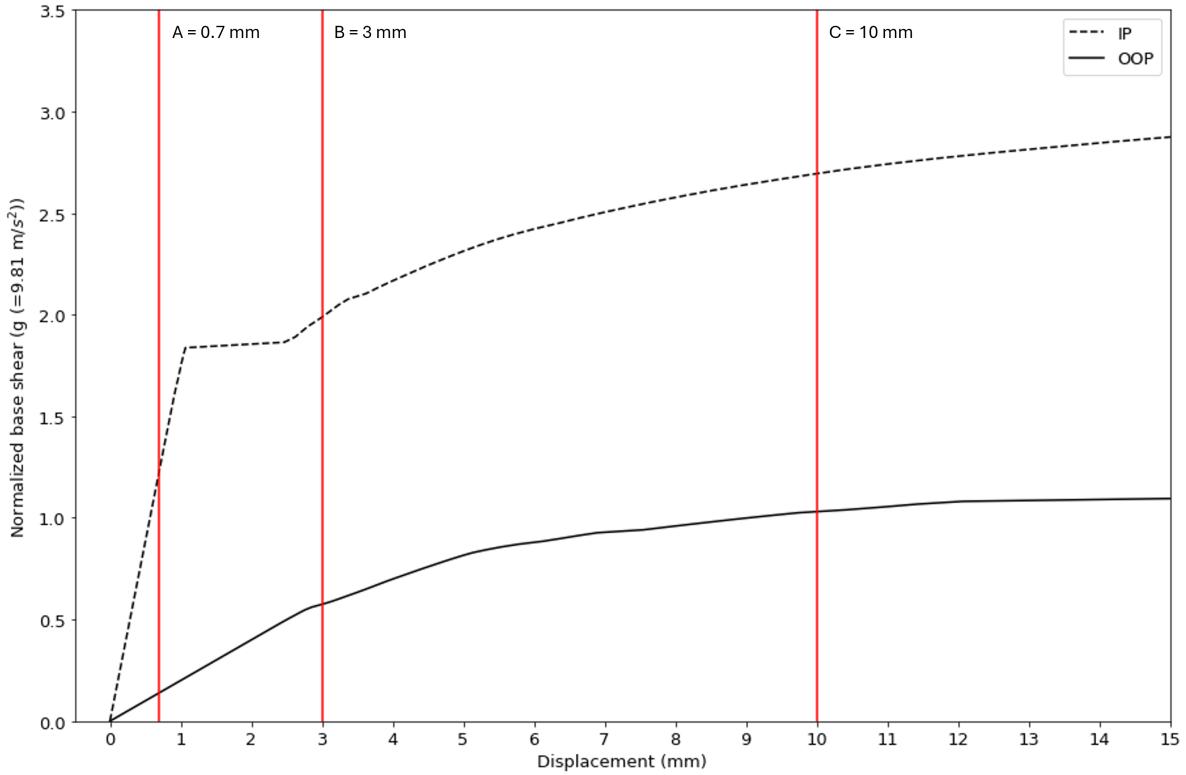

Figure 4.4: Single-material-model: displacement levels

Figure 4.5 till Figure 4.10 show the crack development and the displacements in the structure for both the in-plane and out-of-plane pushover analysis at certain displacement levels, which are indicated in the graph (see Figure 4.4). These levels are chosen at elastic behaviour, post-elastic and at point of significant cracking in the structure. These figures show the failure mechanism for both responses. The failure mechanism of the IP-response shows the structure falling over in plane, mainly resulting in high stresses and cracking in the top of the 4th arch and the bottom of the far right column. The OOP-response shows the second arch from the left toppling over, resulting in the highest stresses and cracking in the columns, especially the two columns of the second arch.

In-plane pushover analysis:

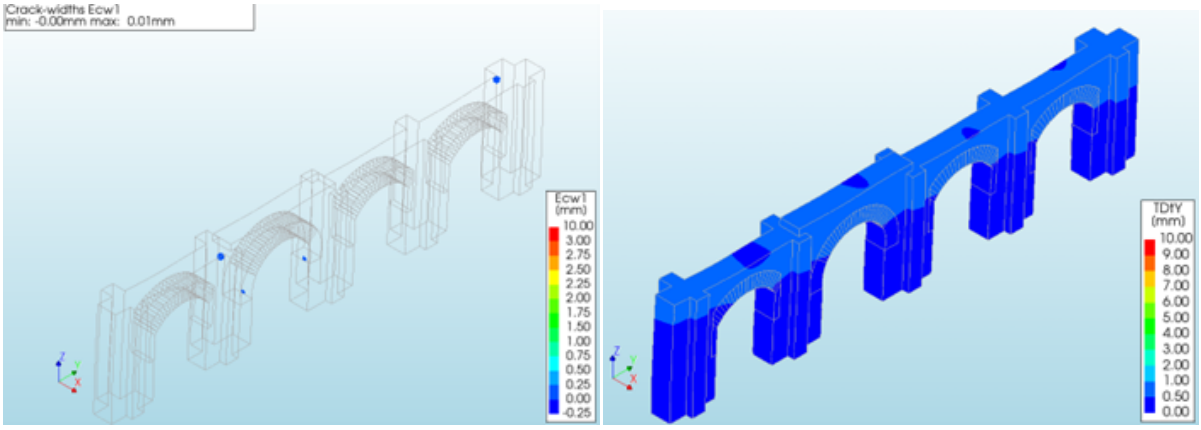

(a) Crack pattern (b) Displacements

Figure 4.5: IP-analysis: displacement level A (Deformation scaling factor: 500)

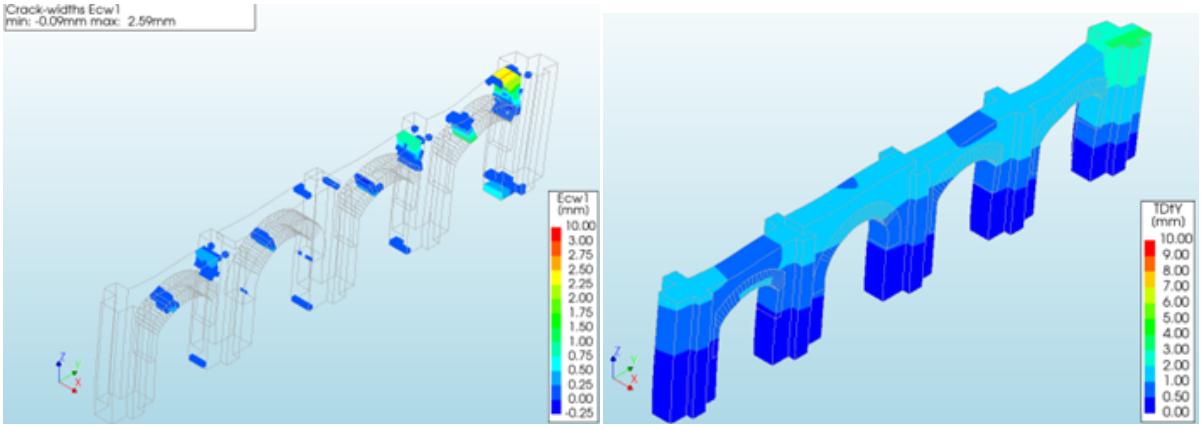

(a) Crack pattern (b) Displacements

Figure 4.6: IP-analysis: displacement level B (Deformation scaling factor: 500)

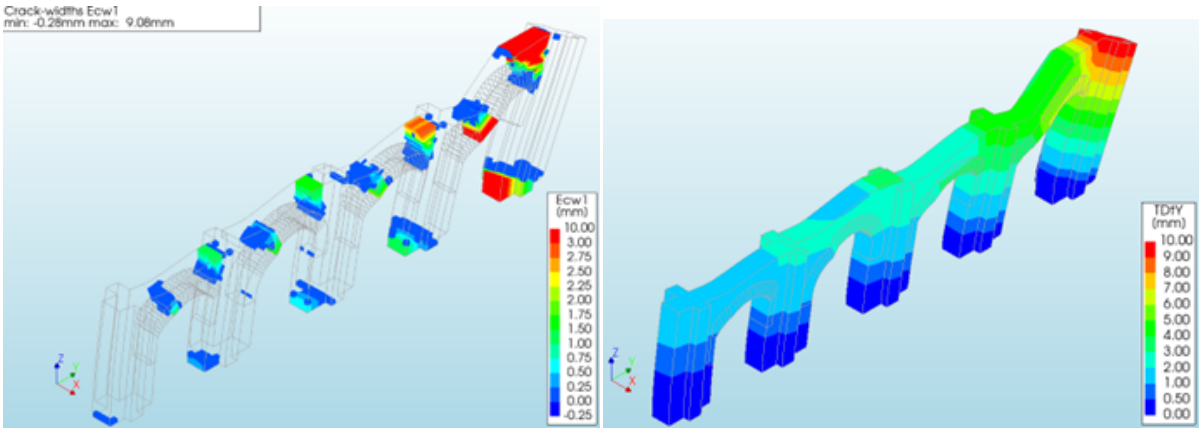

(a) Crack pattern (b) Displacements

Figure 4.7: IP-analysis: displacement level C (Deformation scaling factor: 500)

Out-of-plane pushover analysis:

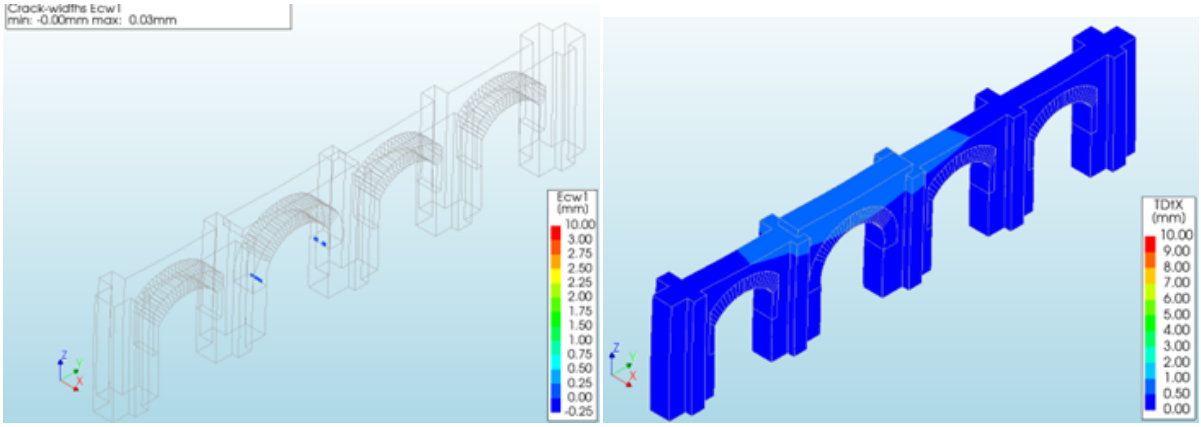

(a) Crack pattern (b) Displacements

Figure 4.8: OOP-analysis: displacement level A (Deformation scaling factor: 500)

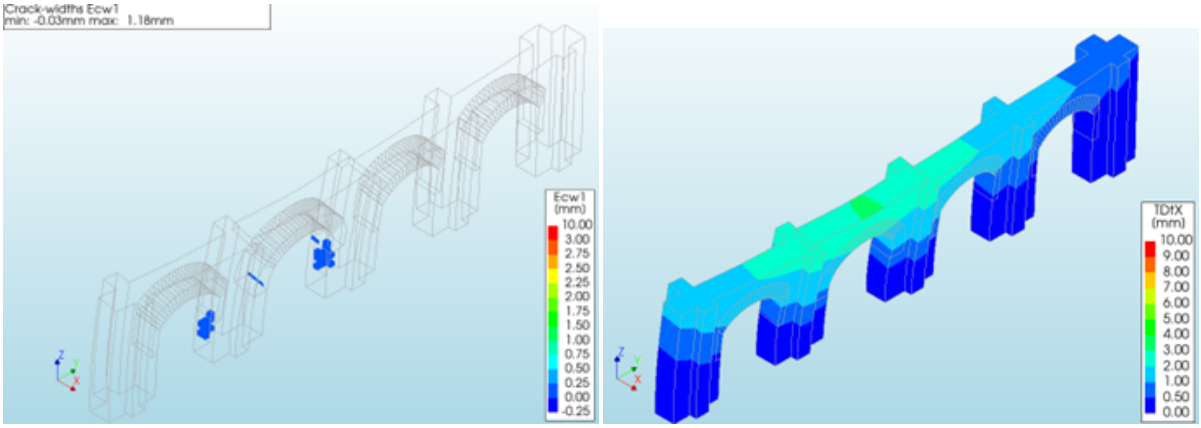

(a) Crack pattern (b) Displacements

Figure 4.9: OOP-analysis: displacement level B (Deformation scaling factor: 500)

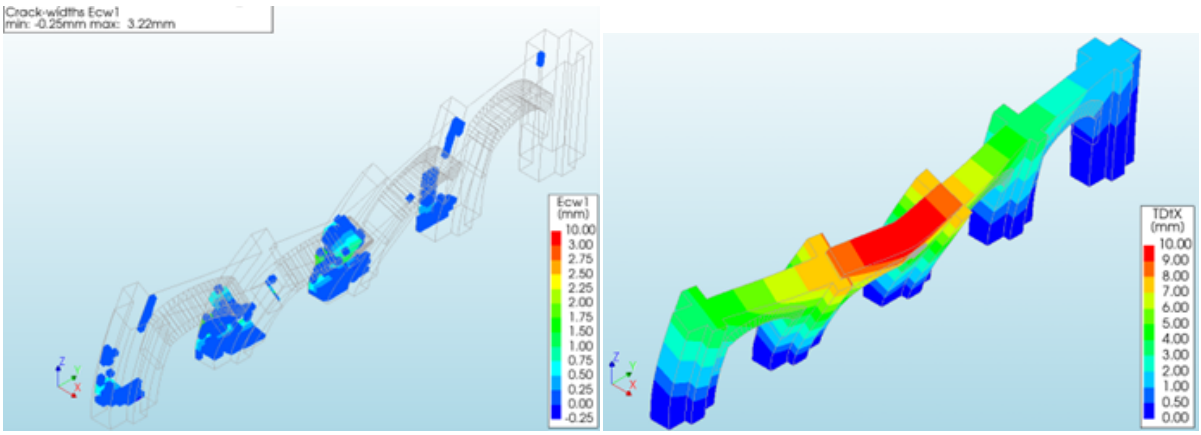

(a) Crack pattern (b) Displacements

Figure 4.10: OOP-analysis: displacement level C (Deformation scaling factor: 500)

4.2.2. Single-material-model: Sensitivity Analysis

An analysis was performed to analyse the sensitivity of two material properties. The properties investigated were the tensile strength and the stiffness of the stone masonry. The sensitivity analysis of the tensile strength was motivated by the results from the prior performed pushover analysis, which indicated that failure was governed by the tensile strength. The stiffness of the masonry was selected to analyse its effect on the failure mechanism of both the IP- and OOP-responses. In both cases the value was halved from the values listed in Table 3.1, giving a tensile strength of 0.05 N/mm^2 and a stiffness of 900 N/mm^2. The sensitivity of a single mechanical property was analysed at a time.

Figure 4.12 shows the response for the Out-of-plane response. Lowering the tensile strength gives only a slight decrease in load bearing capacity, while lowering the stiffness has quite a significant impact. The failure mechanisms do not change. It still fails in tension in the columns of the second arch.

For the in-plane response a similar observation can be made: lowering the stiffness decreases the capacity, lowering the tensile strength does not. The failure mechanisms do not drastically change. Notably, in the case of the lowered tensile strength, cracks start to form at a lower base shear level. Due to the residual strength in the structure the overall capacity at higher forces is higher.

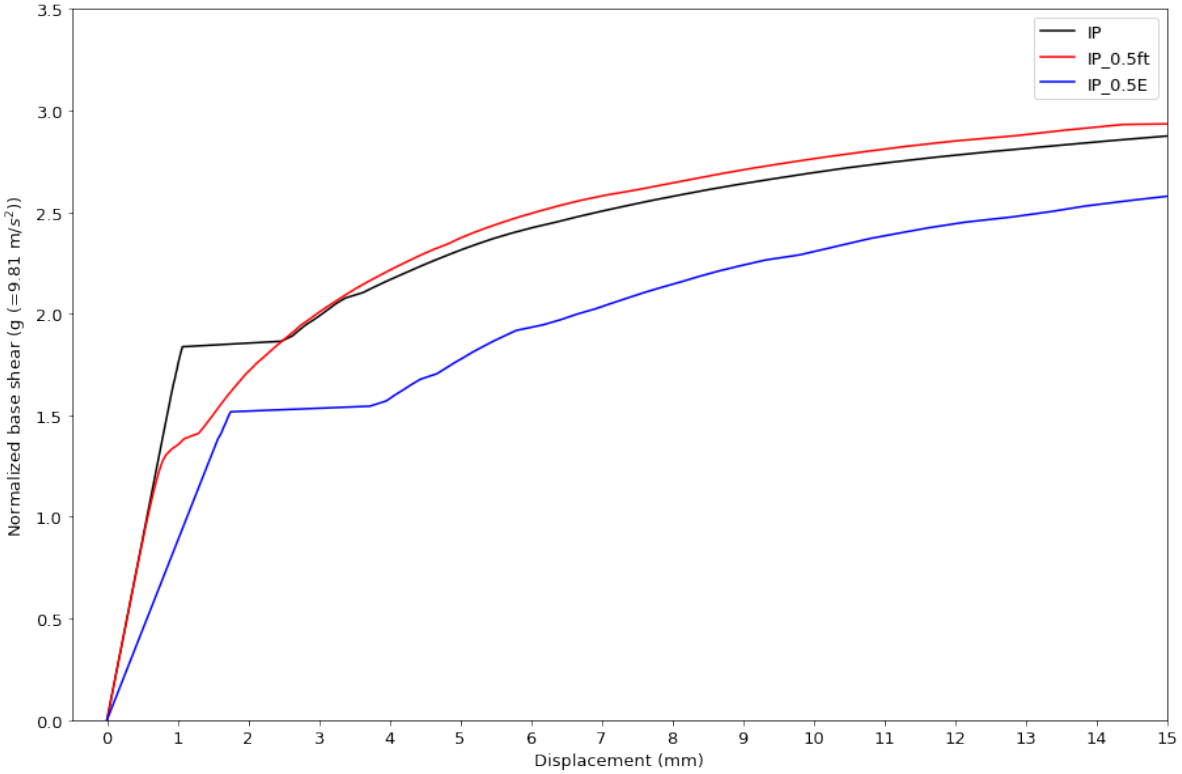

Figure 4.11: IP sensitivity analysis

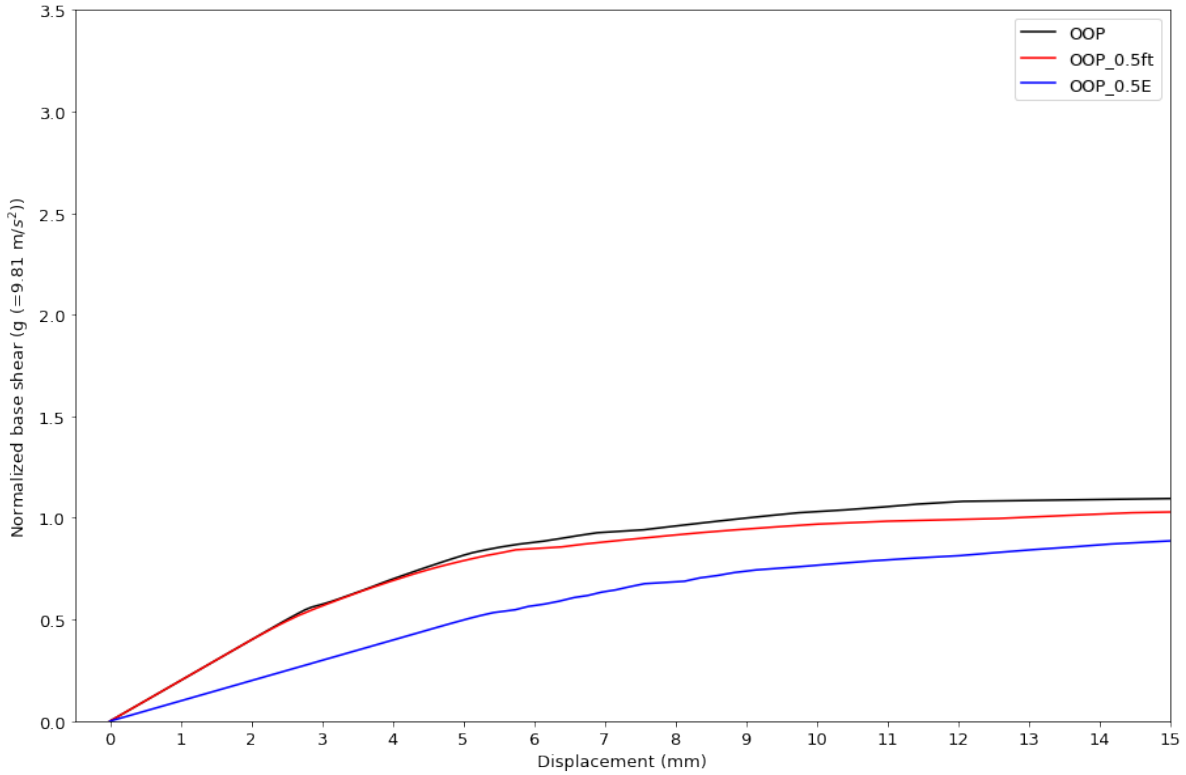

Figure 4.12: OOP sensitivity analysis

4.2.3. Single-material-model: Crushing

The figures (left: OOP & right: IP) below show the moment crushing occurs in the structure in the analyses of the first model. For the OOP-response this is at a displacement of 24.33 mm and for the IP-response at a displacement of 11.16 mm. In both responses the structure shows significant cracking due to high tensile stresses, before crushing occurs in the structure. Therefore crushing is likely not of significance for the overall capacity of the structure. Crushing will not be analysed in the consecutive models.

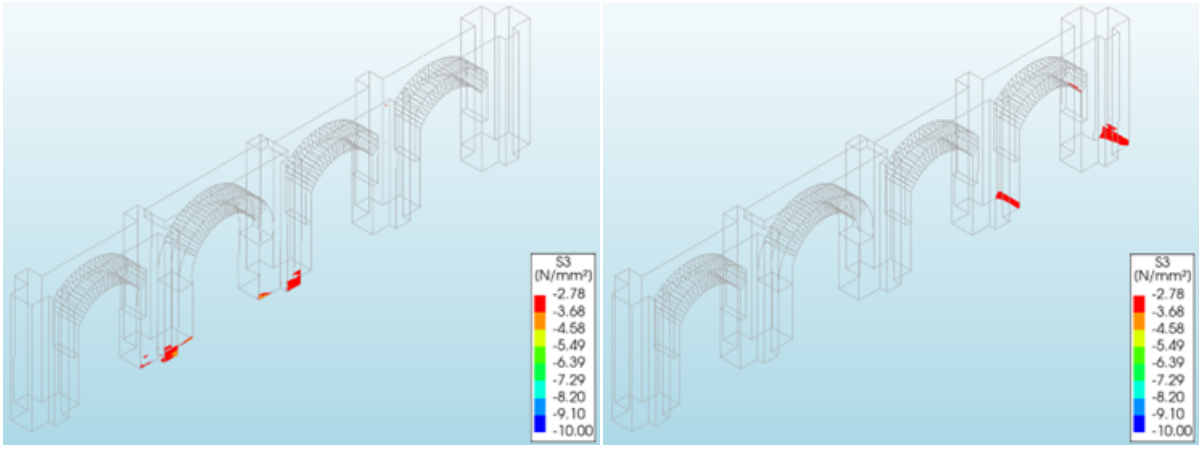

(a) OOP-pushover analysis

(b) IP-pushover analysis

Figure 4.13: Analysis of crushing in the Great Portico

4.2.4. Tri-material-model

The graph in Figure 4.14 shows the responses of the second model. The inclusion of the brick-masonry and stone block materials to the model, only effects the IP-response. The OOP-response is similar to the response from the single-material-model. This is consistent with the observation made from the results of the single-material-model, that from the failure mechanism for the OOP-response the highest stresses develop in the columns, thus in the stone masonry. The initial stiffness of the structure is bit higher, resulting in a slightly higher load bearing capacity. The IP-response gives a higher capacity. The load-level at which the first cracking appears is higher, suggesting that the presence of the brick-masonry and stone blocks in the arches increase the capacity. The figures of the crack development and the displacement show for both responses the same failure mechanisms as in the first model.

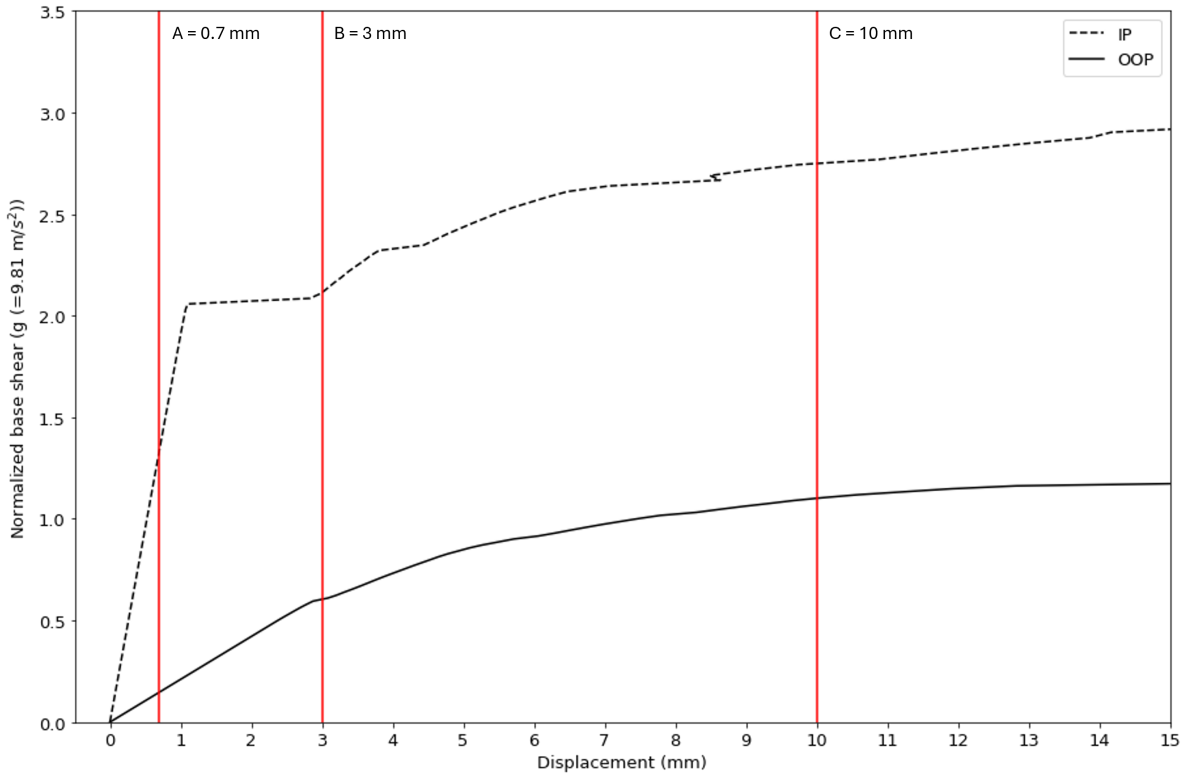

Figure 4.14: Tri-material-model: pushover analysis

In-plane pushover analysis:

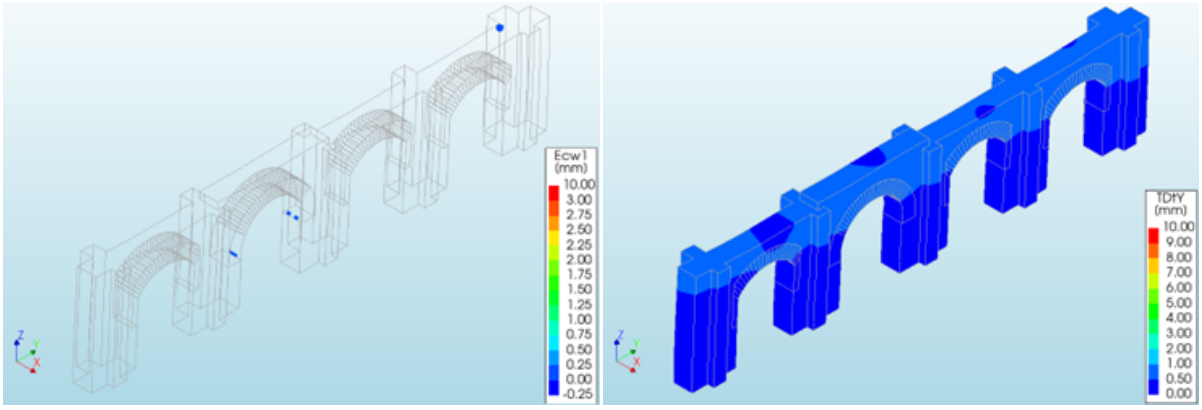

(a) Crack pattern (b) Displacements

Figure 4.15: IP-analysis: displacement level A (Deformation scaling factor: 500)

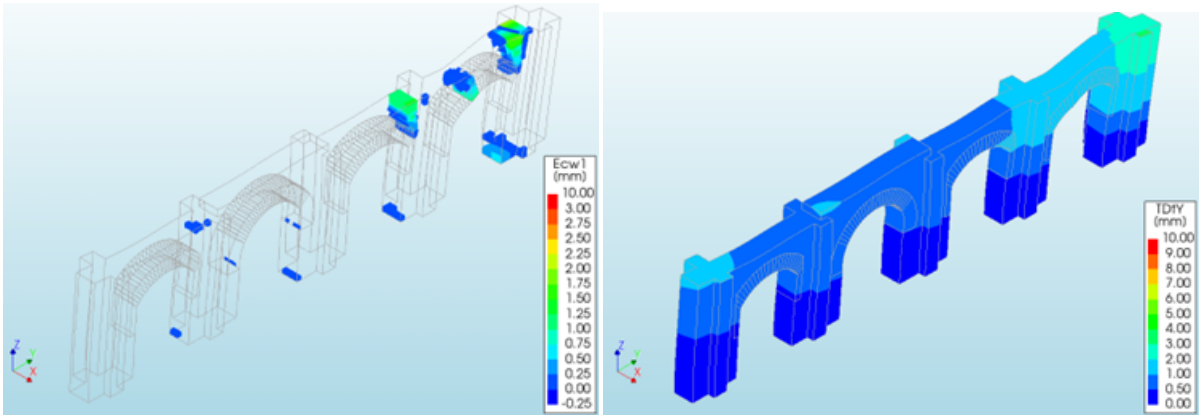

(a) Crack pattern (b) Displacements

Figure 4.16: IP-analysis: displacement level B (Deformation scaling factor: 500)

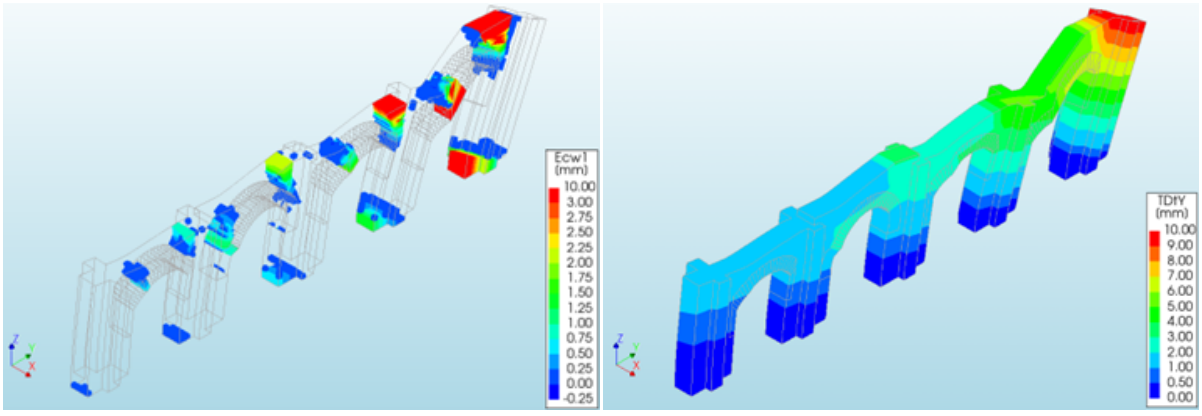

(a) Crack pattern (b) Displacements

Figure 4.17: IP-analysis: displacement level C (Deformation scaling factor: 500)

Out-of-plane pushover analysis:

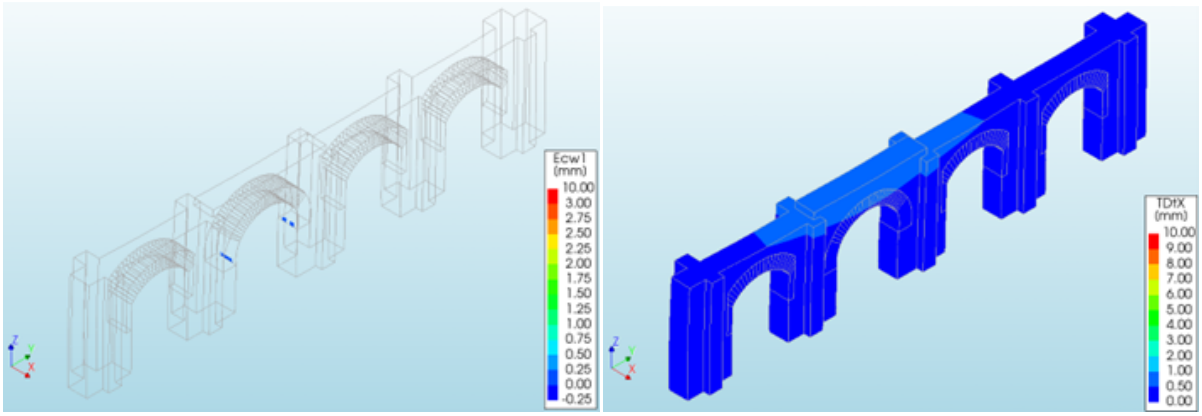

(a) Crack pattern (b) Displacements

Figure 4.18: OOP-analysis: displacement level A (Deformation scaling factor: 500)

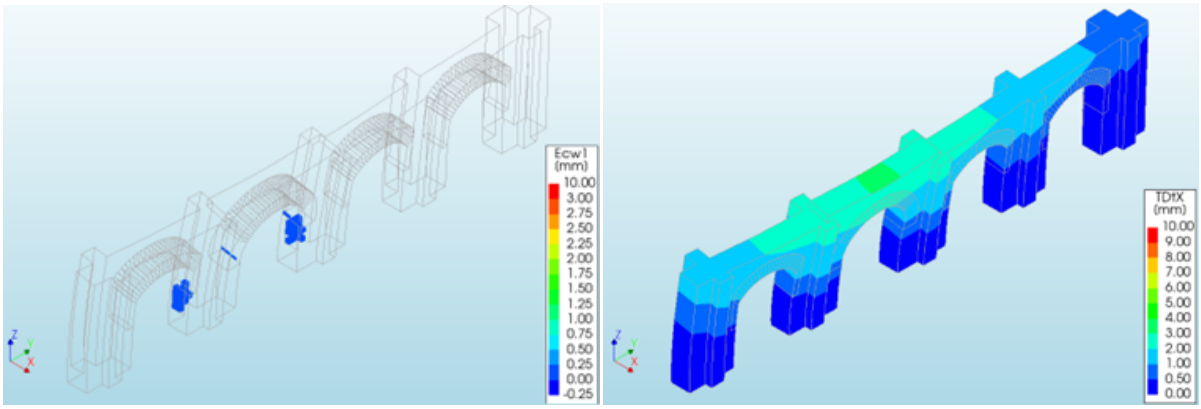

(a) Crack pattern (b) Displacements

Figure 4.19: OOP-analysis: displacement level B (Deformation scaling factor: 500)

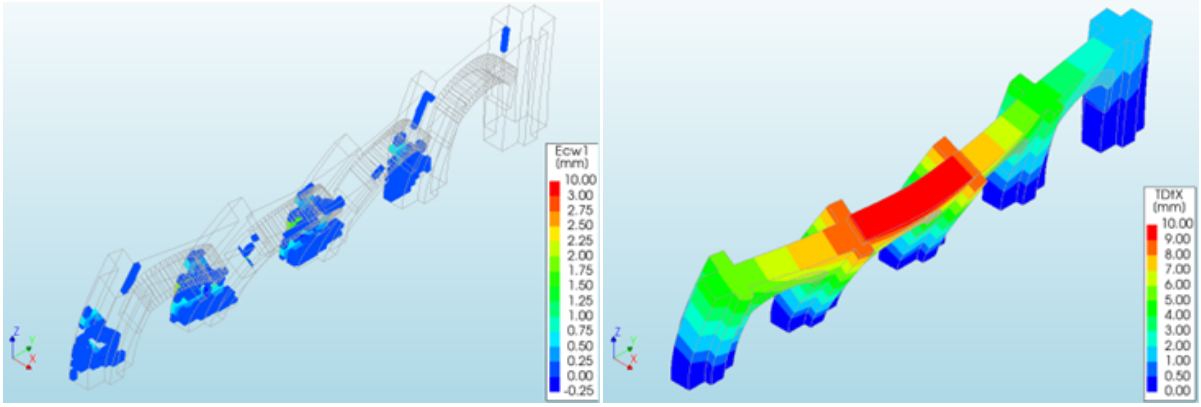

(a) Crack pattern (b) Displacements

Figure 4.20: OOP-analysis: displacement level C (Deformation scaling factor: 500)

4.2.5. Discrete cracking interface-model

The graph in Figure 4.21 shows the response for the model with discrete cracking interface elements. The analysis for the IP-response is stopped at displacement level C_{IP}, because at this point the stresses in at least one interface element are significantly high. At this point the analysis does not converge in the set amount of iterations. Lowering the pushover force increments at these higher stress levels would possibly be a solution for the program to be able to converge and analyse further. This is not included in this research, due to time constraints. The OOP-response is again very similar to the previous models. In the figures of the crack development for the IP-response, it is clear that the interfaces in the 4th arch have an impact on the response and are leading for the structural resistance. However, the failure mechanism does not change. By including the interfaces in the model, the structure has been weakened at a critical point for the IP-response. This is not the case for the OOP-response.

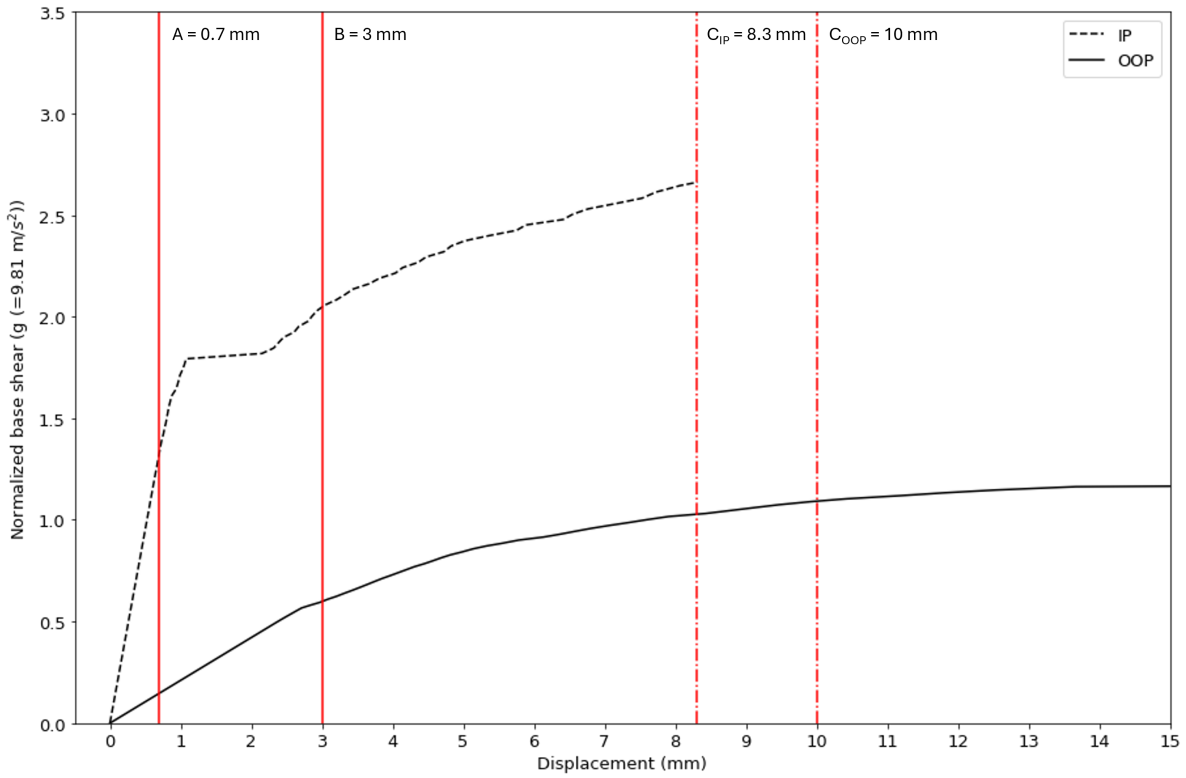

Figure 4.21: Discrete cracking interface-model: pushover analysis

In-plane pushover analysis:

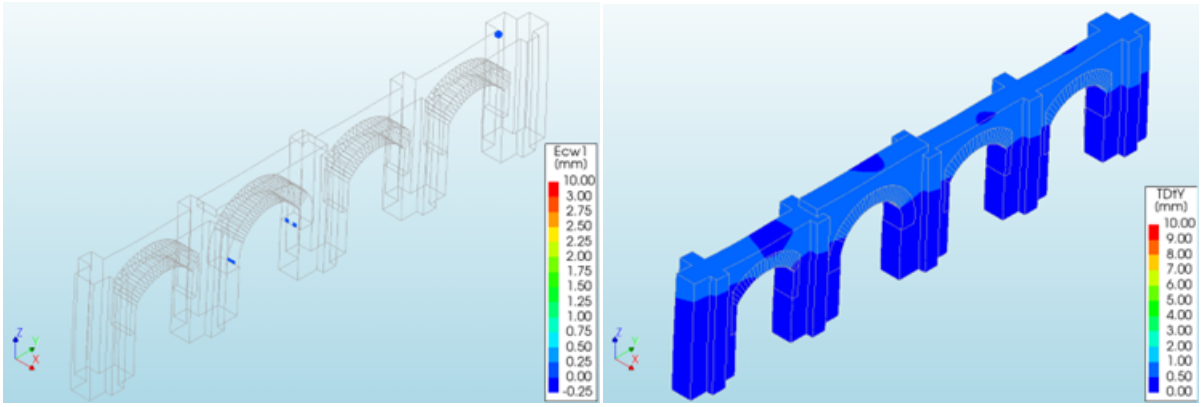

(a) Crack pattern (b) Displacements

Figure 4.22: IP-analysis: displacement level A (Deformation scaling factor: 500)

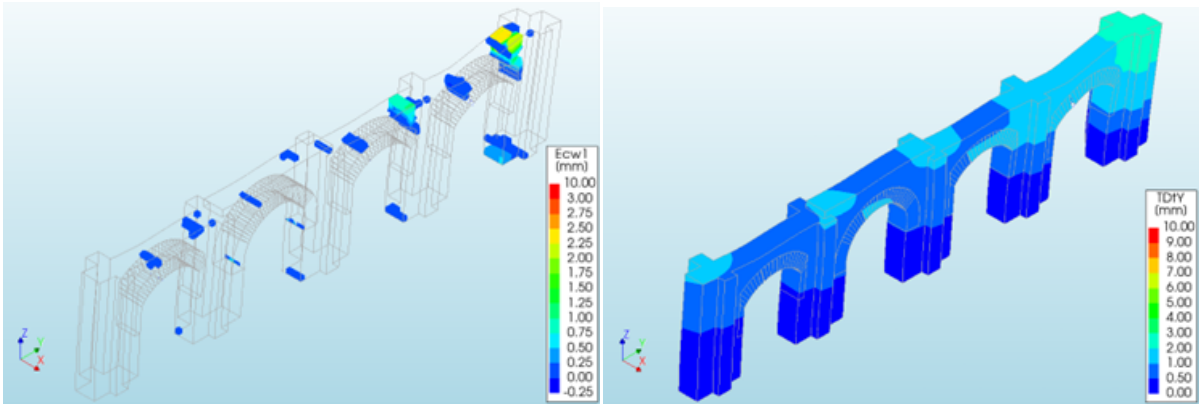

(a) Crack pattern (b) Displacements

Figure 4.23: IP-analysis: displacement level B (Deformation scaling factor: 500)

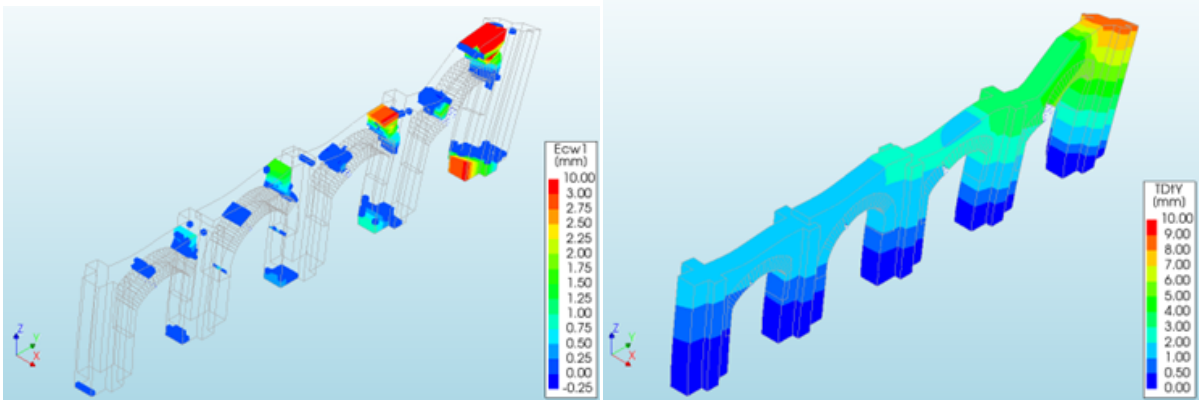

(a) Crack pattern (b) Displacements

Figure 4.24: IP-analysis: displacement level $C_{IP} = 8.3mm$ (Deformation scaling factor: 500)

Out-of-plane pushover analysis:

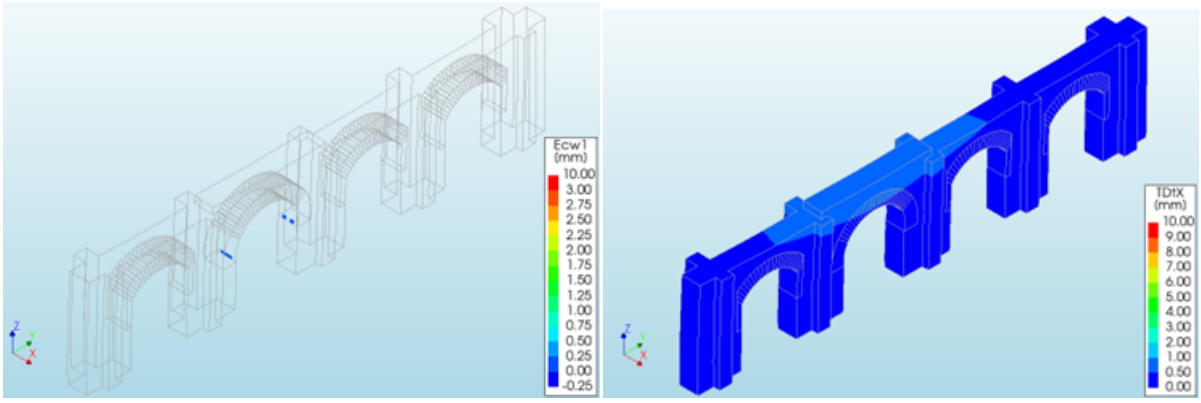

(a) Crack pattern (b) Displacements

Figure 4.25: OOP-analysis: displacement level A (Deformation scaling factor: 500)

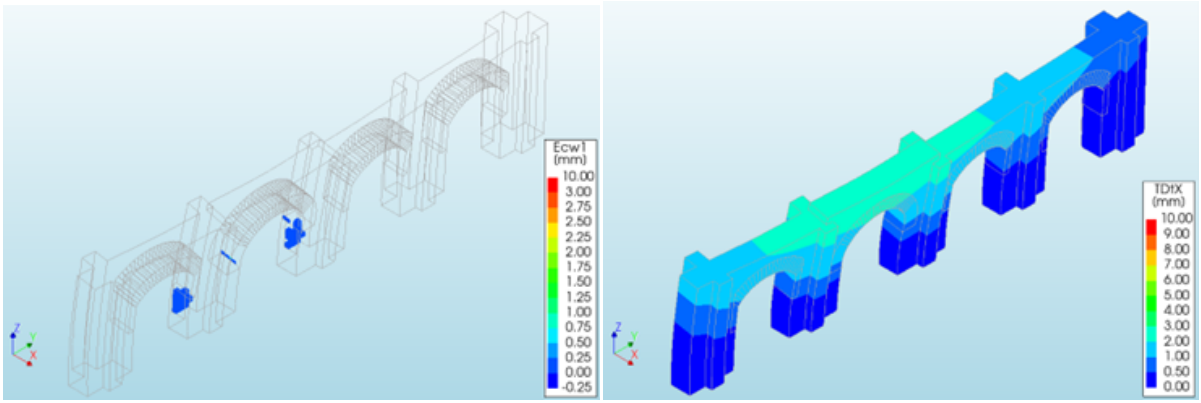

(a) Crack pattern (b) Displacements

Figure 4.26: OOP-analysis: displacement level B (Deformation scaling factor: 500)

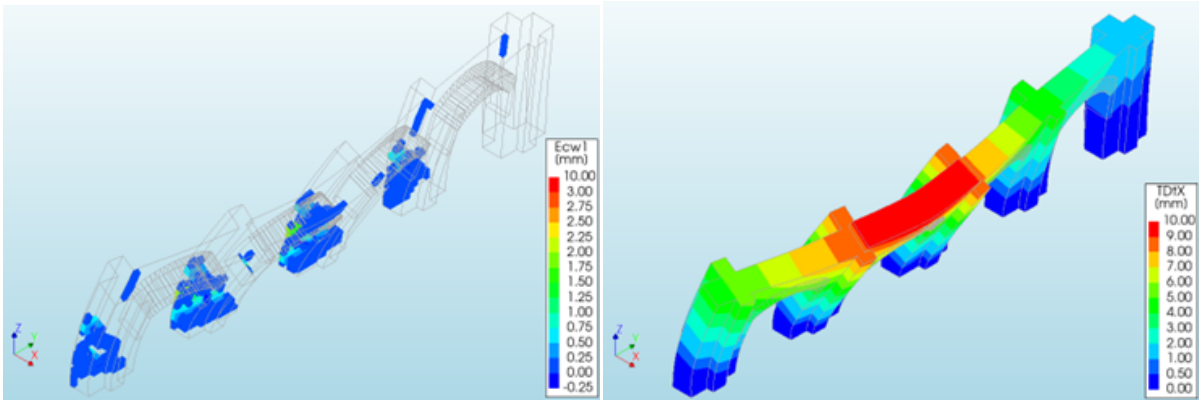

(a) Crack pattern (b) Displacements

Figure 4.27: OOP-analysis: displacement level $C_{OOP} = 10mm$ (Deformation scaling factor: 500)

4.2.6. CCSC interface-model

The model, implementing combined cracking-shearing-crushing interface elements, shows again a similar response to the previous models. Figure 4.28 shows very limited impact on the OOP-response. This is complemented by the crack pattern, which show the highest stresses and strains in the columns for the OOP-response. The implementation of the interface elements has more effect on the IP-response, which is expected as they simulate hard contact between the interfaces, so almost no tensile strength in the mortar in the interfaces. However simulating hard contact seemed to have little impact on the OOP-response.

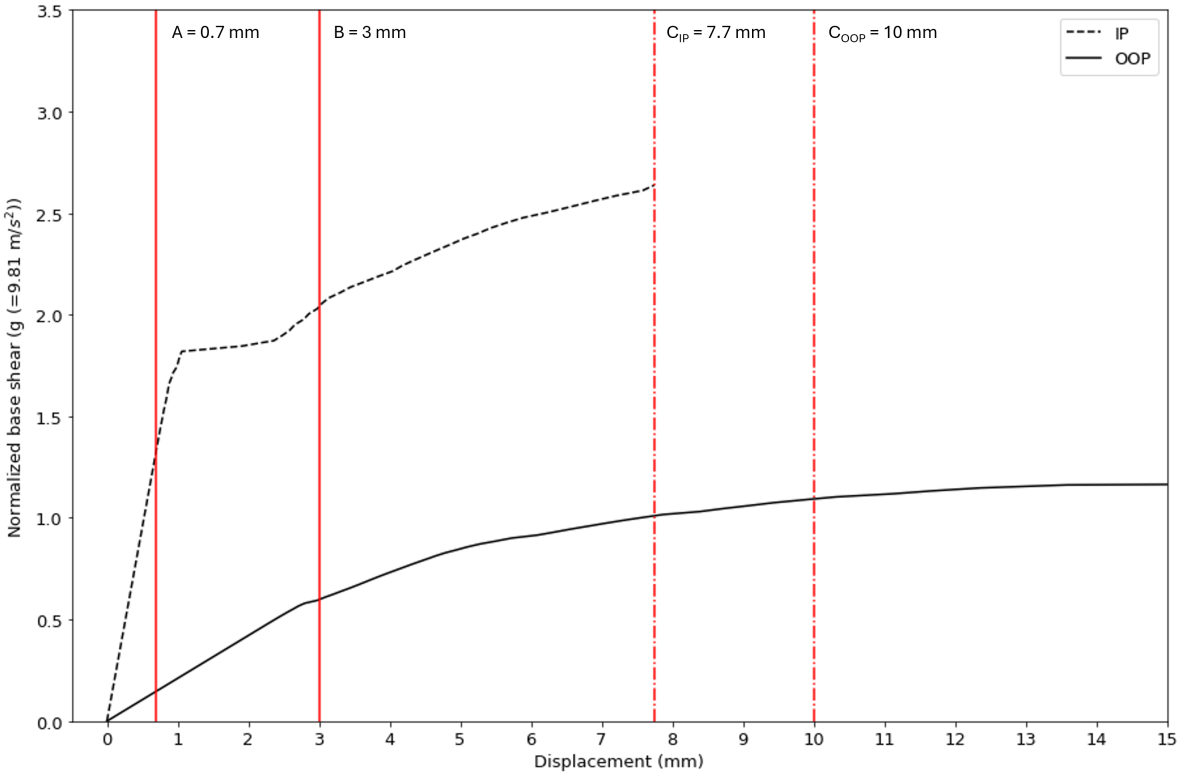

Figure 4.28: CCSC interface-model: pushover analysis

In-plane pushover analysis:

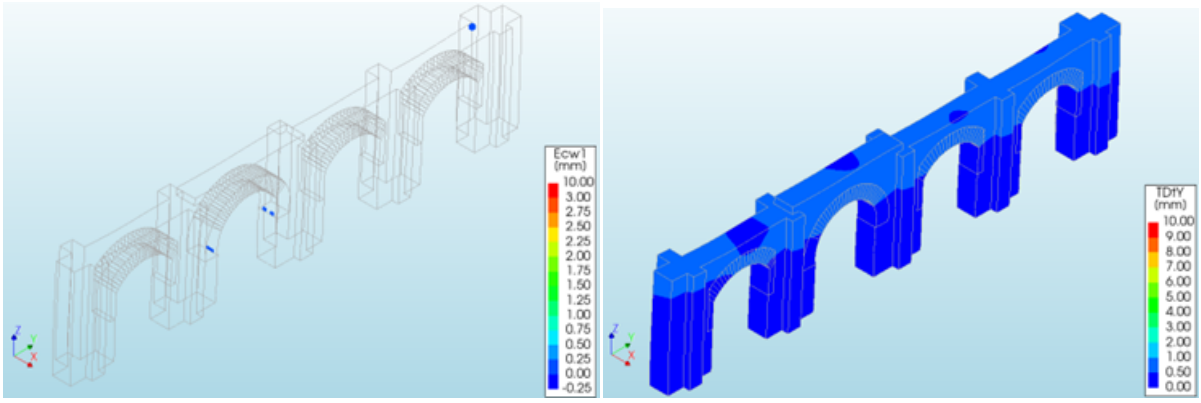

(a) Crack pattern (b) Displacements

Figure 4.29: IP-analysis: displacement level A (Deformation scaling factor: 500)

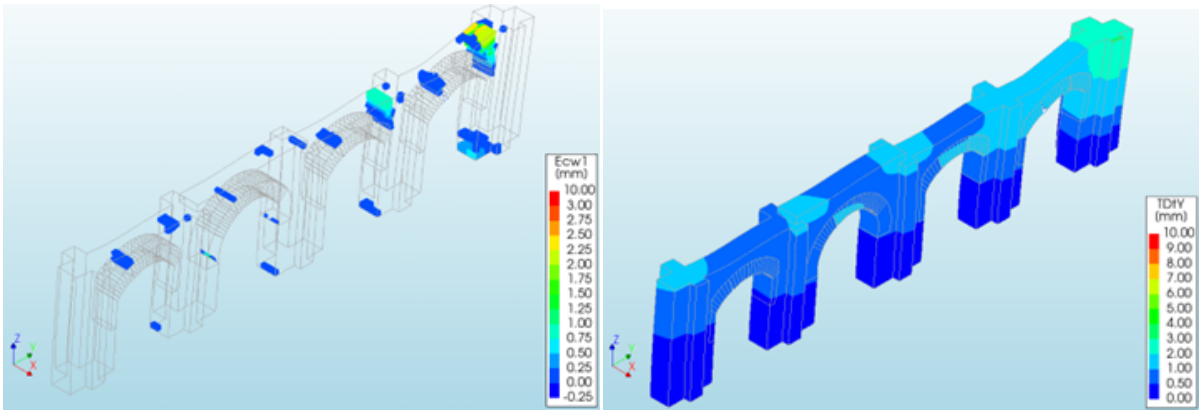

(a) Crack pattern (b) Displacements

Figure 4.30: IP-analysis: displacement level B (Deformation scaling factor: 500)

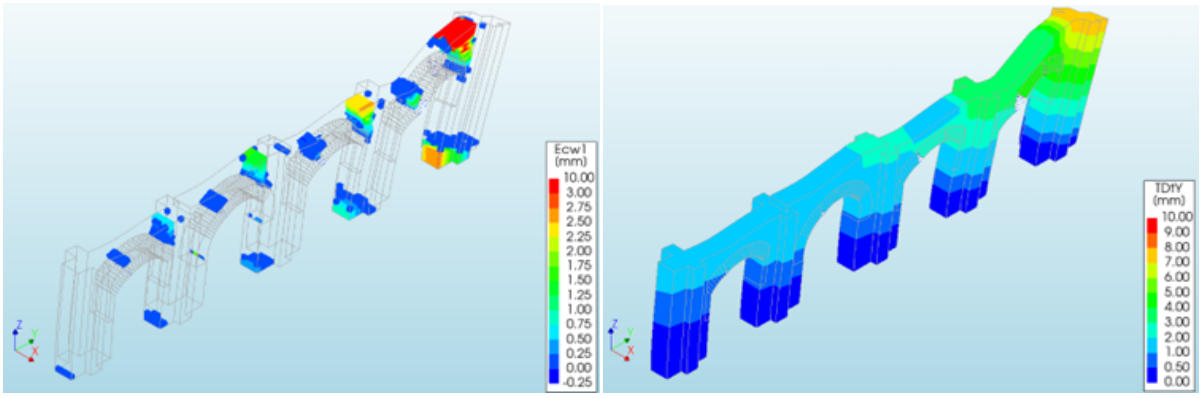

(a) Crack pattern (b) Displacements

Figure 4.31: IP-analysis: displacement level $C_{IP} = 7.7mm$ (Deformation scaling factor: 500)

Out-of-plane analysis:

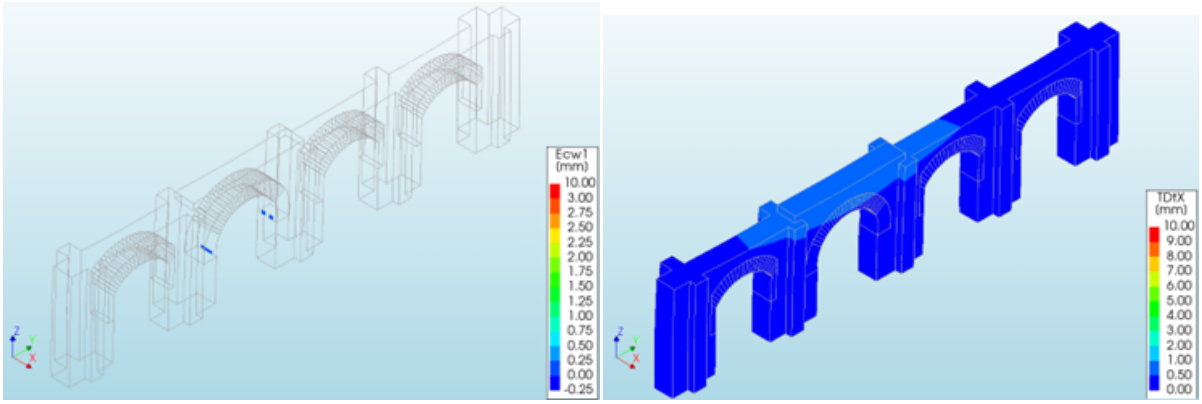

(a) Crack pattern (b) Displacements

Figure 4.32: OOP-analysis: displacement level A (Deformation scaling factor: 500)

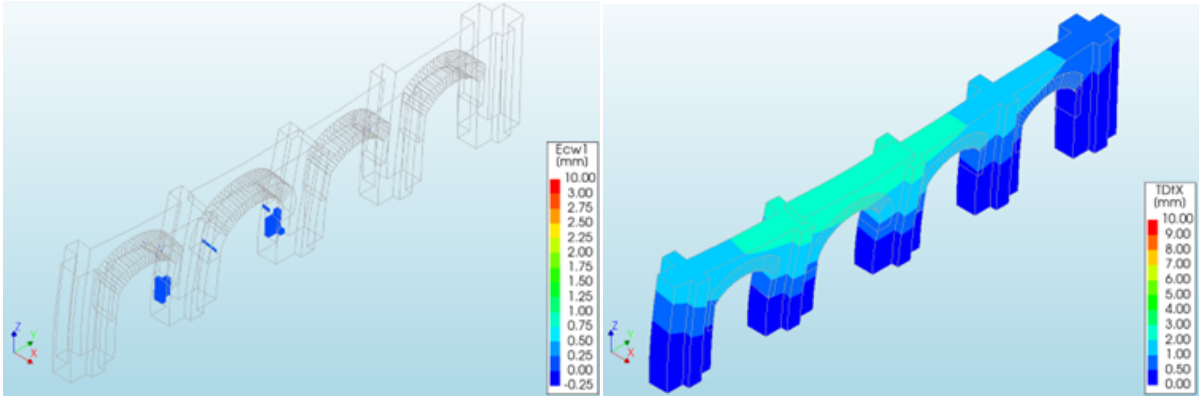

(a) Crack pattern (b) Displacements

Figure 4.33: OOP-analysis: displacement level B (Deformation scaling factor: 500)

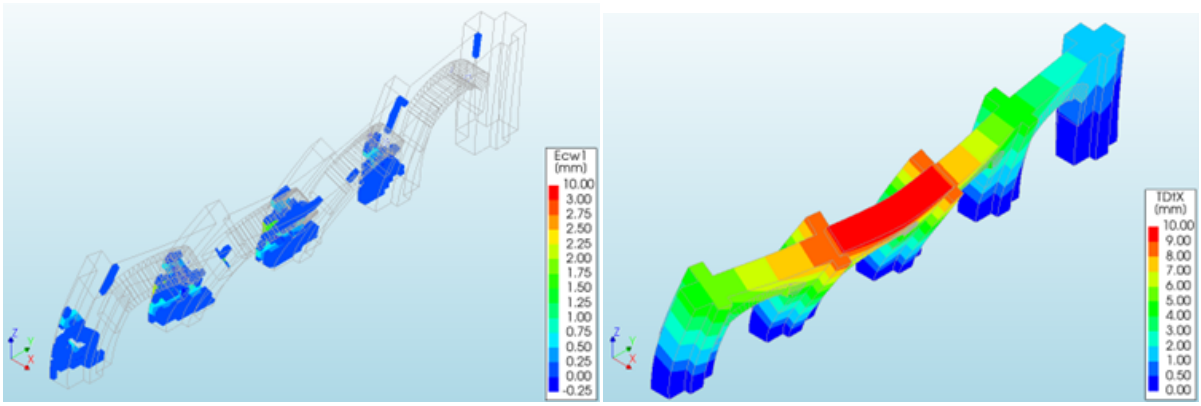

(a) Crack pattern (b) Displacements

Figure 4.34: OOP-analysis: displacement level $C_{OOP} = 10mm$ (Deformation scaling factor: 500)

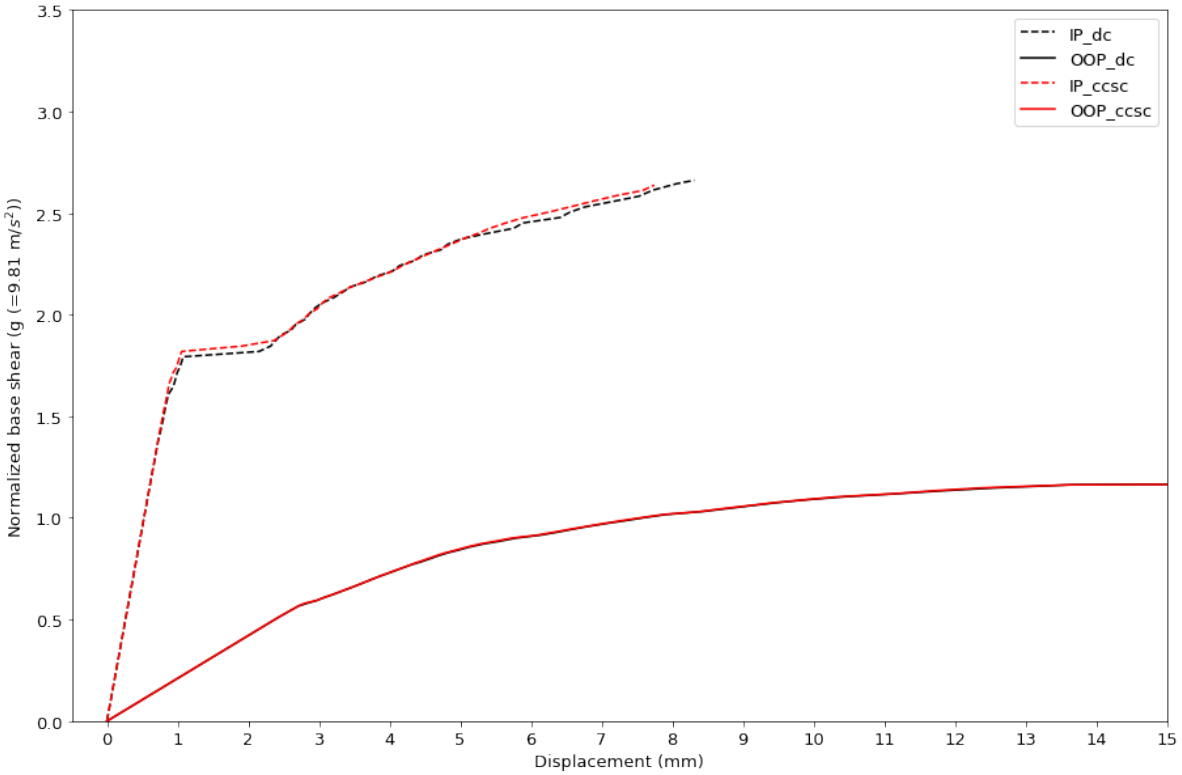

Figure 4.35: Comparison interface-models

The graph in Figure 4.35 shows both interface-models. A different kind of interface elements has little to no effect on the OOP-response. For the IP-response the model with CCSC-interface elements shows a slightly higher load bearing capacity for both the elastic and post elastic response. For the purpose of this analysis the difference between the two kinds of interface elements is negligible. In which case the use of discrete cracking elements would be advised as less properties need be assumed and it is less computationally demanding.

4.2.7. Final-model

The graph in Figure 4.36 shows the normalized base shear over the maximum displacement in IP and OOP-direction, respectively. It is important to note that for the IP-response for all previous models the displacement was taken at the top of the right most column of the structure. However as the top of that column has been removed in this model the displacement is taken at a different point compared to the other models. It is still at the top, but relatively lower in the general geometry. OOP-response gives seemingly the same response. IP-response shows a lower initial stiffness for the elastic response, but has a higher peak elastic load bearing capacity. Also the jump in the IP-response present in the IP-responses of the previous analyses is not there. This could be explained by fact that this brittle response was caused by cracking in the top of the 4th arch, which is removed for the current analysis.

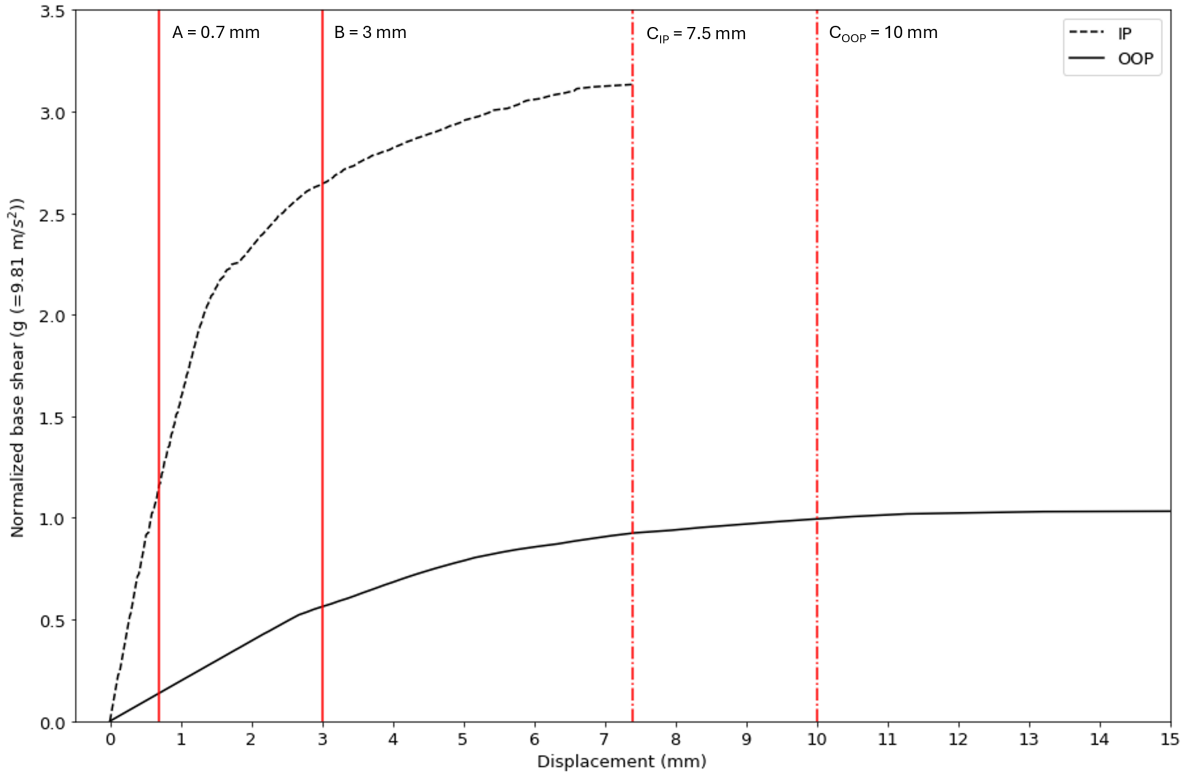

Figure 4.36: Final-model: pushover analysis

In-plane pushover analysis:

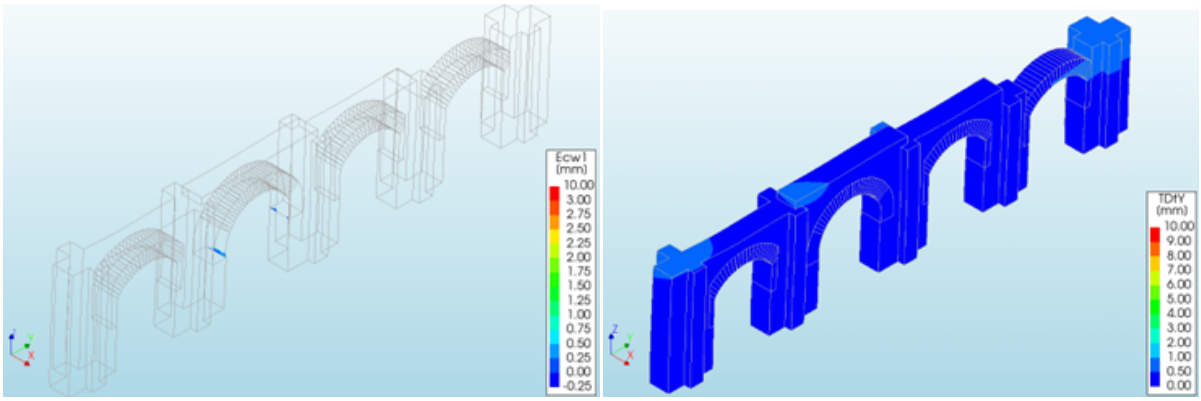

(a) Crack pattern (b) Displacements

Figure 4.37: IP-analysis: displacement level A (Deformation scaling factor: 500)

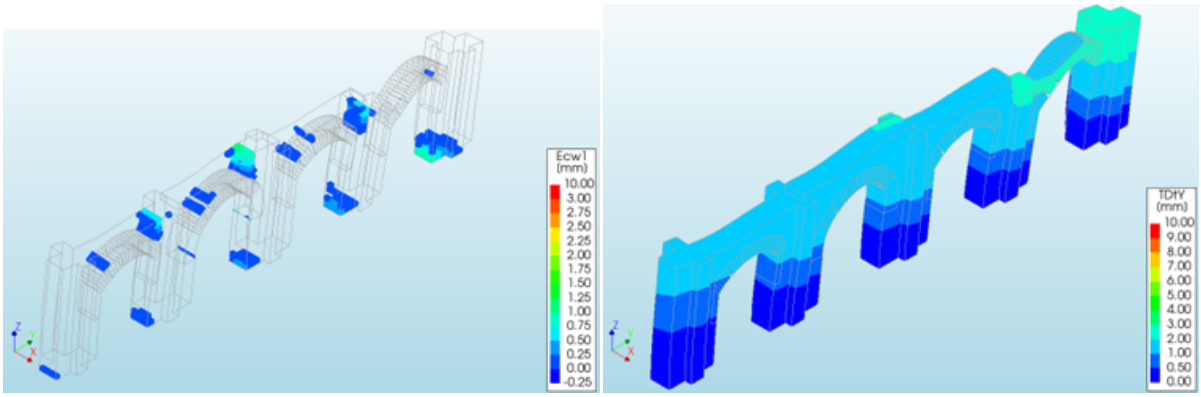

(a) Crack pattern (b) Displacements

Figure 4.38: IP-analysis: displacement level B (Deformation scaling factor: 500)

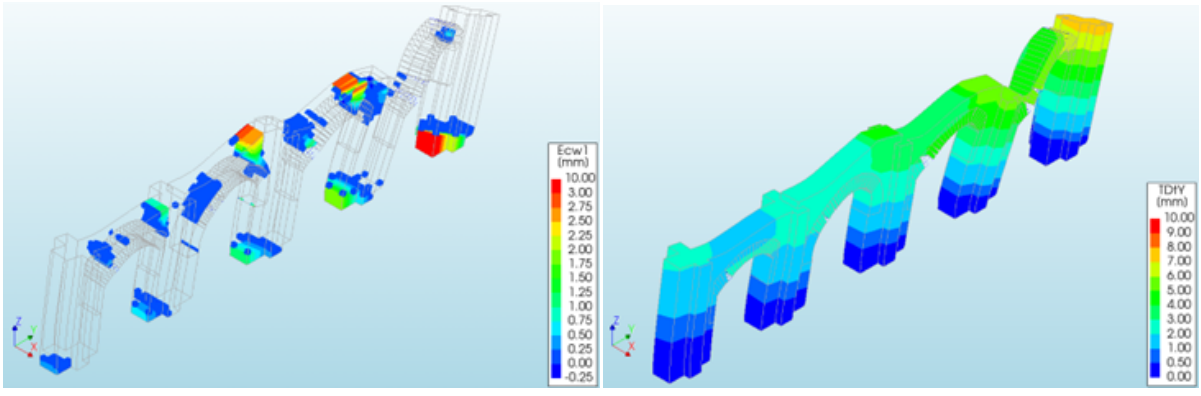

(a) Crack pattern (b) Displacements

Figure 4.39: IP-analysis: displacement level $C_{IP} = 7.5mm$ (Deformation scaling factor: 500)

Out-of-plane pushover analysis:

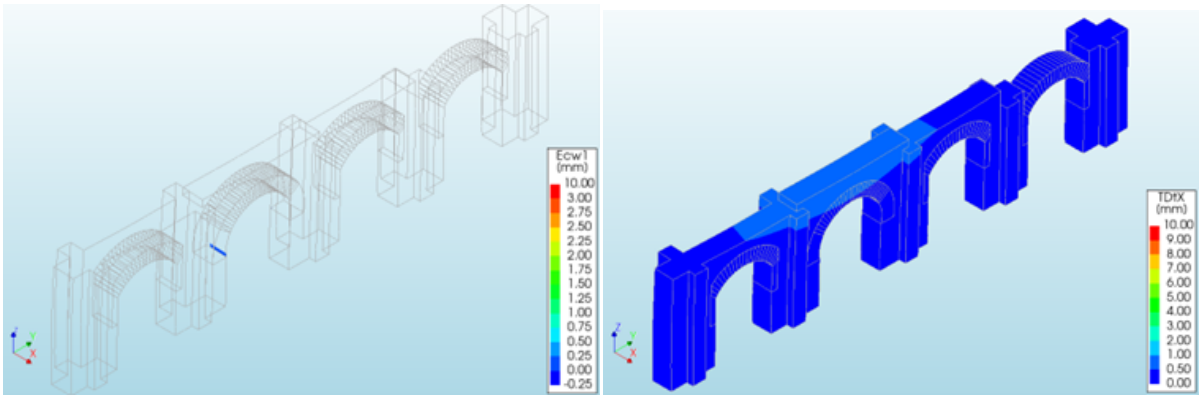

(a) Crack pattern (b) Displacements

Figure 4.40: OOP-analysis: displacement level A (Deformation scaling factor: 500)

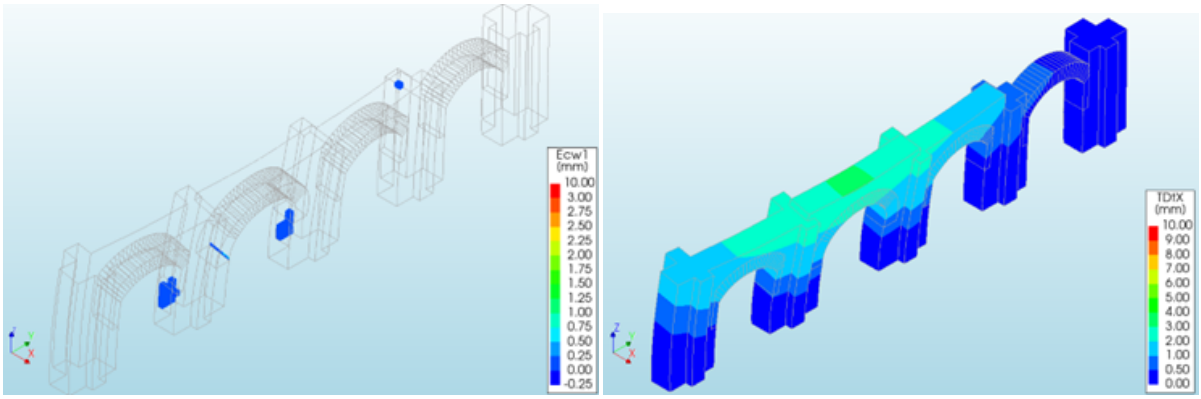

(a) Crack pattern (b) Displacements

Figure 4.41: OOP-analysis: displacement level B (Deformation scaling factor: 500)

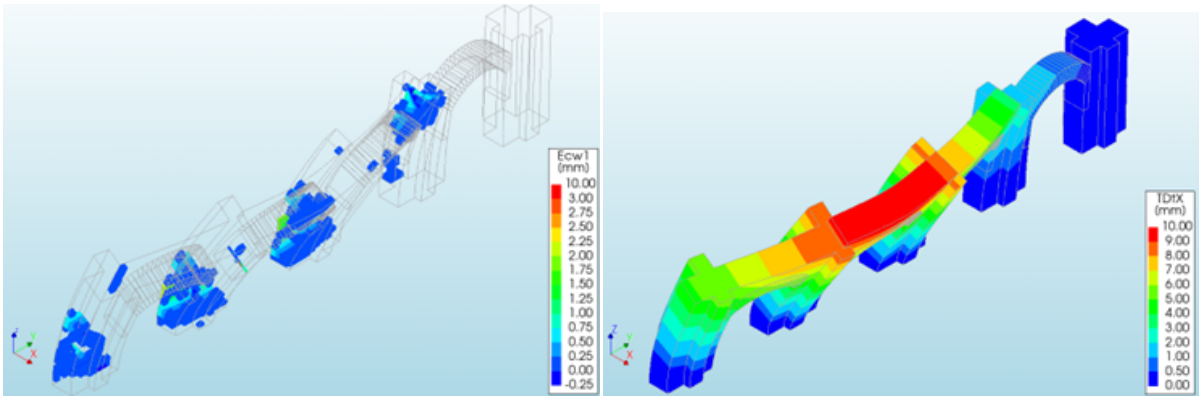

(a) Crack pattern (b) Displacements

Figure 4.42: OOP-analysis: displacement level $C_{OOP} = 10mm$ (Deformation scaling factor: 500)

4.2.8. Model comparison

This section discusses the comparison between all four models for both the out-of-plane and in-plane pushover analyses. The comparison is based on the normalized base shear curves of each model. From the crack pattern figures, it can be observed that all models display the same general failure mechanisms, and no major differences can be identified based on these visual results. The normalized base shear curves provide an indication of how each model represents the structural capacity of the Great Portico under seismic loading. This comparison gives insight into which model sufficiently captures the seismic behaviour of the structure.

For the comparison of the in-plane response, the displacements for the first three models were evaluated at the height corresponding to the reference point used in the final-model, rather than at the top of the right-most column. This adjustment was necessary because the structural element at that location is absent in the final-model. By selecting approximately the same nodal position across all models, the corresponding node in the final-model lies slightly higher due to mesh discretization, a consistent one-to-one comparison between the four models is ensured. As shown in Figure 4.43, the normalized base shear curve of the final model differs more noticeably from those of the other models. The possible explanation for this difference, cracking in the top of the right-most arch, has been discussed in Subsection 4.2.7. The curve of the final model also indicates a higher capacity for the in-plane response. A clear reason for this is difficult to identify, although it could be related to the reduced cracking in certain key areas of the structure, as the elements in the structure where cracks would develop shown in the previous models no longer exist in the final-model.

Figure 4.44 shows the normalized base shear curves of the four models for the out-of-plane analysis. Only small deviations can be seen between the curves, indicating that all models perform similarly in capturing the overall out-of-plane response. The final model shows a slightly lower capacity than the other three, but this difference is not significant. Based on these results, the first model, being the least detailed, captures the structural capacity sufficiently for the out-of-plane analysis.

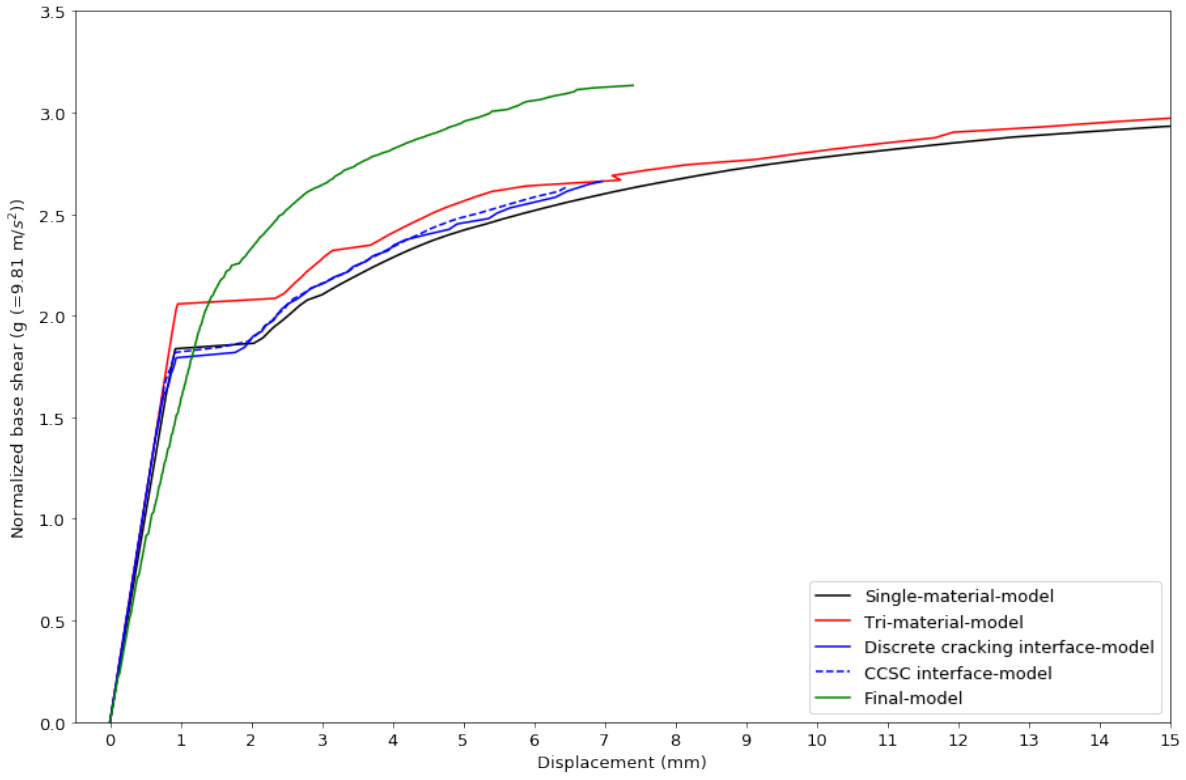

Figure 4.43: IP-analysis comparison

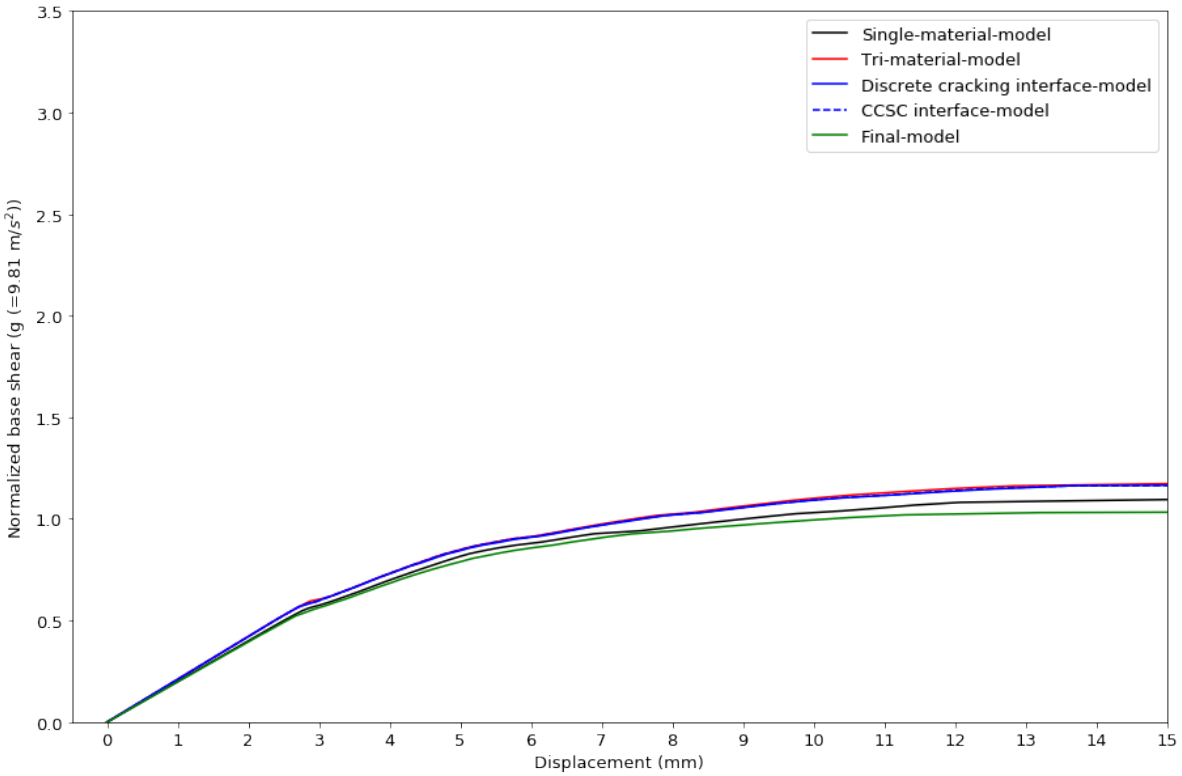

Figure 4.44: OOP-analysis comparison

4.3. Conclusive Remarks

From the results of the seismic analyses performed on the remaining part of the Great Portico, it can be concluded that the out-of-plane behaviour of the structure is more critical than its in-plane behaviour. The arch structure demonstrates a significantly lower capacity against out-of-plane loading in all models used in the research.

For the out-of-plane response, the governing failure mechanism is identified as tensile failure within the stone masonry columns. Once these tensile stresses exceed the masonry's limited tensile strength, cracking initiates and propagates, leading to a loss of stiffness and stability. In this case, the single-material-model, the least detailed model, proves sufficient, as the dominant failure mode is governed by high tensile stresses in the stone masonry.

For the in-plane response, failure is primarily governed by tensile cracking in the brick masonry or within the mortar joints, modelled with interfaces, between the brick masonry and the stone blocks in the arches. The most detailed model, the fourth model, provides the most accurate representation of the structural capacity in this direction, capturing the local stress distributions and the complex interaction between the brick masonry and limestone components.

While localized crushing is observed in small areas of the structure, particularly at points of high compressive stress, this occurs after significant tensile cracking has already developed elsewhere in the structure for both the in-plane and out-of-plane response. Thus, tensile failure remains the dominant and most critical mechanism influencing the seismic performance of the Great Portico.

In modelling the interfaces between the brick masonry and limestone blocks, the use of discrete cracking interface elements is preferred over combined cracking–shearing–crushing elements. The discrete interface approach offers a simpler formulation with fewer underlying assumptions while still providing sufficient accuracy in capturing the cracking in these interfaces and overall seismic response of the structure.

5

Discussion

The research aimed to investigate the seismic behaviour of the Great Portico, a historical masonry arch structure. Researching the structural behaviour of a historical masonry structures is a challenging task. Roca et al. (2010) listed complex geometry, materials, morphology (member composition and connections) and present condition as main challenges. In case of the study on the Great Portico, the materials and present conditions were the main challenges. As part of a UNESCO World Heritage Site, it is difficult to perform tests on the structure, especially laboratory-tests on the building materials. Tests on similar building material from another site, are the best comparable tests to derive the mechanical properties of the Great Portico. Pictures of the Great Portico were used to get an indication of the present condition of the structure. Based on these pictures, an evaluation of the deterioration of the mortar in and between the arch segments was made. Conservatively, the deterioration was likely overestimated. An in-situ assessment could give a better evaluation of the current state of the mortar. It could also highlight detailed places in the structure with a comparatively higher deterioration.

The selection of an appropriate research methodology is also essential. Many approaches can be used to analyse masonry structures. All approaches have their strengths and weaknesses and can be utilized in different kinds of studies. The researcher has chosen to use a continuum model approach. Past experience of the researcher was a factor in the decision. This approach is suitable to assess the global seismic behaviour of a structure. It is a straightforward modelling approach, which makes the modelling process less time-consuming. A drawback of the approach lays in the difficulty to analyse the structure in more detail. For example, the results showed for the out-of-plane response cracking in the columns of the larger horseshoe-shaped arch. The limestone masonry material is modelled as a homogeneous material using continuum constitutive laws, even though masonry is a composite building material. Therefore, it is difficult to determine how exactly the cracks will develop. Determining factors are the masonry configuration and potential weak spots in the masonry, which are either impossible or hard to model using the continuum model approach.

The current research method highlighted specific structural aspects, by incorporating multiple models in an iterative approach. This approach made it possible to focus on potential weak points in the structure. A focus point were the interfaces between the brick masonry and limestone segments in the arches. The pushover analysis showed that cracking in the interfaces occurred, which lowered the overall capacity of the structure in the in-plane response. However, no discernible effect could be seen in the critical out-of-plane response. Therefore, the inclusion of interface elements in the Great Portico models appears to have only a limited influence on the overall structural capacity. Focussing on potential weak points in the out-of-plane response could give more insight in the overall capacity of the Great Portico. One such critical focus point is the mortar within the limestone masonry of the columns of the larger horseshoe-shaped arch. To investigate this vulnerability more effectively, a different modelling strategy may be required. Alternatively, an in-situ assessment of the existing masonry could help identify specific locations within the columns where interface elements should be introduced in the continuum model to better capture local weaknesses. This would require the implementation of more structural segments.

A few modelling simplifications were implemented to streamline the modelling process. Roca et al. (2010) listed the interaction with soil/foundation as one of the desirable features for modelling historical masonry structures. In the research methodology, the foundation conditions are simplified by modelling the

base of the structure using fixed boundary conditions. This approach was adopted primarily due to the limited available information regarding the actual foundation of the Great Portico. Consequently, no soil–structure interaction effects were included in the loading conditions. The omission of the slight inclination in the ground level may also introduce minor deviations. Within the current modelling framework, incorporating this inclination could influence the derived eigenmodes. However, given the relatively small slope compared to the scale of the structure, such effects are expected to remain limited. The large horseshoe-shaped arch would likely still dictate the primary out-of-plane eigenmode. If soil–structure interaction were to be modelled explicitly, e.g. by incorporating a deformable soil domain, the inclination of the ground level could become more influential. Nonetheless, such an approach would considerably increase the complexity of the analysis. Considering the scope of the study, such analysis is deemed unnecessary.

The study used the numerical models to identify the eigenmodes of the structure. To further validate and refine these models, in-situ dynamic identification tests are recommended. The experimental results could subsequently be used to adjust and calibrate the material properties in the models, particularly the material stiffnesses. Based on the modal shapes obtained from the numerical eigenmode analysis, several locations are recommended for sensor placement during dynamic identification. For the in-plane mode, sensors are recommended: at mid-height and top of each column. For the out-of-plane modes, sensors should be positioned: at the top of the second arch at the midpoint of the arch, at the tops of the two outer columns and slightly above mid-height on each of the three inner columns. These placements are expected to provide a clear identification of the eigenmodes and enable a reliable comparison between the numerical and experimentally identified eigenmodes.

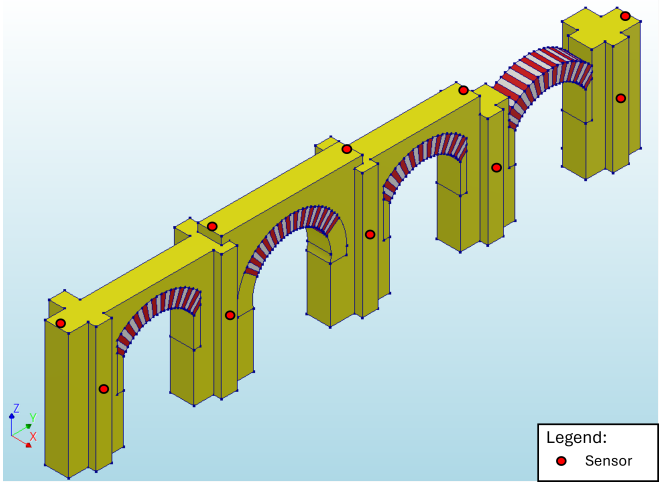

(a) IP eigenmode analysis

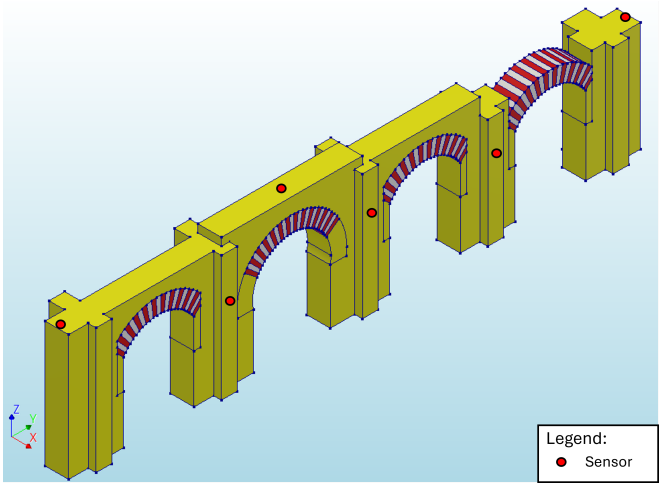

(b) OOP eigenmode analysis

Figure 5.1: Recommended sensor placement for in-situ dynamic identification tests

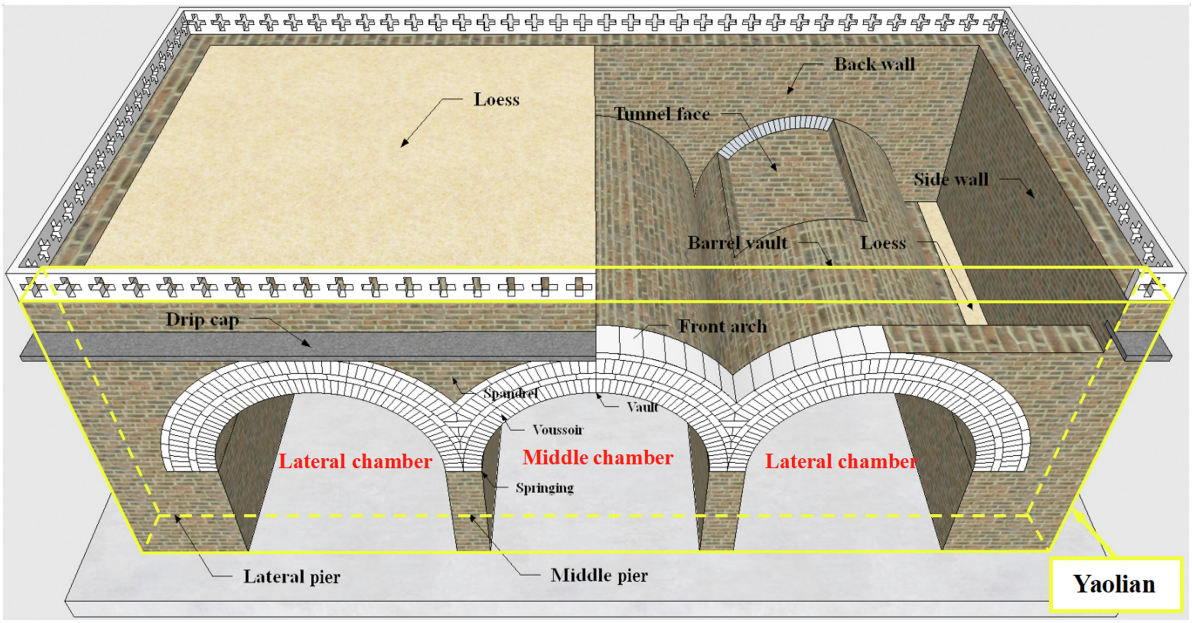

Figure 5.2: Structural diagram of brick cave dwellings (Xue et al., 2021)

The uncertainties, assumptions and simplifications in the modelling of the Great Portico, limit the extent to which the research question can be answered quantitatively. Nevertheless, with appropriate conservatism, the following observation regarding the seismic capacity of the structure can be made. The critical out-of-plane response shows a capacity of approximately 1.0 g (see Figure 4.44). Shake-table experiments have demonstrated that most masonry structures begin to exhibit significant damage at peak ground accelerations in the range of 0.4 g to 0.6 g. Studies by Tomassetti et al. (2018) on a brick masonry building and by Mazzon et al. (2010) on a stone masonry building similarly report substantial damage and notable stiffness degradation at peak ground accelerations below 1.0 g. Xue et al. (2021) performed a seismic analysis on brick cave dwellings in the Loess Plateau of China. These structures are structural comparable to the Great Portico as they include brick-masonry arches. The study indicated a noticeable increase in the structural model's dynamic response and damage when a peak ground acceleration of 0.5 g was reached, while the structural stiffness substantially degraded when the peak ground acceleration reached 0.6 g. In comparison, the estimated seismic capacity of approximately 1.0 g for the Great Portico is relatively high for a masonry structure.

6

Conclusions and Recommendations

The archaeological site of Medina Azahara holds exceptional cultural and historical significance, recognized as a UNESCO World Heritage Site. As a symbol of the architectural and cultural achievements of the Caliphate of Córdoba, its preservation is of great importance. Within this context, the Great Portico represents a key structural and visual element of the site. Understanding its seismic performance is therefore essential to ensure its long-term conservation and to inform appropriate strategies for structural preservation and risk mitigation under potential seismic events. The central research question guiding this study was: **What is the structural response of the remaining structure of the Great Portico of Medina Azahara subjected to seismic loading?**

The results of the eigenmode analysis indicate that both the in-plane (IP) and out-of-plane (OOP) seismic behaviours needed to be considered and are governed predominantly by a singular eigenmode in each respective direction. This suggests that the seismic response of the Great Portico can be effectively represented by considering the dominant mode in each case. However, for the out-of-plane behaviour, further research could explore the inclusion of multiple pushover load distributions to assess whether higher-order modes, despite their lower mass participation factors, might influence the overall response.

The seismic behaviour of the remaining structure of the Great Portico was examined through the pushover analyses in both directions. The results reveal that the out-of-plane response is governed by tensile failure in the stone masonry columns, particularly in the columns supporting the horseshoe-shaped central arch, which represents the most vulnerable portion of the structure. In contrast, the in-plane response is controlled by tensile cracking in the brick masonry and in the mortar joints between the brick masonry and the adjacent limestone blocks in the arches.

The sensitivity analysis focused on the tensile strength and stiffness of the stone masonry, considered the most critical parameters. The analysis indicates that variations in these properties have limited impact on the overall seismic response. The dominant failure mechanisms, tensile cracking in the columns and masonry joints, remained consistent across the tested parameter ranges. The structure's global behaviour and capacity remained largely unchanged, indicating that the seismic response is governed more by the geometric configuration and material composition of the structure than by variations in the mechanical properties of the stone masonry. This limited sensitivity of the results to uncertainties in these two material parameters enhances the robustness and reliability of the conclusions drawn in this study. It suggests that, despite the inherent uncertainties associated with the material characterization of historical masonry, the models capture the essential physical behaviour of the Great Portico with sufficient accuracy to support meaningful seismic vulnerability assessments.

A quantitative evaluation of the seismic vulnerability is constrained by the uncertainty in the mechanical properties of the historical masonry materials. As the exact composition and degradation level of the original materials are difficult to determine, the analyses relied on representative values from literature. This introduces a degree of variability in the predicted response, emphasizing the importance of further experimental research on the material properties. However, the capacity of the Great Portico in the critical out-of-plane response is approximately 1.0 g. Compared to results from shake-table experiments on masonry structures, the capacity is relatively high. Even when accounting for the uncertainties, assumptions and simplifications in the modelling, the results suggest that the Great Portico is unlikely to sustain seismic damage.

Although the capacity of the Great Portico is relatively high, further research would be valuable to investigate the structure in greater detail. The following recommendations for model refinement and key considerations for future in-situ testing are provided:

- A different modelling strategy to capture the composite character of the limestone masonry and to determine detailed crack developments.
- The addition of structural segments and interfaces in the model to investigate potential weak points in the structure.
- The inclusion of multiple modal pushover load profiles. Higher-order modes could have a significant influence on the out-of-plane response.
- An in-situ assessment of the current state of the mortar. Identifying focus points which could be used for the mentioned model refinements.
- Dynamic identification tests to experimentally identify the eigenmodes and, consequentially, to refine the material stiffness parameters.
- Sensor-placement for the dynamic identification tests. For OOP: at the top of the second arch at the midpoint of the arch, at the tops of the two outer columns and slightly above mid-height on each of the three inner columns. For IP: at mid-height and top of each column.

Overall, the conclusions highlight that the out-of-plane behaviour of the Great Portico is the most critical concern for seismic safety, primarily due to the tensile vulnerability of the limestone masonry in the columns. The study suggests that the structure is unlikely to experience significant damage under the expected seismic loading. However, further research is recommended to refine the analysis and evaluate the Great Portico's seismic behaviour in greater detail.

Bibliography

Abdulla, K. F., Cunningham, L. S., & Gillie, M. (2017). Simulating masonry wall behaviour using a simplified micro-model approach. *Engineering Structures*, *151*, 349–365.

Addessi, D., & Sacco, E. (2012). A multi-scale enriched model for the analysis of masonry panels. *International Journal of Solids and Structures*, *49*(6), 865–880.

Almagro Gorbea, A. (2011). *Planimetría de Madīnat al-Zahrā'*. Consejo Superior de Investigaciones Científicas (CSIC).

Angelillo, M. (Ed.). (2014). *Mechanics of masonry structures*. Springer.

Baraldi, D., & Cecchi, A. (n.d.). [a full 3d rigid block model for the collapse behaviour of masonry walls.

Belmouden, Y., & Lestuzzi, P. (2009). An equivalent frame model for seismic analysis of masonry and reinforced concrete buildings. *Construction and Building Materials*, *23*(1), 40–53. https://doi.org/10.1016/j.conbuildmat.2007.07.001

Berto, L., Saetta, A., Scotta, R., & Vitaliani, R. (2002). An orthotropic damage model for masonry structures. *International Journal for Numerical Methods in Engineering*, *55*(2), 127–157.

Blanco-Varela, M. T., Puertas, F., & Palomo, Á. (1997). Rendering mortars in Medina Azahara, Part I: Material characterization and alteration process. *Materiales de Construcción*, *47*(245), 29–43. https://doi.org/10.3989/mc.1997.v47.i245.512

Block, P., Ciblac, T., & Ochsendorf, J. (2006). Real-time limit analysis of vaulted masonry buildings. *Computers & Structures*, *84*(29–30), 1841–1852. https://doi.org/10.1016/j.compstruc.2006.03.010

Block, P., & Lachauer, L. (2014). Three-dimensional (3D) equilibrium analysis of Gothic masonry vaults. *International Journal of Architectural Heritage*, *8*(3), 312–335.

Block, P., & Ochsendorf, J. (2007). Thrust network analysis: A new methodology for three-dimensional equilibrium. *Journal of the International Association for Shell and Spatial Structures*, *48*(3), 167–173.

Brasile, S., Casciaro, R., & Formica, G. (2007). Multilevel approach for brick masonry walls—Part I: A numerical strategy for the nonlinear analysis. *Computer Methods in Applied Mechanics and Engineering*, *196*(49–52), 4934–4951. https://doi.org/10.1016/j.cma.2007.01.018

Bruggi, M. (2014). Finite element analysis of no-tension structures as a topology optimization problem. *Structural and Multidisciplinary Optimization*, *50*(6), 957–973. https://doi.org/10.1007/s00158-014-1110-1

Çakti, E., Saygili, Ö., Lemos, J. V., & Oliveira, C. S. (2016). Discrete element modeling of a scaled masonry structure and its validation. *Engineering Structures*, *126*, 224–236. https://doi.org/10.1016/j.engstruct.2016.03.010

Calero Clavero, N. (2023, April). Gran Pórtico de Medina Azahara [Retrieved October 7, 2025, from https://amedinacordoba.com/gran-portico-de-medina-azahara/].

Caliò, I., Marletta, M., & Pantò, B. (2012). A new discrete element model for the evaluation of the seismic behaviour of unreinforced masonry buildings. *Engineering Structures*, *40*, 327–338.

CEB & FIB. (1993). *CEB-FIP Model Code 1990: Design Code*. T. Telford.

Chiozzi, A., Grillanda, N., Milani, G., & Tralli, A. (2018). UB-ALMANAC: An adaptive limit analysis NURBS-based program for the automatic assessment of partial failure mechanisms in masonry churches. *Engineering Failure Analysis*, *85*, 201–220.

Chiozzi, A., Milani, G., & Tralli, A. (2017). A genetic algorithm NURBS-based new approach for fast kinematic limit analysis of masonry vaults. *Computers & Structures*, *182*, 187–204.

Clemente, P. (1998). Introduction to dynamics of stone arches. *Earthquake Engineering & Structural Dynamics*, *27*(5), 513–522. https://doi.org/10.1002/(SICI)1096-9845(199805)27:5<513::AID-EQE740>3.0.CO;2-O

D'Altri, A. M., de Miranda, S., Castellazzi, G., & Sarhosis, V. (2018). A 3D Detailed Micro-Model for the In-Plane and Out-of-Plane Numerical Analysis of Masonry Panels. *Computers & Structures*, *206*, 18–30.

D'Altri, A. M., Sarhosis, V., Milani, G., Rots, J., Cattari, S., Lagomarsino, S., Sacco, E., Tralli, A., Castellazzi, G., & de Miranda, S. (2020). Modeling strategies for the computational analysis of unreinforced masonry structures: Review and classification. *Archives of Computational Methods in Engineering*, *27*(4), 1153–1185. https://doi.org/10.1007/s11831-019-09351-x

DIANA FEA B.V. (2023). *DIANA FEA* (Version 10.7) [Computer software]. The Hague, The Netherlands, DIANA FEA bv. https://www.dianafea.com

DIANA FEA B.V. (2025). *DIANA Finite Element Analysis: User's Manual – Theory, Release 10.10*. The Hague, The Netherlands, DIANA FEA bv. https://manuals.dianafea.com/d1010/en/1353862-1353862-theory-1010.html

Feenstra, P. H. (1993). *Computational aspects of biaxial stress in plain and reinforced concrete* [Doctoral thesis]. Delft University of Technology.

Fraternali, F. (2010). A thrust network approach to the equilibrium problem of unreinforced masonry vaults via polyhedral stress functions. *Mechanics Research Communications*, *37*(2), 198–204.

Gambarotta, L., & Lagomarsino, S. (1997). Damage models for the seismic response of brick masonry shear walls. Part II: The continuum model and its applications. *Earthquake Engineering & Structural Dynamics*, *26*(4), 441–462. https://doi.org/10.1002/(SICI)1096-9845(199704)26:4<441::AID-EQE669>3.0.CO;2-W

García Hernández, M., & de la Calle Vaquero, M. (2010). Uso y lectura turística de los grandes conjuntos arqueológicos. Reflexiones a partir del Estudio de Público de Medina Azahara / Madinat al-Zahra (Córdoba). *PASOS. Revista de Turismo y Patrimonio Cultural*, *8*(4), 609–626. https://www.cabidigitallibrary.org/doi/full/10.5555/20103307862

Hendriks, M. A. N., & Roosen, M. A. (2022). *Guidelines for Nonlinear Finite Element Analysis of Concrete Structures* (Report RTD:1016-1:2022). Rijkswaterstaat Centre for Infrastructure.

Heyman, J. (1966). The Stone Skeleton. *International Journal of Solids and Structures*, *2*, 249–279.

Heyman, J. (1969). The Safety of Masonry Arches. *Int. J. mech. Sci*, *11*, 363–385.

Heyman, J. (1976). Couplet's engineering memoirs, 1726-33. In A. Rupert Hall & N. Smith (Eds.), *History of Technology, Vol. 1* (pp. 21–44). Mansell.

Hidalgo Fernández, R. E., & Ortiz-Cordero, R. (2020). The Mosque-Cathedral of Córdoba: Evidence of column organization during their first construction s. VIII A.D. *Journal of Cultural Heritage*, *45*, 215–220. https://doi.org/10.1016/j.culher.2020.05.011

Hildebrand, T. (2012). Architectural Origins of the Mosque of Cordoba. *Nebraska Anthropologist*, *27*. https://digitalcommons.unl.edu/nebanthro/175/

Hisari, C., Macorini, L., Amadio, C., & Izzuddin, B. A. (2018). Identification of mesoscale model parameters for brick-masonry. *International Journal of Solids and Structures*, *146*, 224–240.

Lagomarsino, S., Penna, A., Galasco, A., & Cattari, S. (2013). Tremuri program: An equivalent frame model for the nonlinear seismic analysis of masonry buildings. *Engineering Structures*, *56*, 1787–1799.

Lourenço, P. B. (2008). Structural masonry analysis: Recent developments and prospects. *Proceedings of the 14th International Brick & Block Masonry Conference*, 1341–1356.

Lourenço, P. B., Barros, J. A. O., & Oliveira, J. R. M. (2004). Shear testing of stack bonded masonry. *Construction and Building Materials*, *18*(2), 125–132. https://doi.org/10.1016/j.conbuildmat.2003.08.018

Lourenço, P. B., Rots, J. G., & Blaauwendraad, J. (1998). Continuum model for masonry: Parameter estimation and validation. *Journal of Structural Engineering*, *124*(6), 642–652.

Lourenço, P. B., & Rots, J. G. (1997). Multisurface Interface Model for Analysis of Masonry Structures. *Journal of Engineering Mechanics*, *123*(7), 660–668. https://doi.org/10.1061/(ASCE)0733-9399(1997)123:7(660)

Marmo, F., & Rosati, L. (2017). Reformulation and extension of the thrust network analysis. *Computers & Structures*, *182*, 104–118.

Massart, T. J., Peerlings, R. H. J., & Geers, M. G. D. (2007). An enhanced multi-scale approach for masonry wall computations with localization of damage. *International Journal for Numerical Methods in Engineering*, *69*(5), 1022–1059. https://doi.org/10.1002/nme.1956

Mazzon, N., Chavez, C. M., Valluzzi, M. R., Casarin, F., & Modena, C. (2010). Shaking table tests on multi-leaf stone masonry structures: Analysis of stiffness decay. *Advanced Materials Research*, *133–134*, 647–652. https://doi.org/10.4028/www.scientific.net/AMR.133-134.647

Milani, G. (2008). 3D upper bound limit analysis of multi-leaf masonry walls. *International Journal of Mechanical Sciences*, *50*(4), 817–836.

Milani, G., Lourenço, P., & Tralli, A. (2007). 3D homogenized limit analysis of masonry buildings under horizontal loads. *Engineering Structures*, *29*(11), 3134–3148.

Mirmobiny, S. (2015, August). The Great Mosque of Córdoba [Retrieved October 7, 2025, from https://smarthistory.org/the-great-mosque-of-cordoba/].

NEN. (2020, December). *NPR 9998:2020 en: Assessment of structural safety of buildings in case of erection, reconstruction and disapproval – Induced earthquakes – Basis of design, actions and resistances* [Dutch practise guideline; English version of Dutch standard].

O'Dwyer, D. (1999). Funicular analysis of masonry vaults. *Computers & Structures*, *73*(1–5), 187–197. https://doi.org/10.1016/S0045-7949(99)00025-7

Oppenheim, I. J. (1992). The Masonry Arch as a Four-Link Mechanism under Base Motion. *Earthquake Engineering & Structural Dynamics*, *21*, 1005–1017.

Palomar, T., Schibille, N., Cerqueira Alves, L., Díaz Hidalgo, R. J., & Gomez-Morón, M. A. (2023). Historical restorations of the Maqṣūrah glass mosaics from the Great Mosque of Córdoba. *Boletín de la Sociedad Española de Cerámica y Vidrio*, *62*(3), 204–219. https://doi.org/10.1016/j.bsecv.2022.04.004

Pelà, L., Cervera, M., & Roca, P. (2013). An orthotropic damage model for the analysis of masonry structures. *Construction and Building Materials*, *41*, 957–967.

Petracca, M., Pelà, L., Rossi, R., Oller, S., Camata, G., & Spacone, E. (2016). Regularization of first order computational homogenization for multiscale analysis of masonry structures. *Computational Mechanics*, *57*(2), 257–276.

Portioli, F., Casapulla, C., Gilbert, M., & Cascini, L. (2014). Limit analysis of 3D masonry block structures with non-associative frictional joints using cone programming. *Computers & Structures*, *143*, 108–121. https://doi.org/10.1016/j.compstruc.2014.07.006

Requena García de la Cruz, M. V., Romero-Sánchez, E., López Piña, M. P., & Morales Esteban, A. (2023). Preliminary structural and seismic performance assessment of the Mosque-Cathedral of Cordoba: The Abd al-Rahman I sector. *Engineering Structures*, *291*, 116465. https://doi.org/10.1016/j.engstruct.2023.116465

Rinaldin, G., Amadio, C., & Macorini, L. (2016). A macro-model with nonlinear springs for seismic analysis of urm buildings. *Earthquake Engineering & Structural Dynamics*, *45*(14), 2261–2281. https://doi.org/10.1002/eqe.2760

Roca, P., Cervera, M., Gariup, G., & Pelà, L. (2010). Structural analysis of masonry historical constructions: Classical and advanced approaches. *Archives of Computational Methods in Engineering*, *17*(3), 299–325. https://doi.org/10.1007/s11831-010-9046-1

Rodríguez-Pascua, M. Á., Perucha, M. Á., Silva, P. G., Montejo Córdoba, A. J., Giner-Robles, J. L., Élez, J., Bardají, T., Roquero, E., & Sánchez-Sánchez, Y. (2023). Archaeoseismological Evidence of Seismic Damage at Medina Azahara (Córdoba, Spain) from the Early 11th Century. *Applied Sciences*, *13*(3), 1601. https://doi.org/10.3390/app13031601

Rots, J. G. (1988). *Computational modeling of concrete fracture* [Doctoral thesis]. Delft University of Technology.

Selby, R. G., & Vecchio, F. J. (1993). *Three-dimensional constitutive relations for reinforced concrete* (Technical Report, Publication No. 93, Part 2). University of Toronto, Department of Civil Engineering. Toronto, Canada.

Serpieri, R., Albarella, M., & Sacco, E. (2017). A 3D microstructured cohesive–frictional interface model and its rational calibration for the analysis of masonry panels, journal = International Journal of Solids and Structures. *122*, 110–127.

Tomassetti, U., Correia, A. A., Candeias, P. X., Graziotti, F., & Campos Costa, A. (2018). Two-way bending out-of-plane collapse of a full-scale URM building tested on a shake table. *Bulletin of Earthquake Engineering*, *17*, 2165–2198. https://doi.org/10.1007/s10518-018-0507-5

UNESCO World Heritage Centre. (2025). *World Heritage List* [Retrieved November 10, 2025, from https://whc.unesco.org/en/list/].

Van Zijl, G. P. A. G. (2000). *Computational modelling of masonry creep and shrinkage* [Doctoral dissertation, Delft University of Technology]. https://resolver.tudelft.nl/uuid:d6102658-c499-4dd0-8481-a39ae6f7cd09

Xue, J., Hu, P., Zhang, F., & Zhuge, Y. (2021). Seismic behavior of brick cave dwellings: Shake table tests. *Journal of Building Engineering*, 102886. https://doi.org/10.1016/j.jobe.2021.102886

Zapico-Blanco, B., Rodríguez-Mariscal, J. D., & Solís Muñiz, M. (2025). Ultrasonic Evaluation of Mechanical Properties in Heritage Buildings Constructed with Córdoba Freestone. *Heritage*, *8*(11), 462. https://doi.org/10.3390/heritage8110462

A

Single arch analysis

Appendix A covers a case study, about a single arch structure, performed preceding the main research on the Great Portico. This study was performed to explore the possibility of simplifying the final model into a 2-dimensional model instead of a 3-dimensional. Reasoned was that a 2D-model could sufficiently capture the in-plane dynamic behaviour, but not the out-of-plane behaviour. If only the in-plane behaviour needed to be considered a 2D-model was thought to suffice.

A.1. Single arch analysis: Model specifications

For this study the model-geometry was based on one of the arches from the remaining structure of the Great Portico, specifically the third arch from the left, per Figure 3.4a. The geometry of the 3D-model is shown in Figure A.1. For the 2D-model the width of the structure was specified in the thickness of the elements. The structure was fixed at its base. No boundary conditions were added to simulate the rest of the arches, therefore a free standing single arch was considered. The same mesh-size was chosen as for the analyses of the Great Portico-structure: 0.3 meters.

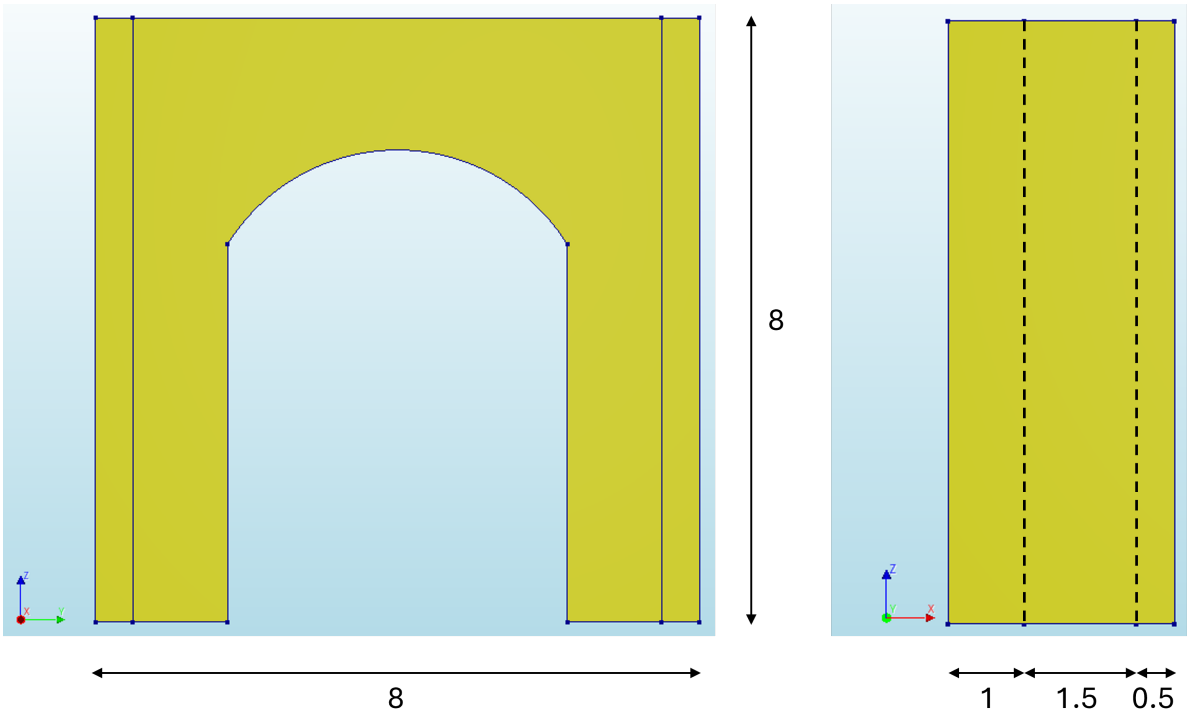

Figure A.1: Model-geometry of the single arch structure (in meters)

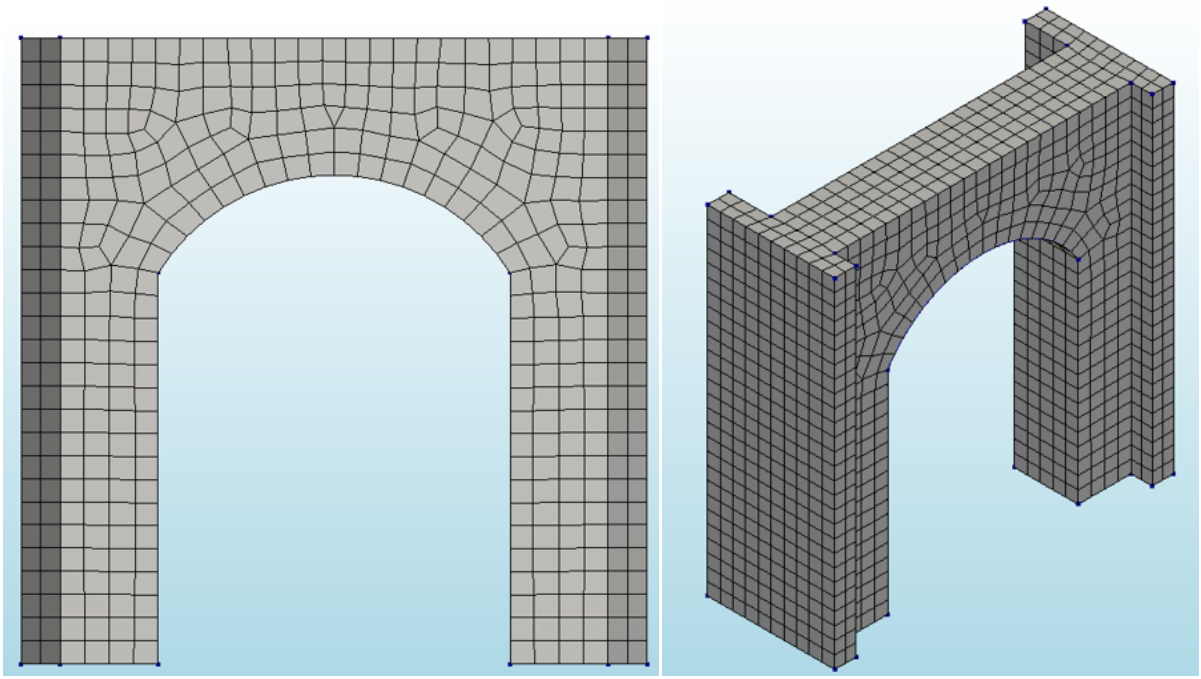

(a) 2D-mesh (b) 3D-mesh

Figure A.2: Model-meshes of the single arch structure

The 3D-model was build with structural solid elements, the elements shown in Subsection 3.1.3. The 2D-model was built with curved shell elements: T15SH and Q20SH (DIANA FEA B.V., 2025). The shell elements were modelled with nine integration points across their thickness. A single material was defined: stone masonry. The same material model was used as in the main study: total based strain crack model. The material-properties are given in Table A.1. The properties are a general set of properties for stone masonry, notably different from the property-set used for the stone masonry-material in the main study.

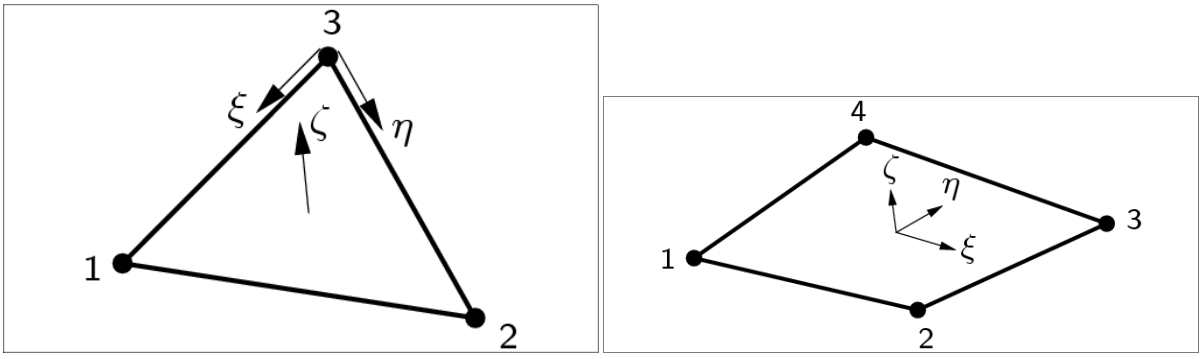

(a) T15SH-element (b) Q20SH-element

Figure A.3: Curved shell elements (DIANA FEA B.V., 2025)

Mechanical property	Symbol	Unit	Stone masonry
Compressive strength	f_c	N/mm^2	4.0
Modulus of elasticity	E	N/mm^2	2200
Density	ρ	kg/m^3	2400
Poisson's ratio	ν	-	0.2
Tensile strength	f_t	N/mm^2	0.2
Fracture energy compression	G_{Ck}	N/mm	6.4
Fracture energy tension	G_{Fk}	N/mm	0.012

Table A.1: Mechanical properties of stone masonry material (Single arch analysis)

A.2. Single arch analysis: Results and Conclusion

The aim of this case study was to explore the possibility to use a 2D-model FEM-model to answer the main research question. Figure A.4 shows the in-plane and out-of-plane pushover analyses of the single arch-structure. The OOP-response shows a similar linear response for the 2D and 3D-model, but post-linear: the 3D-model gives a lower normalized base shear than the 2D-model. The linear IP-response is similar for both models. The 2D model shows a slightly higher initial stiffness for both the IP and OOP-analyses. The post-linear IP-response is uncertain. The analysis diverged around a displacement of 3 mm in both models. No further conclusions were drawn from the IP-response. Based on the OOP-response of the single arch analysis, a 2D-model was deemed insufficient to capture the dynamic response of the Great Portico-structure adequately.

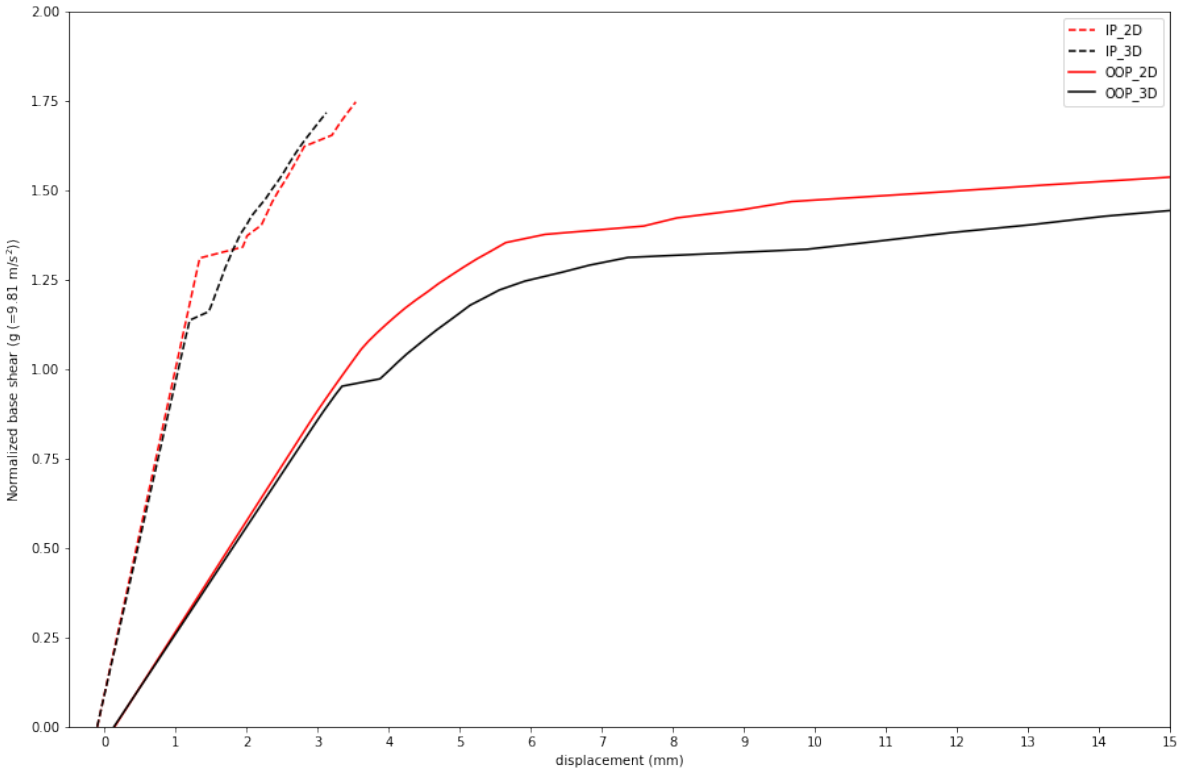

Figure A.4: Single arch pushover analysis

B

Convergence plots

Appendix B presents the convergence behaviour of the pushover analyses conducted for this study. For all analyses, the following convergence criteria were applied: a displacement variation tolerance of 0.01 and an out-of-balance force tolerance of 0.01. Both criteria were required to be satisfied simultaneously to achieve convergence. A maximum of 100 iterations was set for each load step. If convergence was not reached after 100 iterations, the analysis automatically proceeded to the next step. The solution method used was the Quasi-Newton method, utilizing the Broyden-Fletcher-Goldfarb-Shanno (BFGS) method to calculate the iterative stiffness matrix. The first tangent of the next step was taken from the calculated tangent from the previous iteration.

At higher displacement levels (above 30 mm), convergence could not be achieved in all numerical models, primarily due to excessive displacement variation values exceeding 1.0, which are significantly above the specified tolerance norm. These results were therefore excluded from the report.

For the in-plane pushover analyses of the interface-model and the final-model, convergence issues also occurred at lower displacement levels (below 10 mm). In these instances, the residual variations were manually checked; if the displacement variation and out-of-balance force remained below a tolerance of 0.05, the results were considered acceptable and were included in the report.

An exception to the standard iteration limit was applied for the in-plane pushover analysis of the final-model. In this case, smaller load increments and an increased maximum number of iterations were implemented to ensure reliable results for the in-plane analysis. The maximum was set at 200 iterations.

B.1. Single-element-model

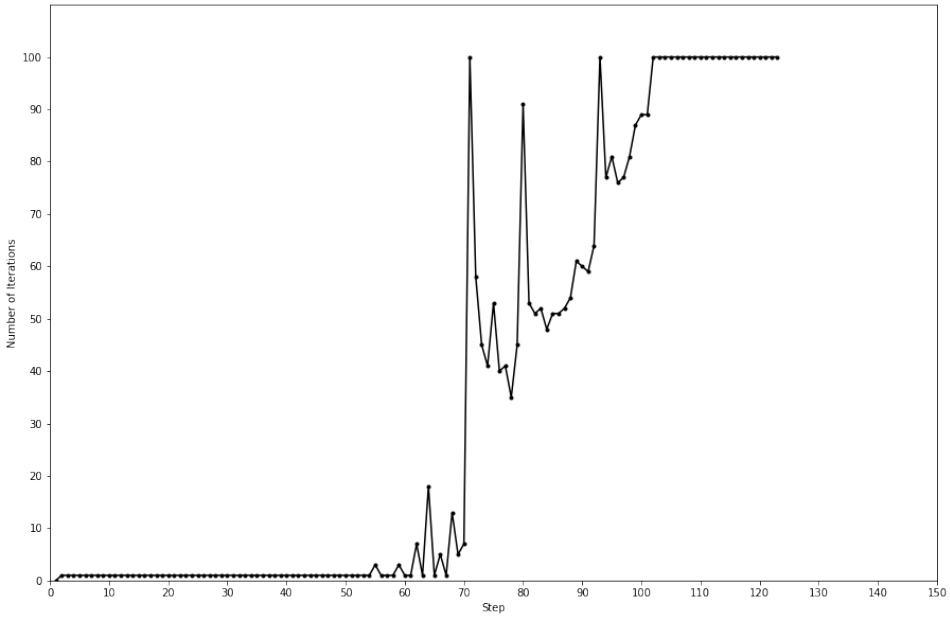

Figure B.1: Convergence-plot IP-analysis

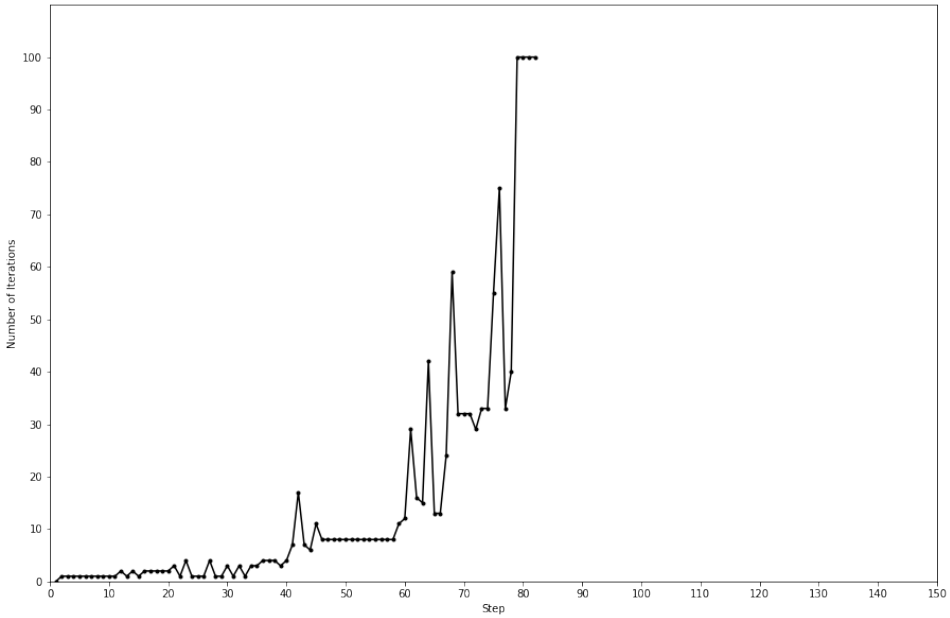

Figure B.2: Convergence-plot OOP-analysis

B.2. Single-element-model: Sensitivity analysis $0.5f_t$

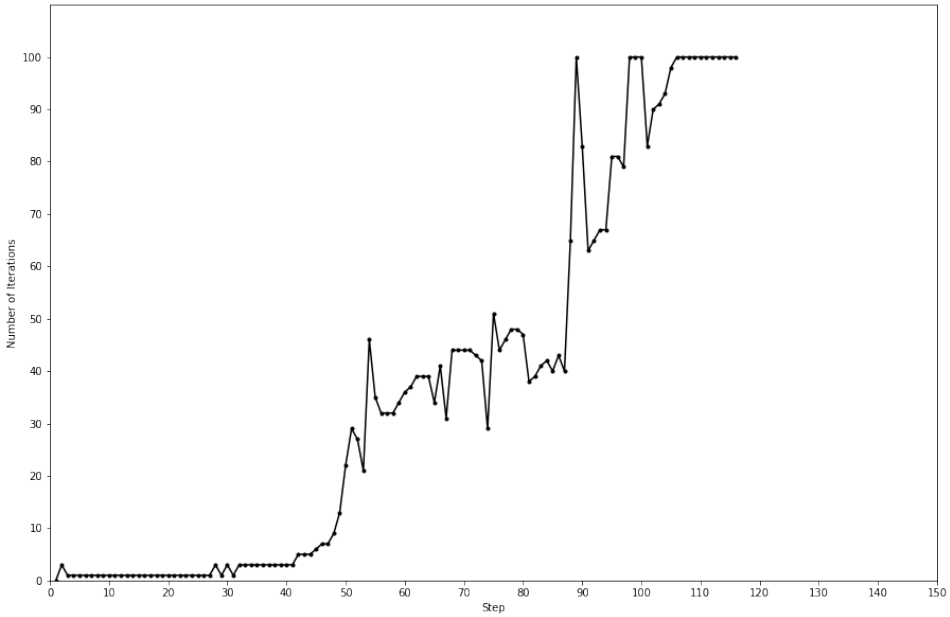

Figure B.3: Convergence-plot IP-analysis

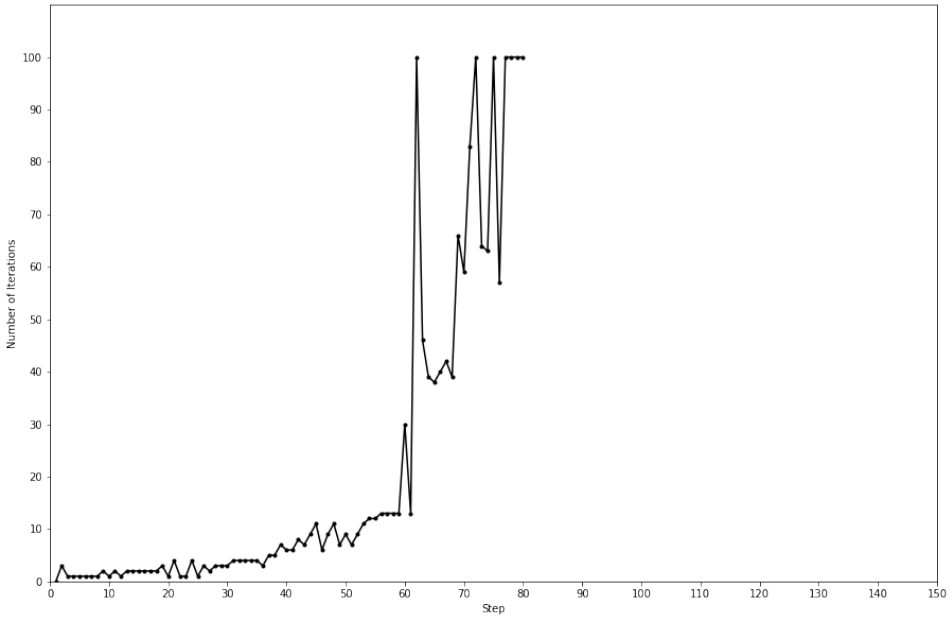

Figure B.4: Convergence-plot OOP-analysis

B.3. Single-element-model: Sensitivity analysis $0.5E$

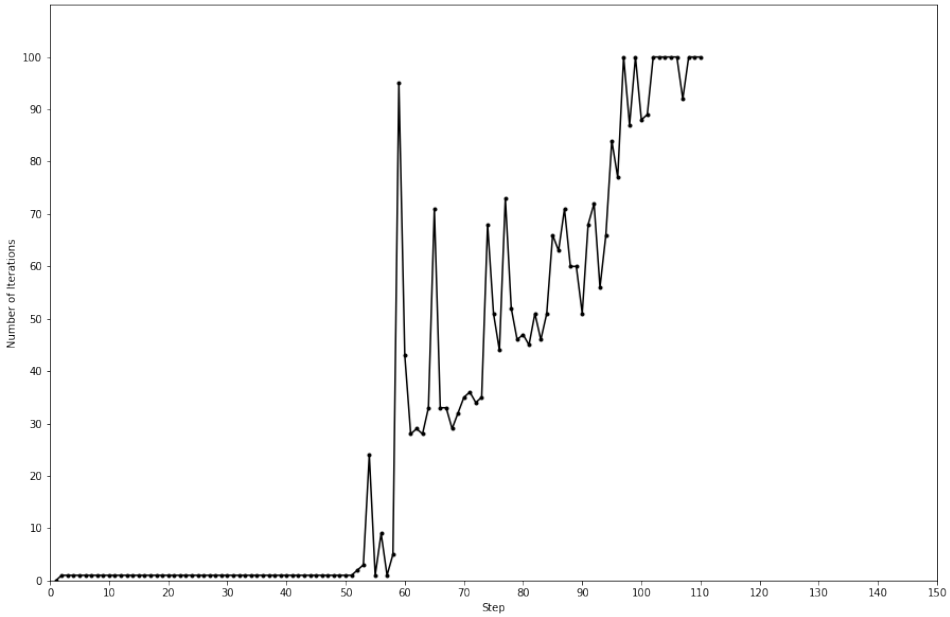

Figure B.5: Convergence-plot IP-analysis

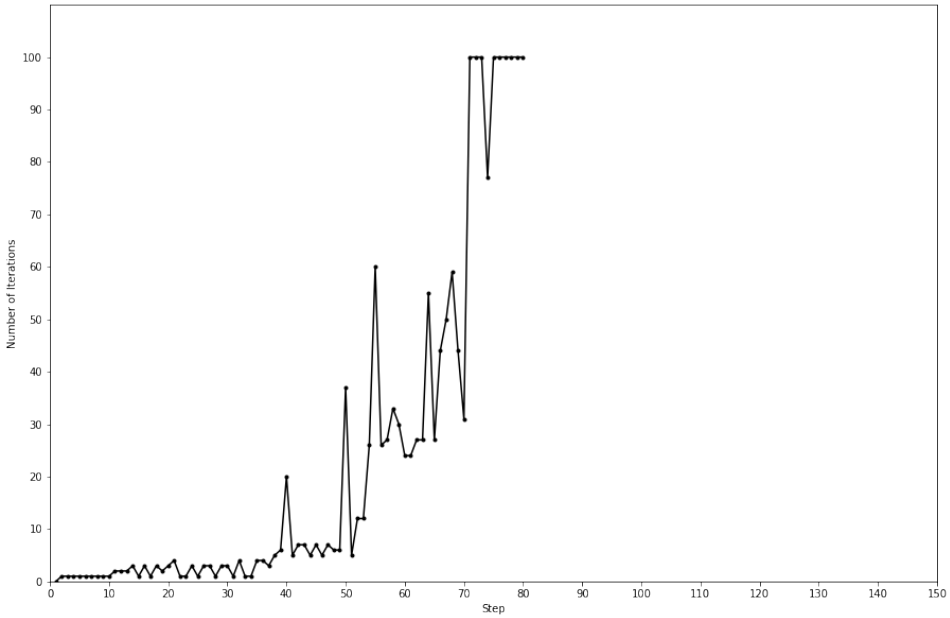

Figure B.6: Convergence-plot OOP-analysis

B.4. Tri-element-model

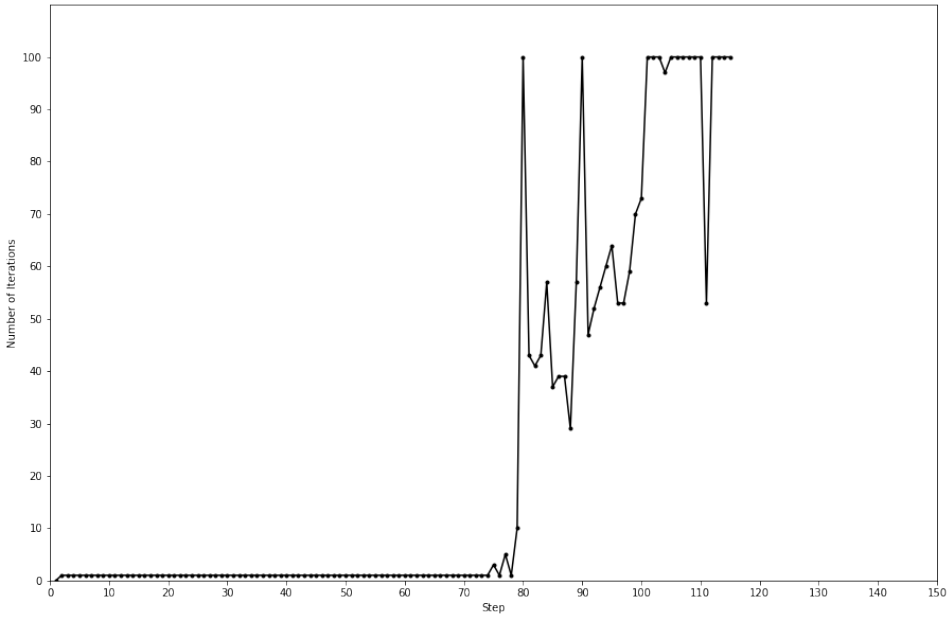

Figure B.7: Convergence-plot IP-analysis

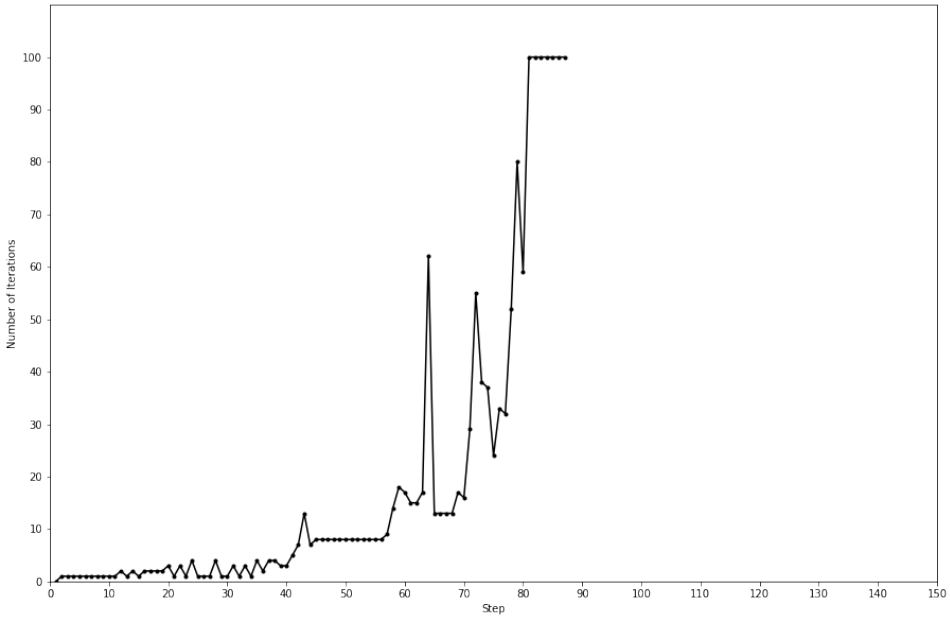

Figure B.8: Convergence-plot OOP-analysis

B.5. Interface-model: discrete cracking interfaces

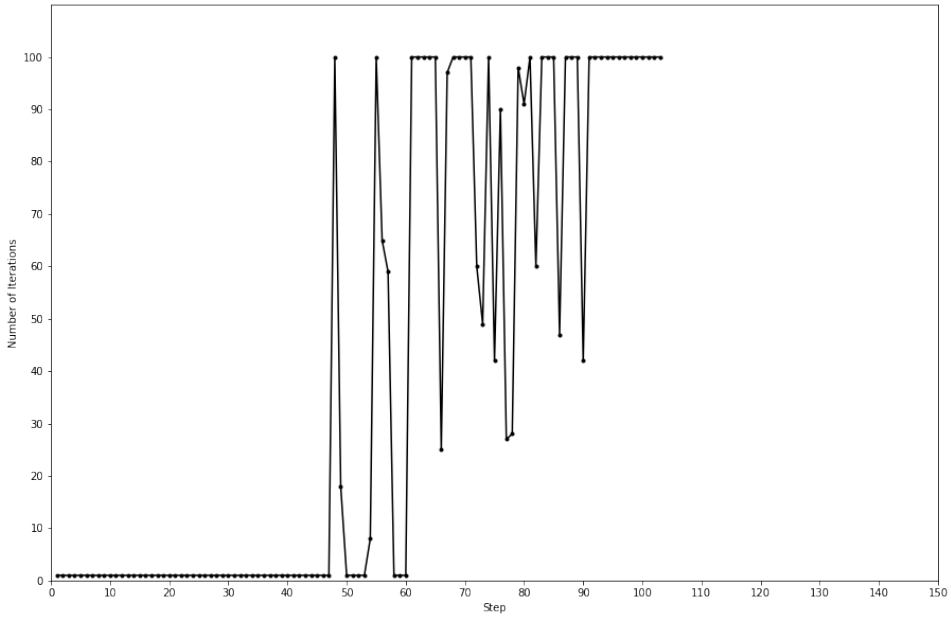

Figure B.9: Convergence-plot IP-analysis

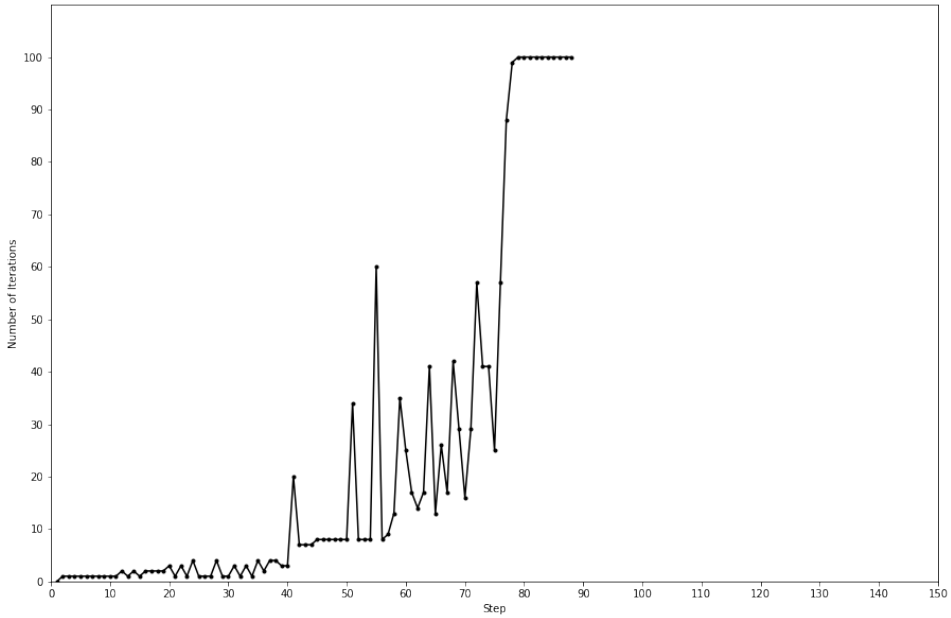

Figure B.10: Convergence-plot OOP-analysis

B.6. Interface-model: combined cracking-shearing-crushing interfaces

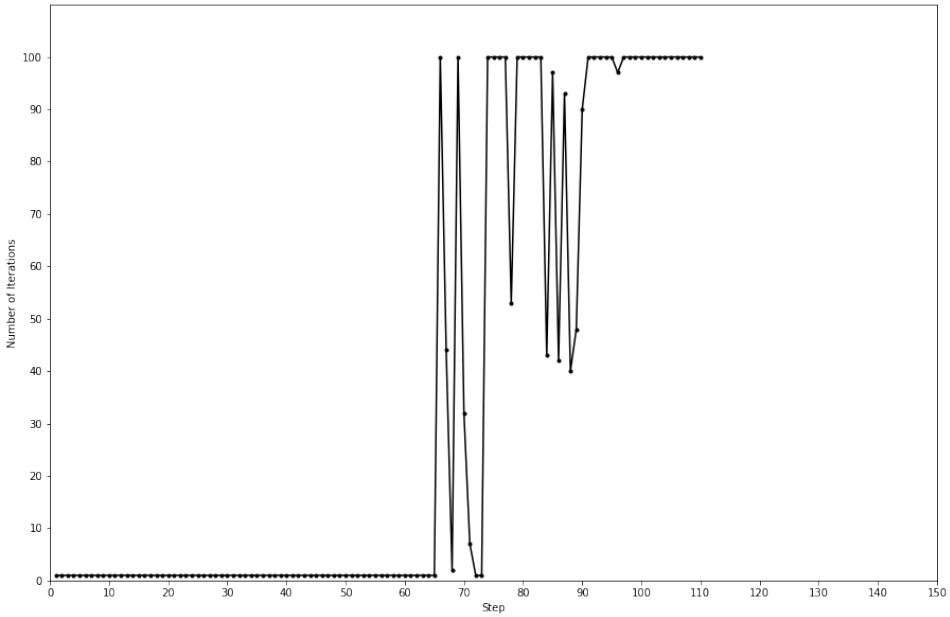

Figure B.11: Convergence-plot IP-analysis

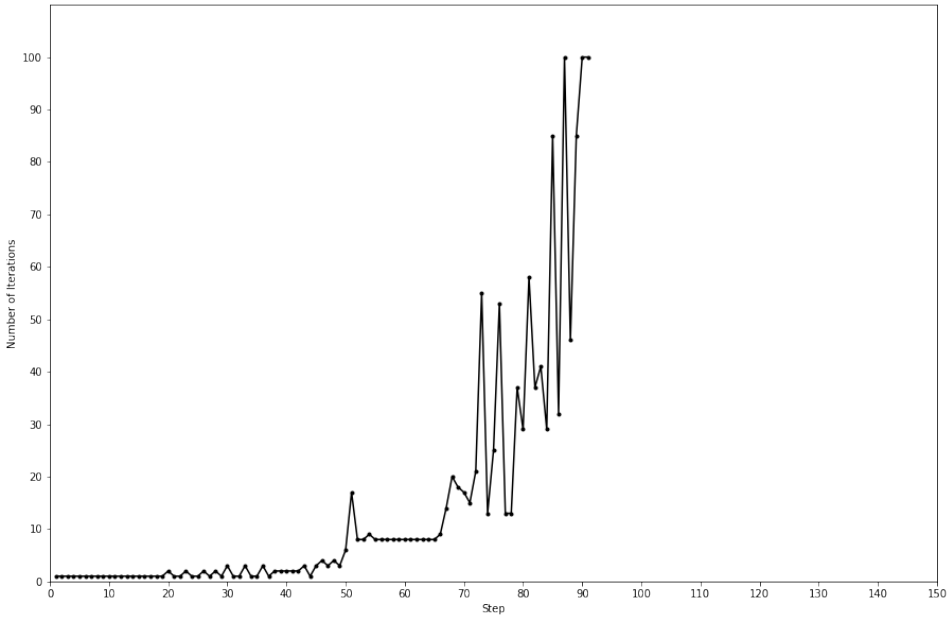

Figure B.12: Convergence-plot OOP-analysis

B.7. Final-model

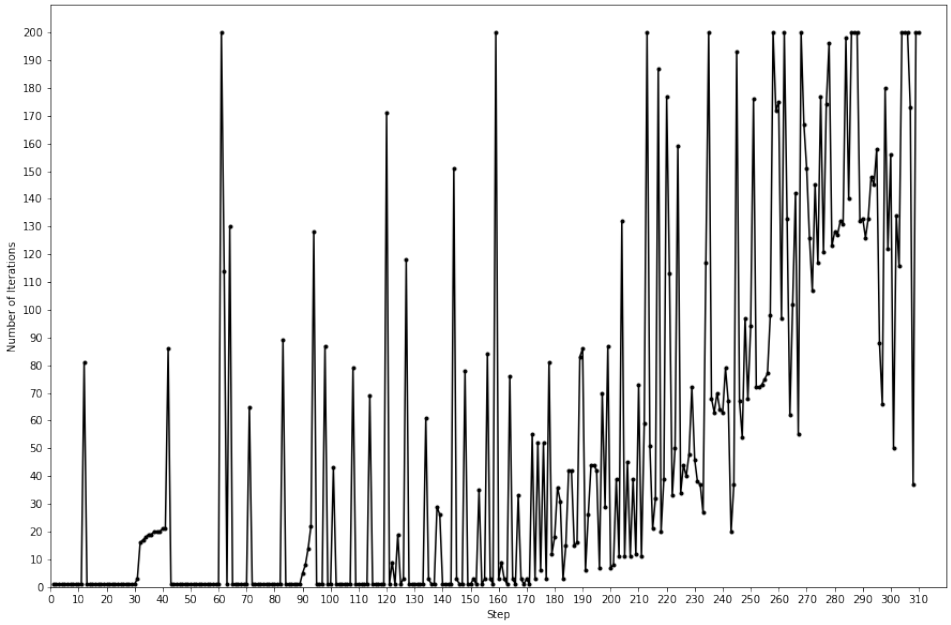

Figure B.13: Convergence-plot IP-analysis

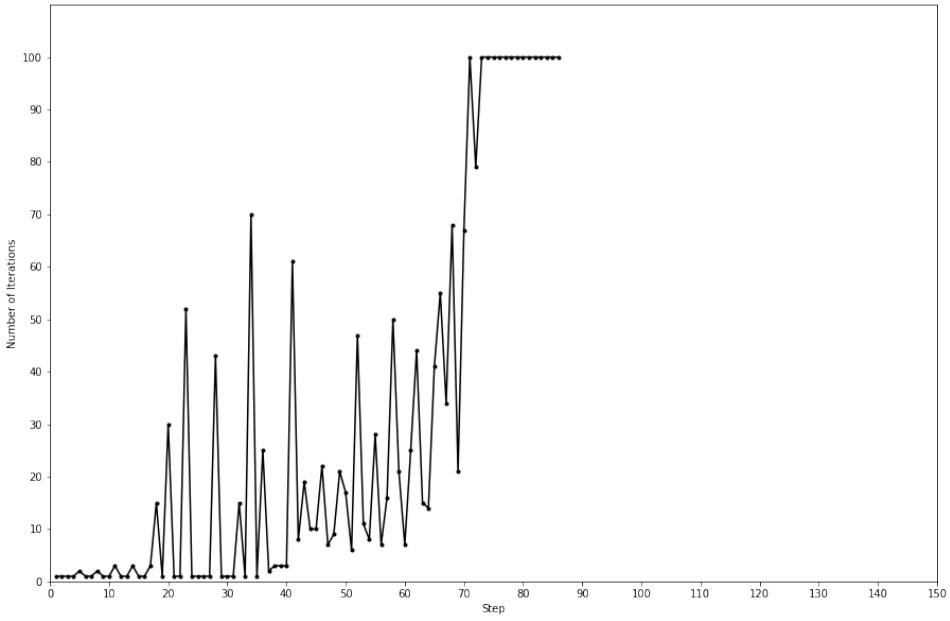

Figure B.14: Convergence-plot OOP-analysis